QUANTIFYING VERTICAL UNCERTAINTY AND THE TEMPORAL VARIABILITY OF THE SEAFLOOR TO INFORM HYDROGRAPHIC SURVEY PRIORITIES

BY

CASSANDRA BONGIOVANNI
B.S. Geology, University of Washington, 2014

THESIS

Submitted to the University of New Hampshire
in Partial Fulfillment of
the Requirements for the Degree of

Masters of Science
in
Earth Science: Ocean Mapping

December, 2018

This thesis has been examined and approved in partial fulfillment of the requirements for the degree of Masters of Science in Earth Science: Ocean Mapping by:

Thesis Director, Thomas C. Lippmann,
Associate Professor of Oceanography

Brian Calder,
Research Associate Professor of Ocean Engineering

Andrew Armstrong,
Co-Director of the Joint Hydrographic Center, NOAA

On November 20, 2018

Original approval signatures are on file with the University of New Hampshire Graduate School.

DEDICATION

To my friends, family, and colleagues that have helped along the way to shape this project, this is for you. I am eternally grateful for your support.

ACKNOWLEDGEMENTS

This work is fully funded by NOAA grant NA15NOS4000200. The author would like to thank Christy Fandel, Patrick Keown, and Corey Allen of NOAA Office of Coast Survey for their input and assistance on this project.

Table of Contents

LIST OF TABLES

LIST OF FIGURES

ABSTRACT

QUANTIFYING VERTICAL UNCERTAINTY AND THE TEMPORAL VARIABILITY OF THE SEAFLOOR TO IDENTIFY HYDROGRAPHIC SURVEY PRIORITIES

By:

Cassandra Bongiovanni

University of New Hampshire, December 2018

As the area of U.S. coastal waters vastly exceeds the capacity of annual hydrographic surveying, prioritization is necessary to optimize survey benefits. Obtaining new survey coverage over the most vital locations allows for an efficient use of funds; however, identifying these locations is a complex task. The current model to address survey prioritization, called the Hydrographic Health Model (or HHM), was created by personnel at the National Oceanographic and Atmospheric Administration (NOAA), the authoritative agency tasked with chart maintenance and hydrographic survey collection. While the HHM incorporates potential sources of bathymetric change, it does not include nor lend itself to the inclusion of actual measured changes associated with these sources. In order to integrate quantified estimates of change, the HHM fundamental equation must be adapted. Here we introduce the Hydrographic Uncertainty Gap (HUG) model as an adapted version of the HHM. Fundamental to HUG is the quantification of hydrographic survey uncertainties and changes to bathymetry, the calculations of which are outlined and performed for Chesapeake Bay and surrounding areas. Ultimately, we argue that the HUG model survey priorities are more realistic and more constrained than those from the HHM.

CHAPTER 1
INTRODUCTION

1.1.1 History of Hydrography

Nautical charts document the depth and physical characteristics of the seafloor to improve navigational safety at sea. The first nautical charts were created as early as the 13th century with only simple navigational directions as a guide. Over the centuries, the details and accuracy of charts have improved immensely due to increases in the amount and availability of hydrographic survey data. The International Hydrographic Organization describes hydrography as:

> *"That branch of applied sciences which deals with the measurement and description of the features of the seas and coastal areas for the primary purpose of navigation and all other marine purposes and activities, including –inter alia- offshore activities, research, protection of the environment, and prediction services."* (IHO Pub. S-32, 1994)

Hydrographic data have been collected for official purposes for the United States of America since the early 1800's when NOAA's original predecessor, the Survey of the Coast, originated through "An Act to provide surveying the coasts for the coasts of the United States."

For the first approximately one hundred years of hydrography in the United States, the standard depth collection method used lead-lines. This process measured depths using lead weights attached to a calibrated line (rope) and thrown from the side of a boat, sinking until it reached the bottom. The depth would then be read from the line and a depth and location would be recorded on the survey sheet. This process was not only slow and arduous but was prone to error due to drift from wind and currents (Van Der Wal and Pye, 2003). To account for these errors, depths were typically rounded down (making them shoaler) to the nearest fathom (Van Der Wal and

Pye, 2003; Calder, 2006). More significant than measurement inaccuracies are measurement frequency and density. Lead line techniques only obtained individual points along the vessel track, leaving the intervening seafloor unmeasured and unknown. Nevertheless, lead-lines continued as the primary method of depth measurement until sonic echosounders were introduced in the 1930s bringing quicker and continuous depth collection methods into the process (Hawley, 1931; Adams, 1942). The mid-1900s also brought advancement in geospatial positioning, moving away from sextant measurements towards electronic positioning in the 1950s and later satellite positioning in the 1990s. These improvements helped shape the performances of both the deep water multibeam systems in the 1980s and the shallow water multibeam systems in the 1990s (Wong *et al.,* 2007).

The profiling echosounder significantly increased hydrographic surveying capabilities by collecting a constant data stream of depths recorded directly under a boat as it moves along a track or course. With the invention of sidescan sonars and multibeam echosounders (MBES), two different types of survey designs became the standard: complete sidescan imaging and complete bathymetric coverage.

NOAA defines complete coverage as 100% of the seafloor is ensonified in one of two ways: either by a multibeam or by concurrent sidescan imaging and multibeam or single beam sonar (NOAA SPECS 2018) The sidescan sonar method collects data from larger swaths than multibeam sonars but are not capable of measuring depths. The exceptions to this rule are phase measuring bathymetric sonars (PMBS) that concurrently collect bathymetric and sidescan imaging from one system. However, PMBS systems are not frequently used in hydrography since their extremely large raw datasets require extensive manual filtering and have greater potential for errors. Traditional sidescans are more prevalent in the hydrographic community and

are primarily used to identify possible dangers to navigation that require additional investigation. Thus, significant areas of the seafloor are left without measured depths.

While the increased functionality of modern hydrographic systems allows users to do much more than ever before, it conversely increases the risk of unintentionally inaccurate data practices. To ensure only the highest quality data is used for chart products, the International Hydrographic Organization (IHO) created a standard (S-44) in 1968 outlining data quality requirements for charting purposes. The Standard has since been frequently updated to include appropriate handling of modern advancements and problems (IHO S-44, 2008), and is currently undergoing revision again.

In recent years, the hydrographic community has begun shifting towards electronic navigational products including electronic navigational charts (ENCs) and with these advancements has come a large push to reevaluate how data uncertainty and quality is assigned and portrayed for the mariner. Specifically, the Category of Zones of Confidence (CATZOC) levels outlined in S-57 (IHO S-57, 2014) are being reassessed and expected to be included in the new S-101 standards for ENCs (IHO S-100, 2015). Since S-101 is not officially released as of the date of this writing, the work discussed herein is based on S-44, S-57, and current NOAA and international standards.

1.1.2 International Uncertainty Standards

The CATZOC concept introduced a consistent methodology of assessing data quality by assigning each area on a chart a CATZOC level (Table 1). A CATZOC level is determined based on the vertical and horizontal uncertainty and type of coverage obtained by the underlying survey

and represents the confidence level in the data's accuracy. While the use of CATZOC, S-57, and S-44 standards allows for quality assurance of international nautical chart products, it also limits the extent by which data uncertainty is displayed and communicated to end-users (Calder, 2006; Calder, 2015). For raster chart products, data quality is limited to a source diagram that groups and labels the charted region by survey data collection year. More modern ENCs now include MQUAL (quality) polygons attributed with the CATZOC level describing the data used to compile any given area on the chart. While the latter approach theoretically allows for a more direct assessment of the confidence of charted soundings, it still has room for improvement. Specifically, the assignment of uncertainty attribution of less-than recent full coverage surveys.

CATZOC LEVEL	POSITION ACCURACY	DEPTH ACCURACY	SEAFLOOR COVERAGE
A1	+/- 5m + 5% depth	0.5m + 1% depth	Full area search
A2	+/- 20m	1m + 2% depth	Full area search
B	+/- 50m	1m + 2% depth	Less than full area search
C	+/- 500m	2m + 5% depth	Not complete and errors expected
D	Worse than ZOC C	Worse than ZOC C	Not complete and large errors expected
U	Unassessed – The quality of the data has yet to be assessed		

Table 1: The International Hydrographic Organization (IHO) S-44 quality standards for assessing survey uncertainty later applied through S-57 Category of Zones of Confidence (CATZOC) Levels. Depth and Position accuracies are at a 95% confidence interval.

Current NOAA and IHO S-57 procedure dictates that MQUALs are to be established for each charted hydrographic survey (IHO S-57, 2014). This process inherently assigns a CATZOC level and associated uncertainty to the entire survey area, whereas that uncertainty only truly pertains to the seafloor that was ensonified. For example, collection of data using other than full-coverage methods discussed above will survey a larger area more quickly with fewer resources but can leave bathymetric coverage gaps with tens to hundreds of meters between survey lines due to the

use of the sidescan in lieu of multibeam. This leaves the only estimation of depth in gap areas to come from either previously collected data (sometimes over one hundred years old) or a modeled estimate from available data (like the NCEI/NGDC Coastal Relief Model, 1999). In this example, the data collected might be of the highest quality and fit the uncertainty requirements of A1, but the survey coverage would cause it to be downgraded to a lesser CATZOC level. Conversely, if the data collected was of worse quality and 100% coverage, it would still result in a lower CATZOC level assignment. Thus, one of the main issues with this process is the inherent assignment of uncertainty to the entire survey area that does not accurately describe the area.

1.1.3 Survey Prioritization

NOAA operates four survey ships and several small survey launches which collect new hydrographic data within U.S. waters, an area of over 3.4 million square nautical miles. Within NOAA, the Office of Coast Survey (OCS) is the program office responsible for the collection and analysis of these hydrographic data that contribute to over 1000 U.S. charts. NOAA estimates that their ships obtain only 3,000 square nautical miles of new coverage annually (Gonsalves *et al*.,2015; Keown *et al*., 2016; Fandel *et al*., 2017; Hicks *et al*., 2017) and contracted survey work accounting for an additional similar amount making it impossible to keep all their charts up to date.

Many alternative strategies have been suggested and are being explored to improve the current challenge of maintaining NOAA's chart quality. One such proposal suggests NOAA utilize outside-source and crowd-source bathymetric data in order to lessen the load placed on their ships and increase the frequency at which charts are updated. However, these data will only

result in small incremental increases in survey coverage. Thus, internal survey prioritization will remain an absolutely essential component of the OCS mission.

1.1.4 Previous Work

NOAA does not currently have a standard way to account for survey degradation over time, entrusting the task of prioritization to their experienced hydrographers (Schultz, 2015). In recent years, attempts have been made to estimate survey degradation through a number of models from hydrographic agencies worldwide. Dorst (2009) performed time series analysis of bathymetric data in the Netherlands to determine survey priorities. The Canadian Hydrographic Service (CHS) started out with a weighted GIS-based model by Grenier and Hally (1991) which later evolved into their current model, the CHS Priority Planning Tool (CPPT), that combines a GIS and matrix approach to identify charts that need updates (Chenier *et al*., 2018). Other approaches have been attempted within the U.S., including NOAA's current model called the Hydrographic Health Model (HHM), the offspring of an Alaska chart assessment outlined in Gonsalves *et al*. (2015).

The HHM is a risk-based approach to approximate the current state of the charted data that relies primarily on survey quality assessments (Figure 1) and the associated risks to these vessels with out-of-date soundings. While the HHM heuristically accounts for some environmental change factors such as storms, tides, and marine debris, it could be improved with the quantification of more dynamic and area specific estimates of change. Specifically, the inclusion of quantifiable hydrodynamic variables could refine the accuracy of the HHM and resultant risk factors as they likely drive regional and nearshore sediment transport patterns.

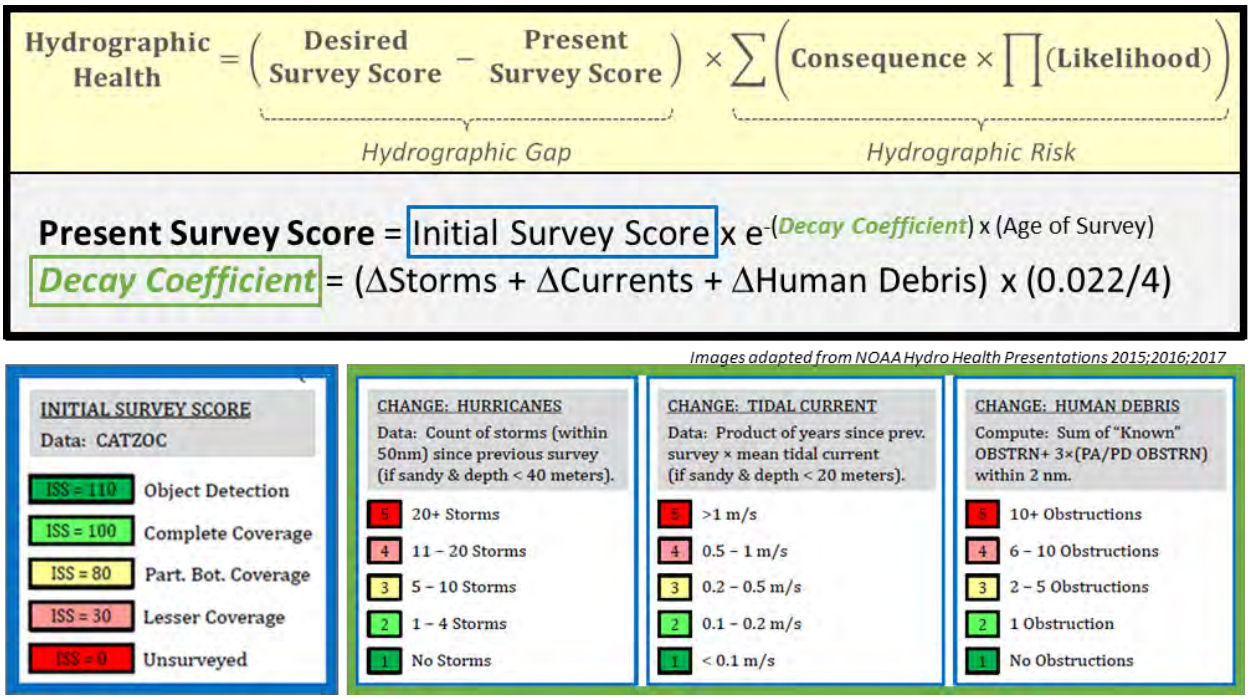

Figure 1: NOAA Hydrographic Health Model equations and inputs are outlined. Blue boxes describe the Initial Survey Score inputs based on IHO CATZOC levels. Green boxes outline the Decay Coefficient inputs for a number of change terms. (Keown *et al*., 2016; Fandel *et al*., 2017; Hicks *et al*., 2017)

1.1.5 Thesis Overview

This thesis presents an alternative methodology for estimating the hydrographic gap based on bathymetric change estimates and will address the problem in the following ways: chapter one discusses the uncertainty of archive (sparse) hydrographic data, chapter two outlines updates to the Hydrographic Health Model, and chapter three addresses conclusions and recommendations for future studies and implementations.

CHAPTER 2

A METHOD FOR QUANTIFYING THE VERTICAL UNCERTAINTY OF LESS-THAN FULL COVERAGE HYDROGRAPHIC SURVEY AREAS

2.1 SUMMARY

The National Oceanographic and Atmospheric Administration (NOAA) and its predecessor agencies have been responsible for the production and upkeep of the United States nautical charts since the nineteenth century. These charts are critical for the safe navigation of marine traffic. Essential to effective charting is curating accurate and up-to-date bathymetric information through cyclical and timely hydrographic surveys and approved analytics. Currently, incoming NOAA hydrographic surveys are attributed with a CATZOC (or Categorical Zone of Confidence) level for charting purposes determined by the limiting factor between survey coverage and vertical uncertainty requirements. Through these categories each survey area is attributed with a CATZOC level that only truly pertains to areas of the seafloor that were ensonified. This practice can lead to the underestimation of vertical uncertainty associated with less-than full coverage hydrographic surveys, ultimately introducing biases on the chart and skewing chart health model results. Here we describe a method using analytics to constrain and quantify the vertical uncertainty of unsurveyed seafloor within less-than full coverage survey areas along the central East Coast of the U.S. with the intention to incorporate estimates of uncertainty of the results into future hydrographic health models.

2.2 INTRODUCTION

Accurate nautical charts are essential for mariner safety and international commerce. The National Oceanographic and Atmospheric Administration (NOAA) is the U.S. authoritative organization responsible for producing up-to-date nautical charts for all U.S. coastal waters since

the early nineteenth century. Each chart is made up of hydrographic data layers that describe the seafloor depicting bottom type, depth, identification of obstructions, etc. all designed to limit mariner risk. This is taken further by periodic surveys, shoal-biasing, and referencing depths to Mean Lower Low Water (MLLW) so that every charted sounding is near shoalest possible depth any given area could be (Van Der Wal and Pye, 2003; Wong *et al*., 2007). However, limited resources restrict NOAA's ability to obtain materially significant new hydrographic data each year resulting in a significant over-reliance on old, sometimes substantially outdated, surveys. Therefore, contributing data on a chart may have been collected as far back as the mid-1800s (Van Der Wal and Pye, 2003; Wong *et al*., 2007; Masetti *et al*., 2018). During this extensive period, many technological advancements have been made which have altered the field of hydrography allowing for progressively more accurate data positioning, increased depth data collection, processing, and archiving capabilities.

While each charted survey utilizes the best possible technology and processing techniques available at the time, there are clear improvements in accuracy achievable with more modern survey techniques. Similar to modern procedures, the quality of archived hydrographic data were assessed upon collection with regards to standards in place at the time and addressed in descriptive reports (DRs) for each survey. However, no quantitative assessment of individual data points was recorded, or at least, not included in the DRs or migrated to electronic data storage (Ladner *et al*., 2017). Instead, the surveys were simply designated as "meets standards" or "did not meet standards". Thus, when NOAA reassessed thousands of archived surveys for uncertainty, the most reasonable assessment (in regards to time and resources) was to use the coverage requirements associated with international hydrographic organization (IHO) CATZOC levels (Table 1) as a way to address confidence.

CATZOC attribution is maintained even with modern surveys and is more accurately established by the limiting factor between survey coverage and uncertainty requirements. As precisely identifying the horizontal and vertical uncertainty of each data point collected is now mandatory, modern attributions of CATZOC more closely align with the IHO's intended purpose.

For both historical and modern surveys, CATZOC levels are assigned for the entire survey area, unintentionally implying that seafloor contained within the bounds of each survey polygon meets the corresponding level uncertainties. However, this is not always the case. CATZOC levels are assigned based on the limiting factor between bathymetric coverage and the vertical and horizontal uncertainties of the data. As the uncertainty of hydrographic data is only known where data exists and cannot accurately be extrapolated between data points, it is not uncommon for data to have larger uncertainties than can estimated without accounting for geophysical processes (Calder, 2006). Additional attention is therefore required to accurately quantify the vertical uncertainty of the entire survey area of less-than full coverage surveys.

It is understood that the uncertainty between data points increases with increased spacing (Oliver and Webster, 2014). For sparse datasets like many archive surveys, uncertainty between data points is essentially unknown making it impossible to know precisely where the seafloor is. Having said this, we can identify where the seafloor depths are at least not presenting a hazard to navigation, given that vessels have successfully traversed certain areas without groundings for many years. If groundings had occurred, the charts were immediately updated to reflect the change. Therefore, using vessel drafts recorded in vessel tracking Automatic Identification System (AIS), it becomes possible to constrain the vertical potential uncertainty between data points (Figure 2).

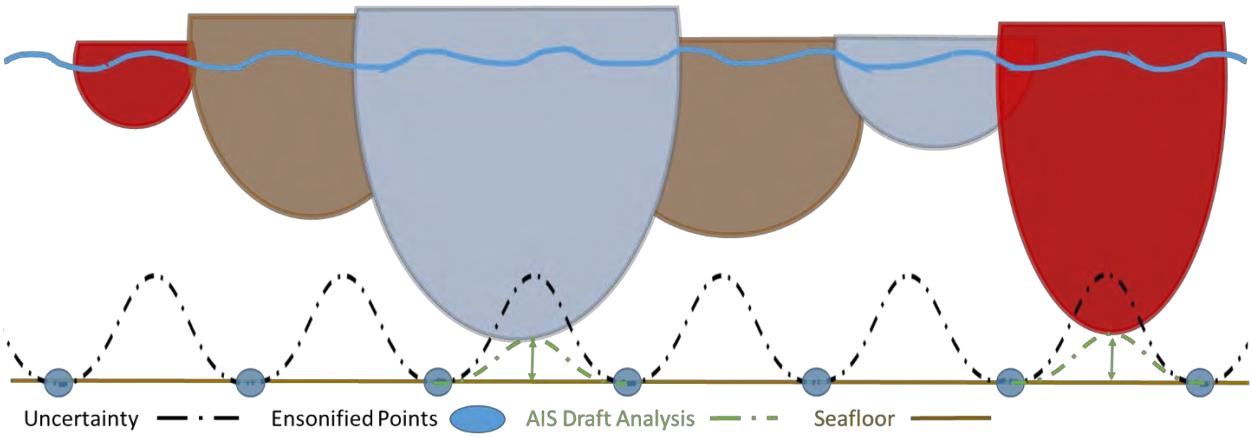

Figure 2: A flat portion of the seafloor is sparsely surveyed with ensonified points. The vertical uncertainty increases with increasing distance between points. Deep vessel drafts can be used to constrain these uncertainties where they pass. This could be particularly effective in shallower waters where the drafts make up a larger percentage of water depth.

To clarify, uncertainty is traditionally understood to be an upper (positive) and lower (negative) limit around a data point or value. For this study, the vertical uncertainty with which we analyze only refers to the upper limit (shallower) of the range as it is the only half that is navigationally significant. For the remainder of this thesis, we discuss uncertainty as the location of the upper limit.

Here we outline a methodology for calculating the uncertainty for an entire survey area with archive data sets, constraining that uncertainty where appropriate using available vessel AIS data, and assess the resulting area uncertainty. To accomplish this, a robust survey archive and an abundance of modern datasets were necessary, making the Chesapeake Bay and surrounding Delmarva area an ideal study area to test this approach. The central East Coast of the United States is known for vast amounts of sediment moving along its coastline, resulting in near constant surveying in some areas to keep up with a dynamic seafloor. Additionally, this region is heavily trafficked by recreational boaters and industrial shipping as a number of major ports are within the bounds of Chesapeake and Delaware Bay, thus providing a wide range of physical

observations to incorporate into the analysis. We anticipate that the methods outlined herein (summarized in Figure 3) could be used to better estimate bathymetric uncertainty on a national scale (discussed further in Chapter 4). Additionally, we expect the final results of this work to not only improve our understanding of currently charted data, but also be included in survey prioritization models (discussed further in Chapter 3).

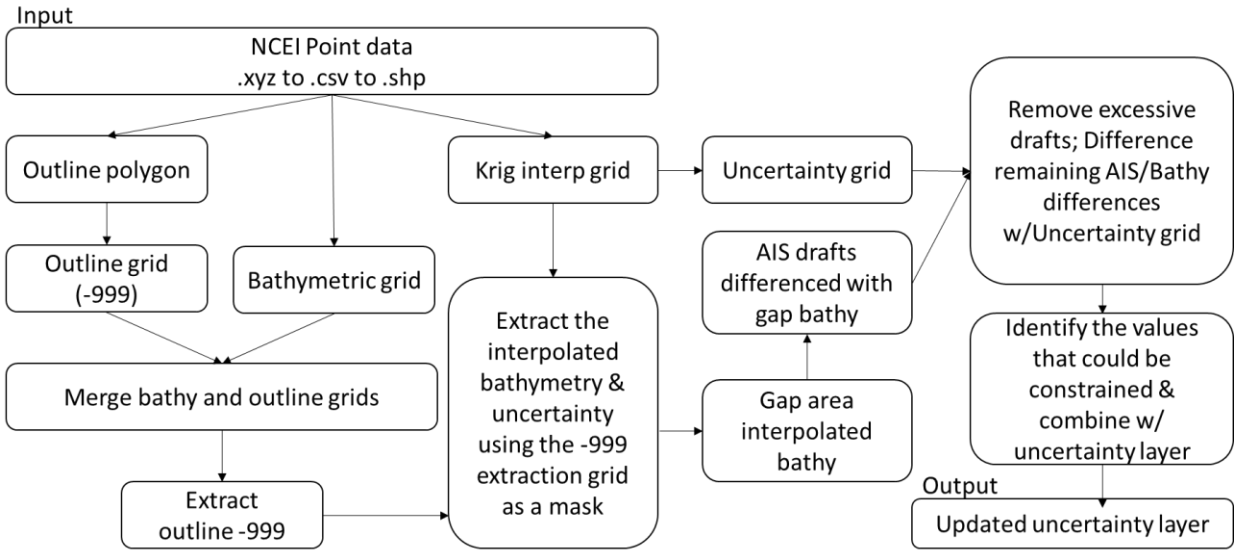

Figure 3: The complete workflow used to calculate and constrain vertical uncertainty of archive datasets using AIS vessel drafts. This workflow was completed using ESRI ArcGIS 10.5.1 and MATLAB 2017b.

2.3 METHODS

2.3.1 Calculating Uncertainty

All bathymetric data (XYZ and BAG formats) in and around Chesapeake Bay, Delaware Bay, and the Delmarva Peninsula were downloaded from the NOAA's National Center for Environmental Information (NCEI – formerly NGDC) (more information detailed in Appendix A). All data were analyzed and processed in ArcGIS ArcMap version 10.5.1. Due to the extensive archive of data in this area, a layered approach was taken.

- Bottom Layer - Any survey that covered a unique section of the seafloor for the first time was considered part of the bottom layer, even if a portion of it overlapped with another survey. The bottom layer includes over 250 surveys and 4.5 million points. The bulk of this layer was primarily collected between the 1940s and 1950s, though some surveys were collected as recently as 2002.
- Upper Layer - Any uncertainty-attributed BAG survey, generally more modern surveys (119 surveys)
- Middle Layer – Any remaining surveys between the bottom and upper layers, or any modern data *not* in BAG format (45 surveys).

All bottom layer XYZ data were imported as point files into ArcMap and additionally attributed with survey name and age. These data were then combined into five groups based on physical location: Upper Chesapeake Bay, Central Chesapeake Bay, Lower Chesapeake Bay, Offshore, and Delaware Bay. This allowed for quicker processing time as well as more realistic interpolation outputs by focusing only on the data pertinent to each group since the same geophysical processes that affect the offshore area do not necessarily influence Central Chesapeake Bay. Additional attention was focused on the mouth of Chesapeake Bay, and a sixth group was created to focus on those surveys.

Similarly, the mid-layer was divided into a few groups: Upper Chesapeake Bay, Lower Chesapeake Bay, and Delaware Bay. A few individual surveys in the mid-layer were too far removed from other surveys to be included in a group but were still included in the evaluation. All data were then analyzed using the ArcGIS 'Geostatistical Wizard' in the Geostatistical Analyst Toolbox to determine the appropriate interpolation (kriging) parameters for each group, or individual survey (Table 2). While the Wizard automatically takes the residuals of the data

and suggests parameters for optimum computing time, these suggestions were not used. Instead, parameters were chosen for optimum interpolation with little regard for computing time. It is possible that the other parameters could result in better interpolation outputs, especially if the universal kriging method is used. That said, the results outlined in Appendix C show a good correlation, a standardized RMS close to 1, and a low standard error.

Group	Method	Model	Lag Size (dd)	Major Range	Partial Sill	Nugget	Search Radius	Cell Size (dd)
B. Upper Ches	Ordinary	Exponential	.000342	.01708	8.3787	0	Variable	.000342
B. Central Ches	Ordinary	Spherical	.000345	.01725	9.1699	0	Variable	.000345
B. Lower Ches	Ordinary	Spherical	.000334	.00734	4.4965	0	Variable	.000334
B. Offshore	Ordinary	Gaussian	.000349	.01782	11.164	0.281134	Variable	.000349
B. Delaware	Ordinary	Spherical	.000293	.01393	.40044	0.070199	Variable	.000293
B. Mouth Ches	Ordinary	Gaussian	.000311	.13037	6.5551	0.307554	Variable	.000311
M. Upper Ches	Ordinary	Circular	.000315	.01259	4.2793	0	Variable	.000315
M. Lower Ches	Ordinary	Gaussian	.000314	.01088	7.3967	0.10388	Variable	.000314
M. Delaware	Ordinary	Gaussian	.000314	.01287	6.1201	0.07364	Variable	.000314
M. H12559	Ordinary	Gaussian	.000314	.01350	0.7487	0.029121	Variable	.000314
M. D00052	Ordinary	Spherical	.000314	.00973	7.4114	0	Variable	.000314
M. H11088	Ordinary	Gaussian	.000314	.01228	23.252	0.02325	Variable	.000314
M. H10934	Ordinary	Gaussian	.000314	.00942	0.9071	0.02656	Variable	.000314
M. H10193	Ordinary	Gaussian	.000314	.00932	21.474	0.34237	Variable	.000314

Table 2: Kriging parameters used for each bottom and middle layer group based on ESRI ArcGIS Geostatistical Analyst toolbox. Parameters were input into ESRI ArcGIS Kriging tool included in the Spatial Analyst toolbox. Kriging was based on the residual depths of each group and the output cell size is in decimal degrees. 'B' designations stand for bottom-layer groups while 'M' designates mid-layer surveys and groups.

In this study, we use kriging to interpolate depths into unknown areas based on the depths of surrounding points. The kriging interpolation method originated from Daniel Krige in 1955 and is now a widely used geostatistical method to predict missing values based on spatial variance. Kriging not only produces estimates of bathymetry, but also calculates the variance associated with each estimation which is readily translated into uncertainty. It is a fairly standard practice within the field of ocean mapping and remote sensing to interpolate between sparse data points using kriging algorithms (Calder, 2006; Dorst, 2009; Bailly *et al*., 2010; Aykut *et al*., 2013) and the kriging implementation in ArcGIS (discussed in Oliver and Webster, 2014) was found to

provide the necessary statistical analysis tools for the purposes of this study. Additional details on the kriging interpolation are discussed in Appendix C.

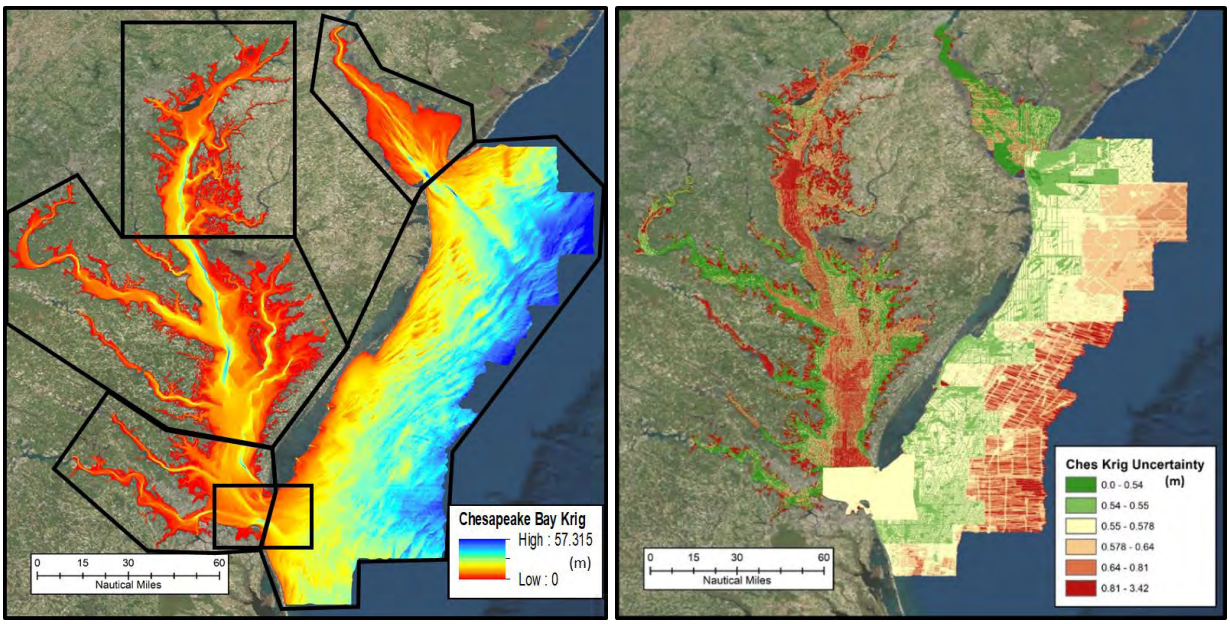

Figure 4: (Left) The bottom-layer krigged depths. The black boxes delineate the six groups: Upper Chesapeake Bay, Central Chesapeake Bay, Lower Chesapeake Bay, Chesapeake Bay Mouth, Offshore, and Delaware Bay. (Right) The bottom-layer combined krigged uncertainties.

The kriging parameters for each group in the bottom layer were input into the 'Kriging' tool in the ArcGIS Spatial Analyst Toolbox and the option for a variance output was selected. The output raster for each group were then masked to the study area and mosaicked together with the 'Mosaic to New Raster' tool using the following supersession order: Chesapeake Bay Mouth, Offshore, Lower Chesapeake Bay, Central Chesapeake Bay, Upper Chesapeake, and Delaware Bay (Figure 4). This process was performed for both the bathymetry and variance raster outputs. The square root of the combined variance raster was calculated to obtain the uncertainty. Both the bathymetry and uncertainty rasters had a cell size of ~40 m.

The kriging process was also performed on the mid-layer groups and surveys. However, as the purpose of the kriging interpolation was to estimate bathymetry and uncertainty gaps in coverage, the upper layer surveys were excluded from this processes since the BAG file format can include both bathymetry and uncertainty determined for each survey. Once both bathymetric and uncertainty estimates are obtained, the next step is to identify the area between data points and attempt to constrain the uncertainty.

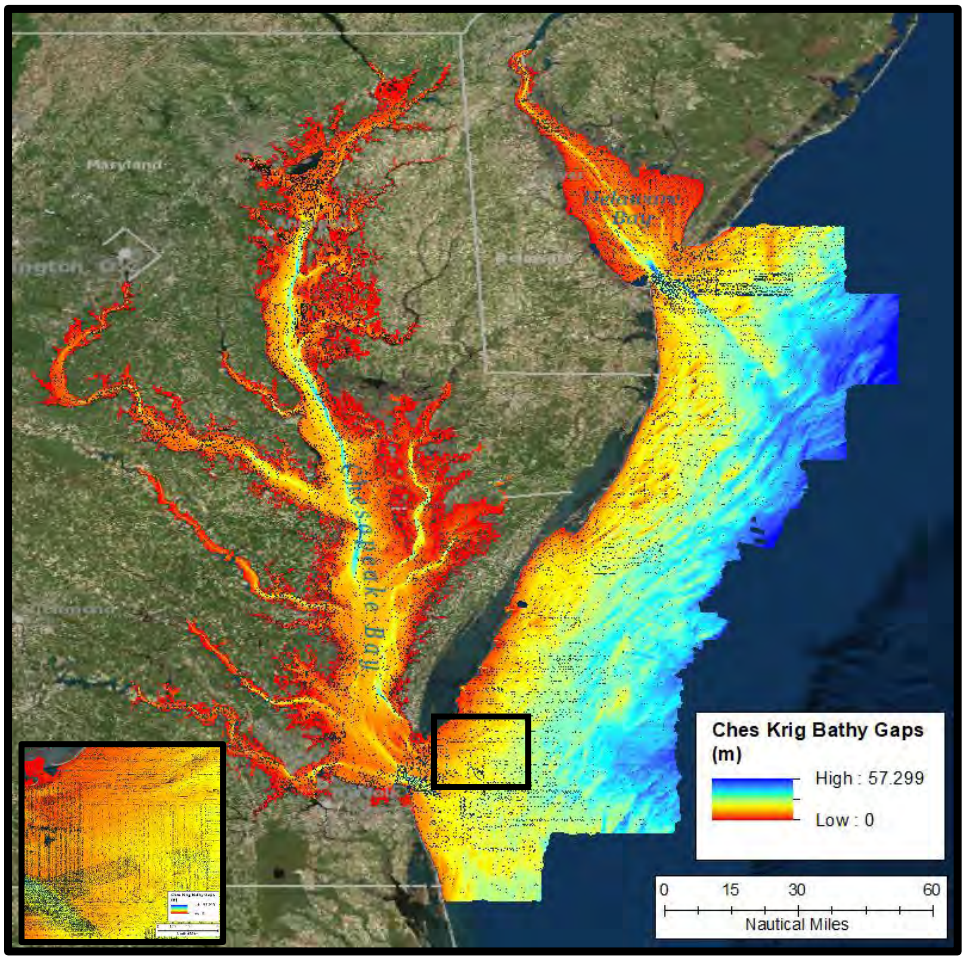

Figure 5: Bottom-layer gap bathymetry – areas between actual data points. A close-up near the mouth of Chesapeake Bay is outlined in the black box and shown in the bottom left to highlight the preservation of survey track lines.

2.3.2 AIS Analysis

To achieve constraint for uncertainties between bathymetric data, these gap areas must first be isolated from where true data exists. Thus, the bathymetric point datasets (XYZ) for each group were converted into 30 m cell-size raster grids populated with the recorded depth of each point. Due to sparseness of these archive bathymetric data, a 30 m grid resolution maintained the true point nature of the data and avoided the appearance of complete coverage which would be inherent with larger cell sizes. The ArcGIS 'Aggregate Point' tool was used to delineate coverage (or outline) polygons for each area, with a radial search distance of 1.5 nautical miles. Each outline polygon was attributed with an arbitrary value of '-999' that was then used to populate an overview raster grid of each area at a resolution of ~25 m using the 'Polygon to Raster' tool.

Both bathymetric and overview grids were mosaicked together using the ArcGIS 'Mosaic to New Raster' tool, with priority cell population going to the bathymetry. This process attributes the gaps between soundings with the arbitrary value of -999, making them easier to identify. Using the ArcGIS 'Extract by Attributes' tool, the gaps were extracted into separate rasters and mosaicked together for the entire study area. A bathymetry raster of only interpolated depths was produced by using the 'Extract by Mask' tool to the bathymetric values from the kriging interpolation (discussed in the previous section) (Figure 5).

Publicly available AIS tracklines for 2011 and 2013 were then downloaded from Marine Cadastre[1], brought into ESRI ArcGIS as shapefiles, and clipped to the study area. The attribute table for each year was exported as an Excel table and brought into MATLAB 2017b 9.3.0. It is

[1] Marine Cadastre website: http://marinecadastre.org

commonly understood that the AIS data has inherent errors due to uncontrolled user input fields. More specifically, the errors pertinent to this project result from incorrect units where the required units are meters but are commonly recorded in feet. These unit errors are scattered throughout the data and are easily identified when large values are recorded (~25 m) but can be hard to identify when they fall within a normal range (< 3 m vs. < 3 ft).

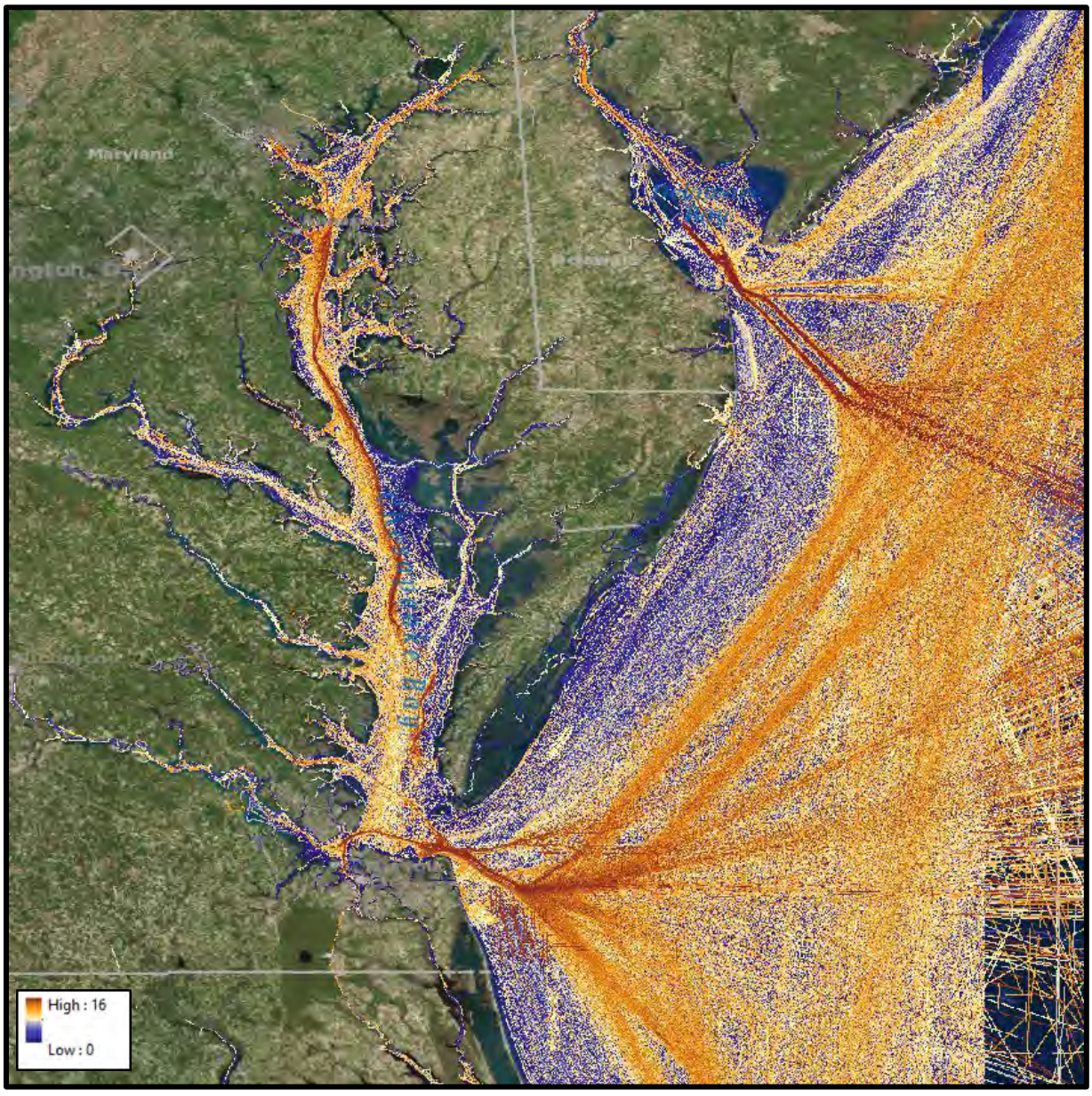

Figure 6: Combined raster surface of MATLAB edited AIS draft values from 2011 and 2013. The raster cell assignment was based on deepest draft values.

For this reason, we normalized these data, limiting these errors, by filtering the recorded draft values through a MATLAB script (Appendix B) that compared AIS recorded vessel type and corresponding draft depths with a list of maximum allowable drafts (Appendix B). If a maximum allowable draft was not identified for any vessel type, the maximum depth of the study area (16 m) was used instead (described further in Appendix B). Any draft values that exceeded the maximum allowable draft for a given vessel type were assumed to be recorded in feet instead of meters, and appropriately converted. Draft values less than or equal to the maximum allowable were not altered through this process and assumed to be reasonable.

After the drafts for both years were normalized and edited, they were combined and imported back into ArcGIS to populate a 20 m raster grid based on the deepest recorded drafts (Figure 6). To identify the areas where uncertainty can be constrained, we need to establish how the AIS drafts compare with the sea floor. These values can then be directly compared with the uncertainty values already established (Figure 4) and areas susceptible to constraint can be identified. These steps are depicted in Figure 7.

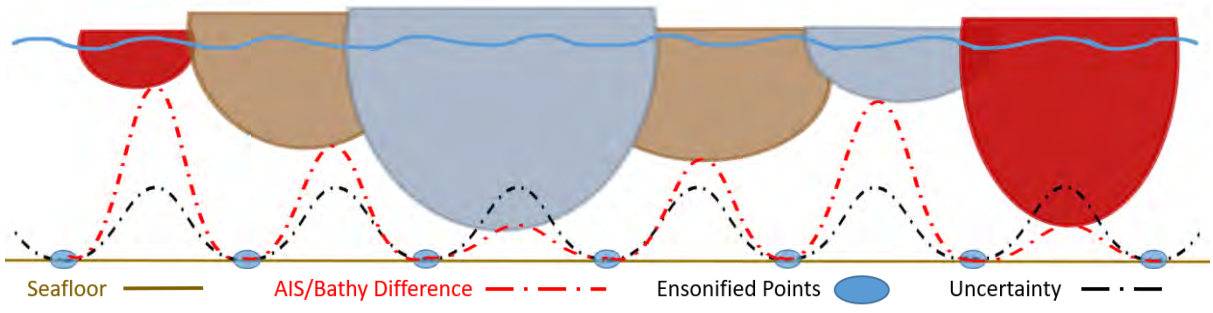

Figure 7: Draft comparison with bathymetry results in a curve (red) that can be compare with the uncertainty curve (black) and ultimately identifies the areas where the uncertainty curve can be constrained by AIS drafts.

As such, the combined AIS draft surface was compared with the bathymetric gap raster to determine the distance between the draft and seafloor. However, negative values indicated recorded drafts that exceeded the bathymetry and were removed from the study due to ambiguity outlined in the discussion section (Figure 8). The remaining values were then compared to the uncertainty raster to identify areas that could be constrained. The resulting values identified areas that could be constrained by AIS drafts and were differenced with the uncertainty to produce an updated uncertainty estimate. Finally, the updated uncertainty values and the original uncertainty were mosaicked together with the updated values having priority (Figure 9). In short, the measure of the draft of a boat passing over a given area constrains the uncertainty providing higher certainty of a minimum depth (Figure 7).

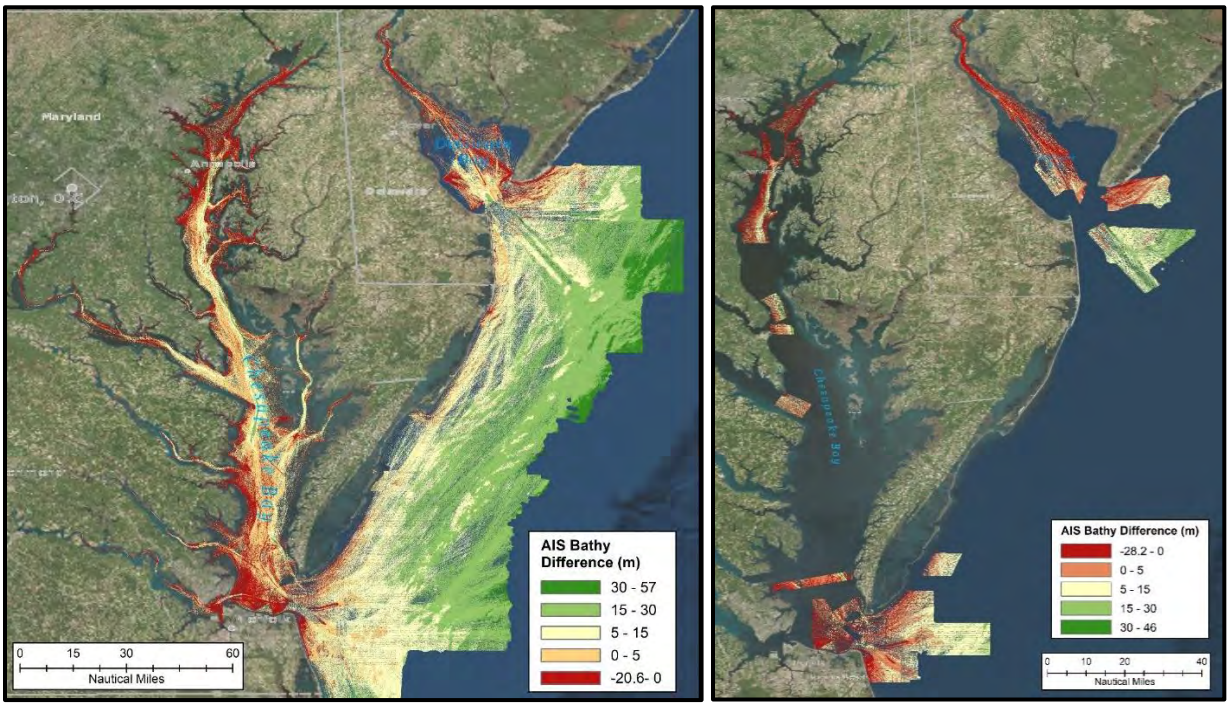

Figure 8: Bottom-layer (left) and mid-layer (right) AIS draft/bathy comparison. Negative vales are red and signify that the AIS drafts exceed estimated bathymetry and were removed.

This process was repeated for the mid-layer surveys. Since this AIS analysis and uncertainty constraint procedure serves to better estimate gaps in bathymetric coverage of the seafloor, the upper layer surveys (BAG) were excluded as they are essentially point data with known bathymetry and uncertainty. As such, the upper layer survey uncertainties were mosaicked together with the most recent survey taking priority. A final uncertainty layer was produced from all updated uncertainty layers by mosaicking them together – with priority (or supersession) increasing from the bottom, middle, and top layers (Figure 10). This order was chosen as it is theoretically how data is prioritized on the chart. The result is in an updated uncertainty picture of charted data within the study area.

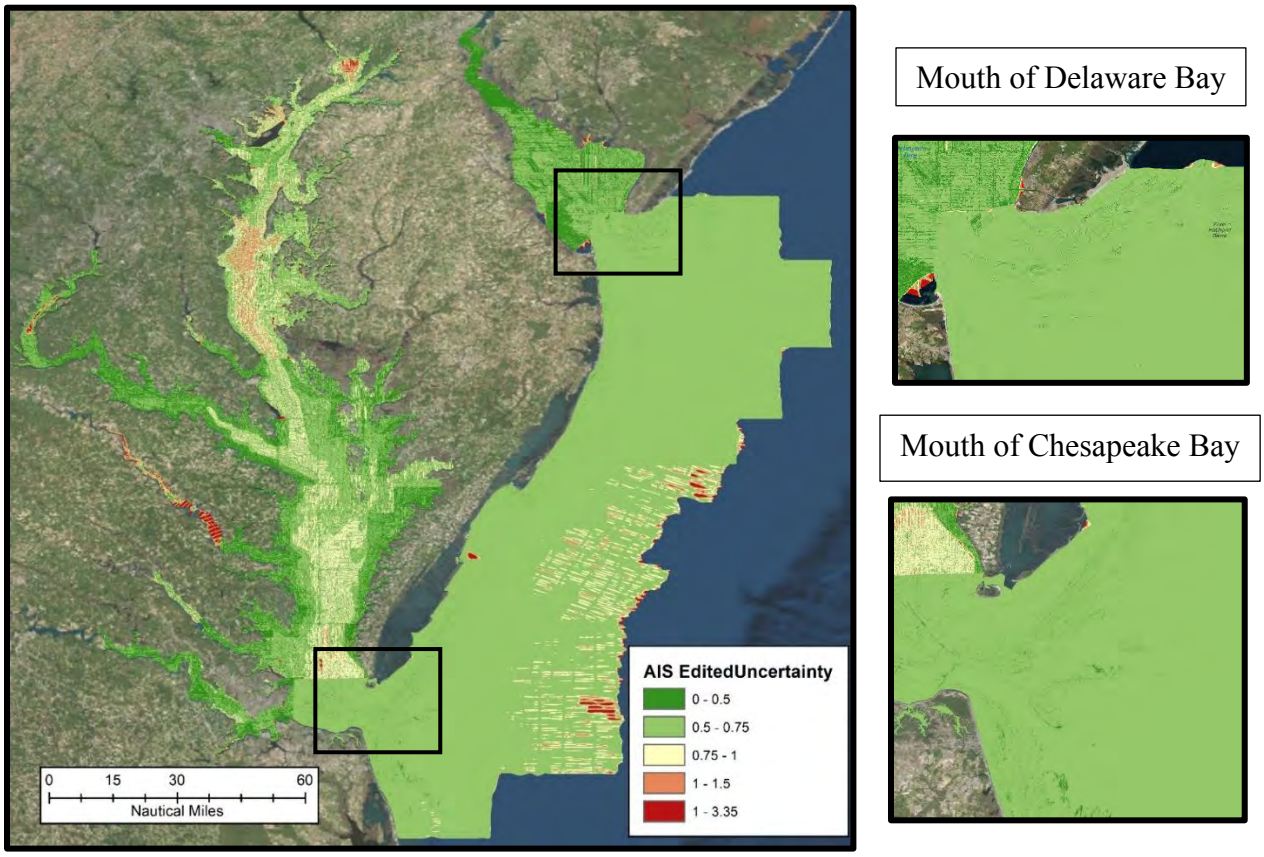

Figure 9: AIS updated lower-layer uncertainties (left). Close ups of the Chesapeake Bay and Delaware Bay mouths shown on the right.

2.4 RESULTS

2.4.1 Kriging Interpolation

An estimate of uncertainty for the entire study area was achieved through kriging. As mentioned previously, the lowest layer data were broken into groups to increase processing speed and interpolation accuracy. Different parameters were used for each group to match the variability within each dataset, and ultimately to create a complete bathymetric surface. Through the interpolation process, the true data point values are not necessarily maintained as data density and output cell size can influence the final result (Oliver and Webster, 2014). For example, a cluster of five points within a 20 m x 20 m area, and a designated output cell size of 20 m results in only one value that will populate the single cell that covers those points.

A point-to-point comparison was performed to determine how much change occurred to the true data points. Using the 'Extract Multi Values to Points' tool in ArcGIS, the depth value generated from kriging was extracted at the location of the measured data points and added to their attribute table. Both the true depth and interpolated depth were plotted, a trend established, and standard deviation was calculated (Table 3). The largest changes to true depth values occurred in the Upper Chesapeake Bay and Offshore regions, with the lowest differences found in the Mid-Layer data and Delaware Bay. It's possible these differences could result from spatial biases in the kriging calculation which could be rectified through universal kriging (that uses a variable mean) as opposed to ordinary kriging (that uses a stationary mean). This is discussed further in the discussion.

Group	Trend Equation	Standard Deviation	# of Points	Survey Year Range
B. Upper	y=0.9980x+0.0610	0.5746 m	945,966	1897-2002
B. Central	y=0.9948x+0.0244	0.4150 m	1,498,972	1860-1974
B. Lower	y=0.9921x+0.0527	0.5078 m	391,519	1886-1980
B. Offshore	y=0.9917x+0.1567	0.5864 m	1,234,166	1934-1999
B. Delaware	y=0.9949x+0.0276	0.3246 m	256,761	1971-2002
B. Mouth	y=0.9876x+0.1334	0.5079 m	276,826	1886-1990
M. D00052	y=0.9987x+0.0143	0.1093 m	3,149	1985
M. H10193	y=0.9887x+0.1567	0.4311 m	10,341	1986
M. H10934	y=0.9901x+0.1239	0.1325 m	27,899	2000
M. H11088	y=0.9967x+0.0480	0.2581 m	42,718	2004
M. H12559	y=0.9961x+0.0355	0.1943 m	18,775	2013
M. Lower	y=0.9937x+0.0764	0.3102 m	718,462	1965-2013
M. Upper	y=0.9935x+0.0726	0.3389 m	770,427	1965-2013
M. Delaware	y=0.9967x+0.0498	0.3313 m	222,031	1965-2013

Table 3: Kriging point to point validation results for each group of the bottom and middle layers. Variance and standard deviation was calculated for the differences between the measured and kriged depths.

2.4.2 AIS Filtering

The first stage of filtering ignored 22% of drafts for each AIS year (2011 and 2013) as draft data had simply not been entered. The MATLAB code (Appendix B) edited 7.3% of the 2011 drafts, with the majority coming from the tug boats vessel class (Figure 11). Similarly, 12.7% of the 2013 drafts were edited and a majority contribution coming from tug and pilot vessel classes (Figure 12). Further, a combined 10% of the publicly available AIS draft data were edited using the maximum draft by vessel category approach.

The second stage of filtering was performed by differencing the combined edited drafts with gap bathymetry. For the lower layer, 12% of the drafts exceeded estimated bathymetry and were removed. For the mid-layer, 24% of the drafts exceeded the bathymetry. The removed AIS data for both layers was primarily isolated to nearshore areas and within current designated navigation channels. Both regions could be explained by physical changes to the seafloor that

occurred in the time between each survey and AIS data collection and is explored further in the discussion section.

2.4.3 Final AIS-constrained Uncertainty

Two percent of the lowest layer uncertainties were constrained by AIS drafts. The surface overall has an average uncertainty of 0.6 m and a standard deviation of 0.17m. Over 85% of the lowest layer has an uncertainty over 0.5 m, but only ~4% of that area is greater than 50% of the water depth indicating that most of the larger uncertainties are confined to deeper areas. This is not unexpected as deeper areas with less navigational influence tend to have sparser datasets and larger uncertainties. However, the ~4% that is greater than 50% of the water depth is confined to nearshore regions where depth measurements are more difficult to obtain (Figure 13).

Three percent of the mid-layer uncertainties were constrained using AIS drafts. The average uncertainty for the mid-layer is 0.34 m with a standard deviation of 0.18 m. Only 3% of the mid-layer had uncertainties over 0.5 m, although these areas were not confined to the nearshore areas. The majority of the large uncertainties are isolated to two surveys with minimal survey coverage: D00052 (1985) and H10193 (1986).

A total of 2% of the combined study area uncertainty was updated through the AIS draft analysis, and a complete chronological estimate of uncertainty was achieved for Chesapeake Bay and surrounding areas. In comparison, current CATZOC methodologies would use kriged bathymetry and the IHO uncertainty variables for each 95% confidence interval per CATZOC level (Table 1) to calculate vertical uncertainty. A direct comparison between the CATZOC output and the uncertainties calculated here show that 96% of our uncertainties are smaller than

CATZOC (Figure 14). Additionally, the larger uncertainties come from two main sources: modern multibeam surveys and an edging effect resulting from resolution differences between the two models. As coarser grids populate large geospatial areas with single values, finer grids allow for more variability to be captured and comparing the two can result in large differences particularly on the outer edges of each grid.

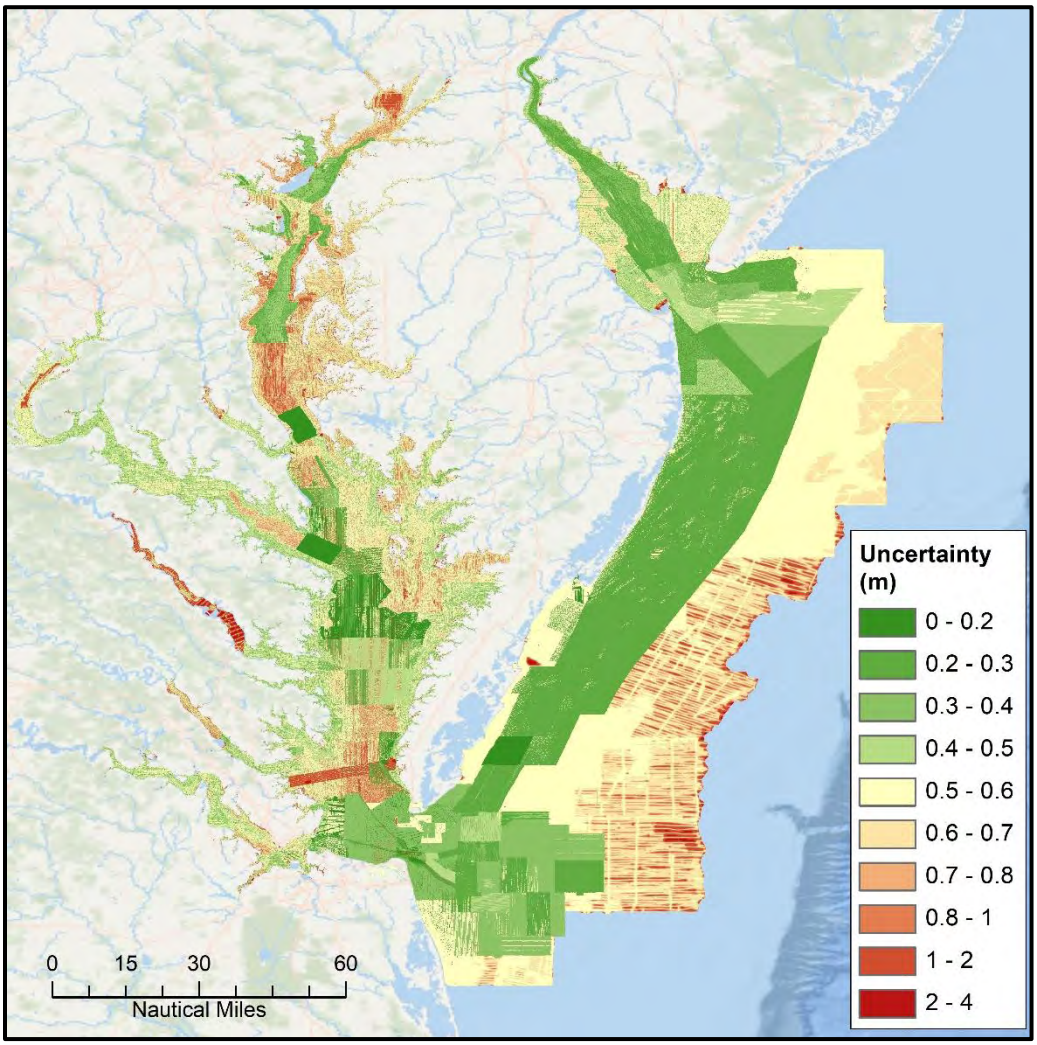

Figure 10: Final merged uncertainty surface with AIS constraints. Temporally prioritized cell assignments – the newest surveys having priority over archive surveys.

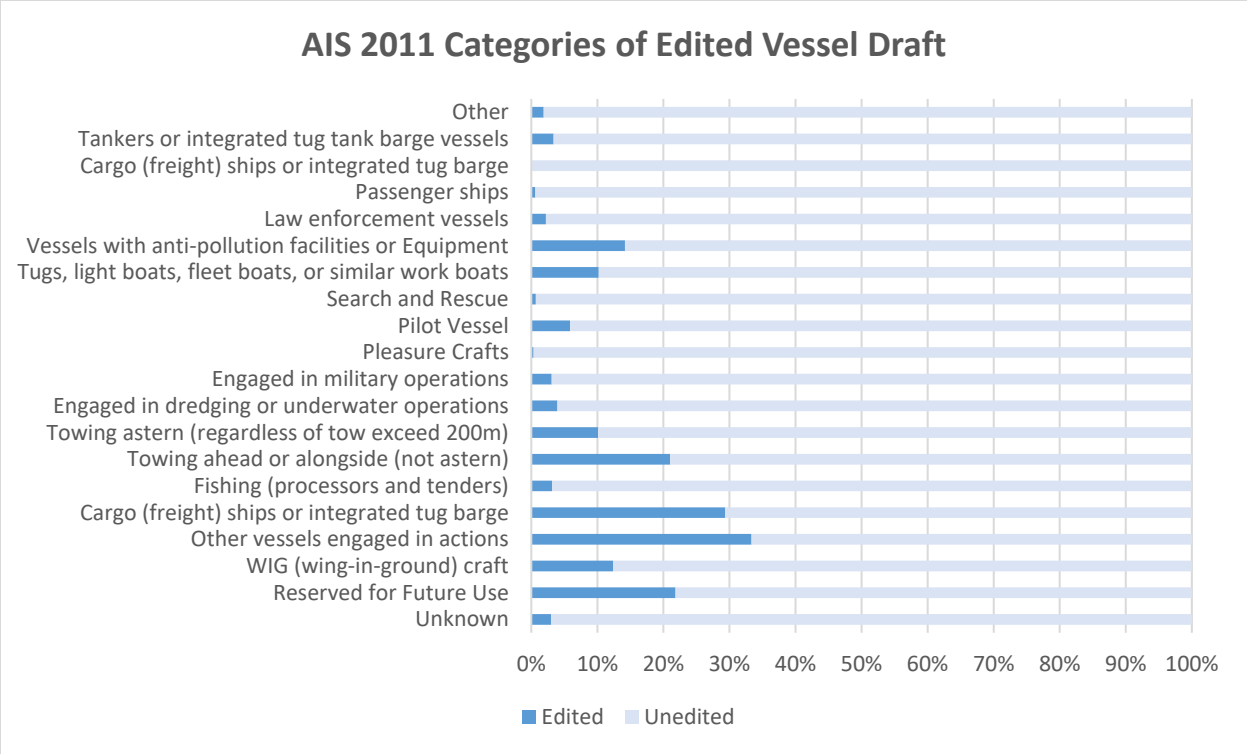

Figure 11: 2011 AIS composition of MATLAB edited drafts.

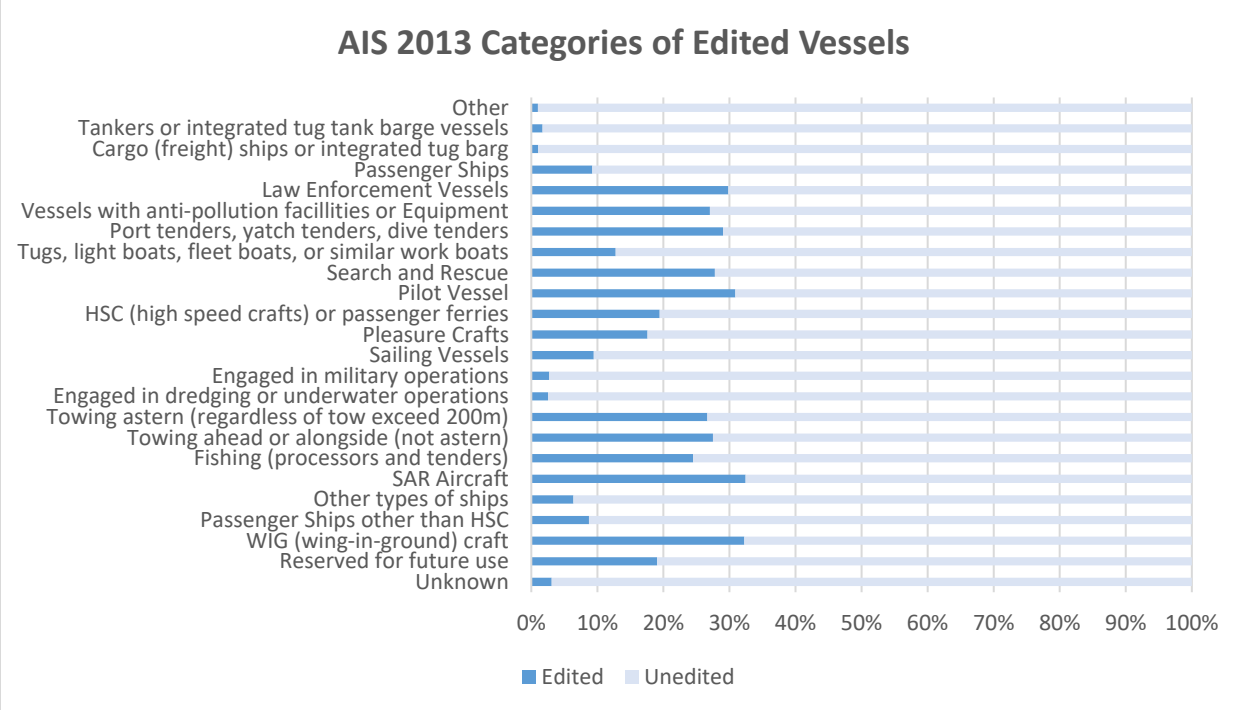

Figure 12: 2013 AIS composition of MATLAB edited drafts.

2.5 DISCUSSION

2.5.1 Kriging Interpolation

Previous attempts to analyze archived hydrographic surveys have focused on their comparison with modern coverages (Calder, 2006; Wong *et al*., 2007; Dorst, 2009). Calder (2006) found the ambiguity from spatial aliasing hard to capture through kriging, even after accounting for inaccuracies with historic hydrographic techniques. However, considering the Wizard-decided optimum lag size equated to > 250 m, the vast amount of archived data utilized in this study allows coverage gaps from one survey to be covered by another, capturing smaller-scale spatial fluctuations during interpolation and permitting a lag ~35 m. This is particularly true for the lowest layer bathymetry and uncertainty estimates where the inclusion of hundreds of surveys results in significant survey overlap.

On the other hand, some surveys had to be individually kriged in the mid-layer as they were not near other surveys. For these surveys, the uncertainties produced have higher probabilities of suffering the same issues outlined by Calder (2006), particularly H10193 and D00052. Both of these surveys were collected in less than 45 m of water with over 100 m between survey lines. While they may have included feature investigations, they were flagged with extreme uncertainty values due to the lack of coverage and large spacings.

It should also be noted that each kriging group exhibits high spatial variability in part due to their size, but also the kriging method choice. Ordinary kriging was chosen for this study as it is designed to work well in most situations (Oliver and Webster, 2014), but with a trend, more accurate results could be achieved through universal kriging.

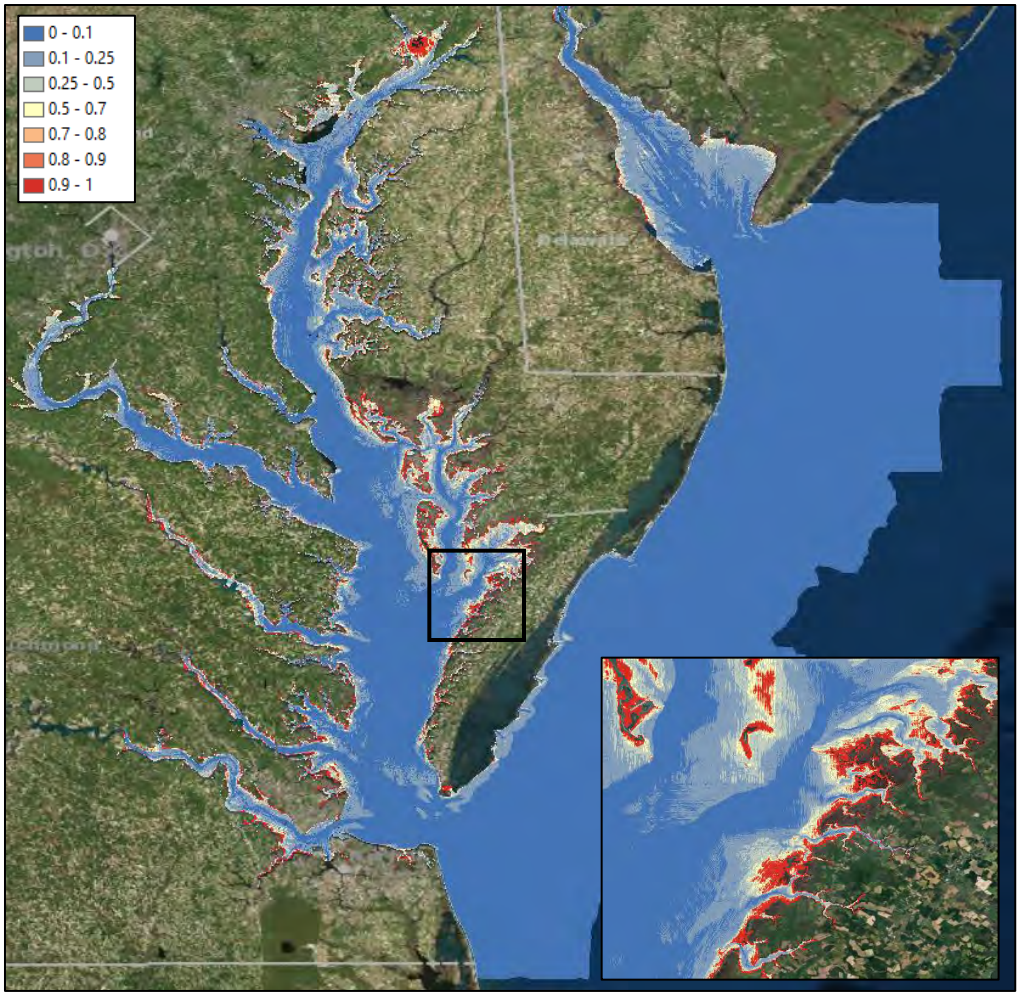

Figure 13: Lower-layer uncertainties as percent water depth. Larger uncertainties (in red) are constrained to nearshore environments.

2.5.2 AIS Filtering

AIS drafts are required by the U.S. Coast Guard to be input in meters, yet U.S. customary units are in feet. Thus, it is not surprising that AIS datasets contain errors. The MATLAB draft editing discussed in the Methods section of this chapter (and outlined in Appendix B) set the absolute maximum allowable vessel draft to be 16 m (~52.4 ft) to be close to the maximum maintained channel depth of 52 ft. This method could introduce skewing as the chart datum is MLLW and not mean sea level (MSL). Additionally, this does not account for tides that allow larger vessels to successfully pass than would otherwise be possible at higher tides. While the tides are only

maximum 1 m above MLLW and 0.5 m above MSL at the Chesapeake Bay Channel, this is still enough to change the output uncertainty raster. The method outlined in this chapter would ultimately produce more conservative uncertainty estimates by accounting for tides and datums. However, allowing for an increased maximum draft more reflective of true maximum vessel drafts would likely increase the amount of ambiguous data found in the differencing of AIS drafts and the bathymetry.

Additionally, AIS vessel tracking was not mandatory in the U.S. until 2009. Since then, only a few years have been made public, and of those, only two include vessel tracklines (2011 and 2013). Therefore, the differencing of AIS drafts and early bathymetry (described previously) use data that are from two different time periods separated by an average of 50 years. The resulting areas that show AIS drafts exceeding the interpolated bathymetry could result from other sources. First, the AIS draft could still have been recorded using standard U.S. units of feet instead of the required input of meters despite the MATLAB filtering outlined previously. Second, the seafloor could have been dredged allowing for deeper draft vessels to move where they formerly could not (and vice versa). Finally, the bathymetry could have been recorded incorrectly as the available technology at the time was conducive to larger geospatial errors than modern systems. However, distinguishing the true cause of the 'error' was impractical, and thus these data were ignored.

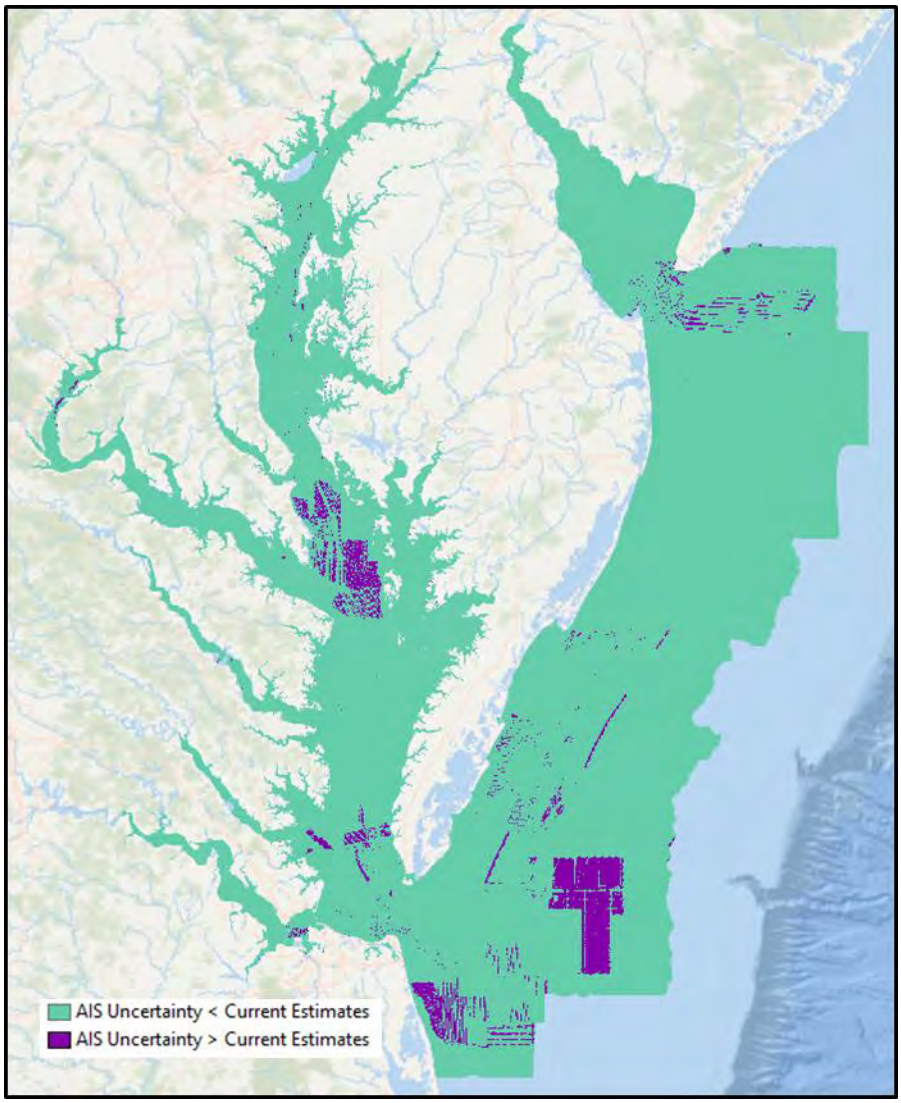

Figure 14: In comparison with current methods: 96% of the uncertainties calculated in this study have smaller uncertainties (in teal) than achievable through CATZOC estimates. Larger uncertainties (in purple) result primarily from edging effects and modern surveys.

2.5.3 Final AIS-Constrained Uncertainty

Final uncertainty grids were mosaicked together sequentially with more recent BAG survey uncertainties superseding kriged uncertainties of archived surveys. This order was chosen to approximate the charted data order; although there are arguments to be made for both a minimum or maximum value cell assignment as realistic chart order is more complex than simply age. In particular, a minimum value supersession approach could more closely capture

the charted order. However, the uncertainty values identified in this study are almost entirely less than those identified through standard CATZOC estimations, indicating that our minimum value might not be the same as the CATZOC minimum used for charting. Alternatively, using a maximum value approach would show the worst-case scenario for a given region, which is also how charts are compiled. This does not mean that the worst bathymetric data is used, but instead that the higher uncertainties are included in the charting process to provide the mariner the most conservative estimates. Nonetheless, temporal supersession accounts for technological and procedural advancements and were deemed the most appropriate choice.

2.6 CONCLUSIONS

A methodology that produces a complete coverage uncertainty estimate for the entire study area was calculated through kriging. Of these uncertainties, 2% were successfully constrained using publicly available AIS drafts from 2011 and 2013, totaling ~420 km^2. While 2% improvement in confidence constraints might seem fairly minor, the maximum annual coverage area for the NOAA fleet is less than 0.1% of US waters, a small fraction of what this analysis has produced. Further, this analysis is a proof of concept. Gaining access to more accurate AIS data through the Coast Guard or private crowdsourcing companies could also increase the final percentage of constrained uncertainties. Ninety-six percent of the uncertainties presented here are smaller than those obtained from current authoritative uncertainty calculations. The few larger uncertainties result primarily from an edging effect and more modern datasets, implying an over-estimation of archive surveys and an under-estimation of modern surveys. Future work should focus on including additional years and sources of AIS data and accounting for tides.

CHAPTER 3

ESTIMATING SEDIMENTATION RATES NEAR CHESAPEAKE BAY AND DELMARVA PENINSULA AND THE ASSOCIATED IMPLICATIONS FOR SURVEY PRIORITIES

3.1 SUMMARY

There is no standard methodology for assessing the validity of survey data and charted information as they age. NOAA's current approach uses the Hydrographic Health Model (HHM) which is a risk-based methodology aimed at determining hydrographic survey priorities. The HHM incorporates a number of crucially important maritime variables including heuristic changeability terms (based on the seabed sedimentary material), history and frequency of large storms, tidal currents, and anthropogenic obstructions. We propose an enhanced approach that supports quantifiable estimates of chart health by modeling the sedimentation and erosion rates determined by successive bathymetric surveys, sediment cores, and numerical algorithms. This model can more accurately identify rapidly degrading regions that exceed acceptable IHO standard variability. The proposed enhancements are evaluated in the Chesapeake Bay and Delmarva Peninsula where frequent hydrographic surveys are required to monitor significant sediment transport in heavily trafficked regions. This work creates a link between hydrodynamic models and hydrographic survey priorities more objectively prioritizing current and future survey needs and investments.

3.2 INTRODUCTION

Survey prioritization is fundamental to nautical chart maintenance and fiscal management by identifying which coastal U.S. areas are more "at risk" and in need of modern coverage than others. This decision making has primarily been based on knowledge of groundings, wrecks, current coverage and survey age, stakeholder requests, and boat scheduling with significant

weight put on the presence or absence of modern survey coverage. With less than 0.1% of new survey coverage collected annually, the possibility for out-of-date chart soundings as a result of physical changes to the seabed between repeat surveys along the coastal U.S. could be quite high in dynamic coastal areas. This implies that survey quality will decay more rapidly with time as a result of prolonged exposure to ocean waves and currents.

Determining how a survey depreciates over time is a complex problem with no uniformly applicable procedure. Presently, the National Oceanographic and Atmospheric Administration (NOAA) does not have a standard way to account for survey depreciation over time. The task of prioritization is entrusted to their experienced hydrographers.

Due to the importance in safety and commerce, building consensus on the best methodology has become a focus of much research in recent years. Hydrographic agencies across the globe have begun investigating automated prioritization methods as a more accurate avenue for identifying charted areas subject to significant change. The Canadian Hydrographic Service (CHS) initially designed a GIS-based model by Grenier and Hally (1991) that weights 19 variables based on hydrographic and cartographic needs. Their current model, the CHS Priority Planning Tool (CPPT), combines a GIS and matrix approach to identify charts that need updates (Chenier *et al*., 2018). Dorst (2009) looked into time series analysis of bathymetric data in the Southern North Sea around the Netherlands as a method to determine survey priorities for the Royal Netherlands Navy. Calder (2015) created a risk-based approach to mitigating uncertainty in transit on an individual ship basis. Additional statistical methodologies have been applied to assess survey priorities (Calder, 2016). Other approaches have been attempted within the U.S., including NOAA's current model called the Hydrographic Health Model (HHM), the offspring of an Alaska chart assessment outlined in Gonsalves *et al*. (2015).

The HHM is a risk-based analysis implemented in ESRI ArcGIS that determines the current state (or the "health") of charted data to identify survey priorities at a 500 m resolution. The HHM is based on a simple formula

$$HHM = H_{gap} \sum R \quad (1)$$

that multiplies the estimated hydrographic risk, $\sum R$, by the hydrographic gap term of a specific area, H_{gap}, resulting in a health rating from less than 0 to 100, with the healthiest (or most recent surveys) scoring near or below 0 (Figure 1). The hydrographic risk is a mathematical weighting function that rates consequences and likelihoods on a scale of 1-5 with 5 presenting the most risk (Keown *et al*., 2016; Fandel *et al*., 2017; Hicks *et al*. 2017). The hydrographic gap of currently charted data is determined by

$$H_{gap} = DSS - PSS \quad (2)$$

the difference between the estimated present survey score (PSS) and the user-defined desired survey score (DSS).

The PSS and DSS terms are populated with values (0-110) that closely correspond to CATZOC level coverage specifications (IHO S-57, 2014; Keown *et al*., 2016; Fandel *et al*., 2017; Hicks *et al*. 2017) and depreciate by an exponential decay of the survey's current score, ζ, based empirically on the age of the survey, *T*, and several empirical changeability terms, C, such that

$$PSS = \zeta e^{-CT} \quad (3)$$

While the PSS changeability terms incorporate heuristic estimates of change specifically through the parameter *C* that includes the number of large storms, tidal currents, marine debris, and an empirical factor (Keown *et al*., 2016; Fandel *et al*., 2017), these variables do not always result in

physical change. Similarly, the absence of these changeability variables does not equate to a stable environment. This is also true for the calculation of the entire HHM including the $\sum R$ as the risk is subjectively established. To truly estimate hydrographic health, both components should be quantitatively calculated. However, here we focus on the imperative need to establish a quantitative and area-specific approach for change estimates to achieve a robust assessment of chart adequacy. Additionally, local hydrodynamic variables drive sediment transport patterns and their inclusion could markedly improve the accuracy of predicted chart health estimates. However, a direct application of these estimates into the current iteration of the HHM is not presently possible. In the present work, an alternative methodology for estimating the hydrographic gap (Hgap) is presented.

Risks due to charted depth inaccuracy can be characterized by quantification of uncertainty using annually observed average rates of change (Taylor, 1982). Thus, the modified gap equation proposed herein uses the difference between estimated Present Survey Uncertainty (PSU) and Maximum Allowable Uncertainty (MAU) terms,

$$\tau_{HUG} = \left(\sigma_{present} - \sigma_{max}\right) \tag{4}$$

where $\sigma_{present}$ is the PSU and the σ_{max} is the MAU which would take the place of the PSS and DSS respectively in (2) and Hgap in (1). Here, the PSU incorporates temporal variability and average rates of change through

$$\sigma_{present} = (\Delta T \frac{\Delta z}{\Delta t}) + \sigma_{initial} \tag{5}$$

where $\sigma_{initial}$ is the initial survey uncertainty (ISU) values, ΔT is the change in time, and $\Delta z/\Delta t$ is the temporal variability component. The proposed modification to the HHM hydrographic gap

term is henceforth referred to as the Hydrographic Uncertainty Gap (HUG). HUG is implemented in ESRI ArcGIS 10.5.1.

Quantifying the total vertical uncertainty (TVU) is a common NOAA practice for each hydrographic survey and is referenced in chart compilation by assigning a CATZOC level. Unfortunately, these levels are inherently attributed to an entire survey area even if complete coverage was not achieved. As discussed previously, the uncertainty of the entire survey area must be quantified to truly estimate what the current and future states of hydrographic chart data are or will be. Thus, the Initial Survey Uncertainty (ISU, $\sigma_{initial}$) component of the proposed PSU term will use the process outlined in Chapter 2.

The other key component of the PSU is the quantification of temporal variability; that is, the rate of change of seabed elevations. In this assessment, we discuss two methods to account for temporal variability. The first is by using sedimentation rates which can be determined from a literature review, bathymetric differencing of two surveys separated in time, and/or observations from sediment cores. The second method is based on numerical sediment transport models.

The temporal variability ($\Delta z/\Delta t$) output in (5) is multiplied by a time component (ΔT) that corresponds to the survey age but can also be used to represent future changes. Understanding how a given area will change in the future allows for more comprehensive resource allocation, updates to disaster response requirements, and better understanding of climate change scenarios. It is important to note that the various temporal variability estimates are not required to be used together to establish the overall temporal variability of a given location. Instead, through this assessment, we expect to show how to utilize publicly-available data to better estimate bathymetric change, and to further outline how numerical modeling could be useful.

The MAU (σ_{max}) is a user-defined variable derived purely from the calculated uncertainty from a desired CATZOC level using the IHO uncertainty equation

$$MAU = \sqrt{(a^2) + (bd)^2} \quad (6)$$

where 'a' and 'b' are IHO S-44 order-dependent variables (IHO S-44, 2008) and 'd' is depth (in meters). Differencing the PSU and MAU estimates the hydrographic uncertainty gap (HUG) of a given charted region, and dividing by the water depth (d) can give these results in terms of the fraction of water depth. Positive results from this calculation indicate the uncertainty exceeds allowable limits, while negative results indicate the area is within the desired uncertainty limit.

One area of known variability is offshore Virginia near the mouth of Chesapeake Bay (Figure 15). This area has experienced near-constant dredging over the last thirty years and demands frequent hydrographic surveys, indicating sediment is being transported and reformulated in this region on a large scale. For this study, the HHM Hydrographic gap (H_{gap}) component is reworked (τ_{HUG}, (4)) to better incorporate local sedimentation rates (5) in order to more accurately assess the current state of charted data and determine the changes expected under a variety of conditions. Through this work, we hope to provide an example of how this concept can be applied to a specific area, suggesting a new standard for future application to additional U.S. coastal areas.

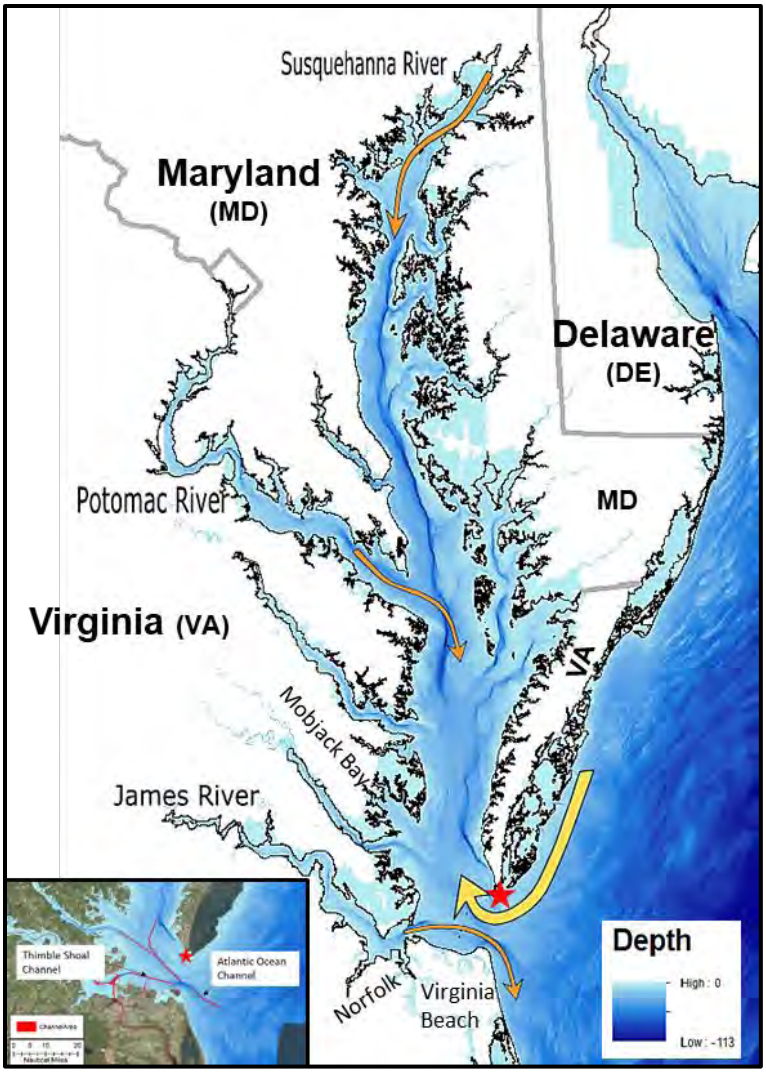

Chesapeake Bay Dredge History	
Atlantic Ocean Channel	
Year	Maintainted to
2017	52 ft (~16m)
2014	52 ft (~16m)
2012	52 ft (~16m)
2010	52 ft (~16m)
Thimble Shoal Channel	
Year	Maintainted to
Apr-17	50 ft (~15m)
Oct-16	50 ft (~15m)
Apr-16	50 ft (~15m)
Jun-14	50 ft (~15m)
Apr-13	50 ft (~15m)
York Spit Channel	
Year	Maintainted to
Aug-15	50 ft (~15m)
Cape Henry Channel	
Year	Maintainted to
Mar-15	50 ft (~15m)

Figure 15: (Left) Bathymetric map of Chesapeake Bay and nearby offshore regions. The arrows denote sediment transport pathways identified from previous studies. Orange are riverine and yellow is shelf sediments. The red star is Fisherman's Island. (Bottom Left) Subset of Chesapeake Bay mouth with navigational channels designated in red and Fisherman's Island designated with a red star. (Right) USACE Chesapeake Bay navigational channel dredge history.

3.3 GEOLOGIC BACKGROUND

Chesapeake Bay is the largest estuary in North America and connects the Atlantic Ocean to a number of major rivers including the Potomac, the James, and the Susquehanna Rivers. As there are major cities and ports lining Chesapeake Bay's borders, this region has been heavily trafficked by large vessels since early European settlements (Brush, 1984). Studies of sediment cores throughout the bay have identified a clear correlation between increased sedimentation

rates and post settlement anthropogenic influence on the land (Brush *et al*., 1984; Donoghue, 1990). Cores have also shown that sedimentation rates are not uniform throughout the bay with nearly 80% of sediment coming from the Susquehanna, Potomac, and James rivers (Donoghue, 1990; Valle-Levinson *et al*., 2001). Hobbs *et al*. (1992) reported that the Chesapeake is filling at both ends by both sediments discharged by the rivers and sediments coming through the inlet from the inner continental shelf and adjacent beaches.

As the cities along the Chesapeake Bay have grown, so too have the demands of the population and the ships that cater to their needs. Multiple deep-draft shipping channels have subsequently been created and maintained by the U.S. Army Corps of Engineers (USACE) in both the Maryland and Virginia areas of the bay to allow for such activities. These channels are said to be maintained to the deep-draft limit of 42 ft (12.8 m) according to current NOAA Charts, although various USACE reports indicate the channels are maintained to a minimum of 52 ft (16 m) with a request to deepen to 59 ft (18 m; USACE Norfolk Report and Environmental Assessment, 2017). Regardless of the specific deepest depth, maintaining the channel to an appropriate depth has proved to be a challenge. Bi-annual dredging has been performed on a majority of the lower Chesapeake Bay channels since their creation (Figure 15- Right), indicating significant sediment movement in a short time period.

Numerous sand wave fields identified in the Chesapeake Bay provide further evidence of substantial sediment transport. Perillo *et al*. (1984) found that the sand waves in the middle of the Chesapeake are relics from previous energetic events. Additional studies on turbulence and resuspended sediments found that wind-driven currents can have a significant effect on the ability to resuspend sediments in the shallower regions of the upper and middle bay (Ward *et al*., 1985; Sanford *et al*.; 1991; Sanford *et al*., 1993; Sanford *et al*., 1994) while tidal currents have a

lesser effect on these sediments. Conversely, the lower bay (between the mouth of the bay and Mobjack Bay) is significantly influenced by tidal fluctuations and currents (Perillo *et al*., 1984; Colman *et al*., 1988). Studies on the lower bay sand waves found that the sand waves are active and move as cohesive units (Colman *et al*., 1988). The dichotomy of primary sediment forcing between the upper (inland) and lower (near inlet) bay areas implies the likely sediment sources infilling the navigational channels.

Identifying these sediment sources and their transport patterns could prove useful for the accuracy of nautical charts for this region and, ultimately, the maintenance of the bay channels. Skrabal *et al*. (1991) used sediment cores to determine that Thimble Shoal Channel is primarily infilling from the James River discharge sediments rather than shelf sediments owing to a lack of illite (an indicator of shelf sediments) in the channel sediments shown in Figure 15 (Left). Conversely, the north side of the bay mouth was found to be fed by shelf sediments that extend into the bay along the eastern boundary and are driven by a strong longshore current from the Delmarva Peninsula (Colman *et al*., 1988). The proximity of the Cape Henry Channel to the active sand wedge off Fisherman's Island would imply Delmarva coastal sediments are the source of its infill. Additionally, Ludwick (1978) found a northward propagating sand stream in the coastal region off Virginia Beach with occasional reversals southward as a result of storms. The infilling observed at the Atlantic Ocean Channel could be a result of this sand transport pattern and ultimately determined by longshore currents in the nearshore.

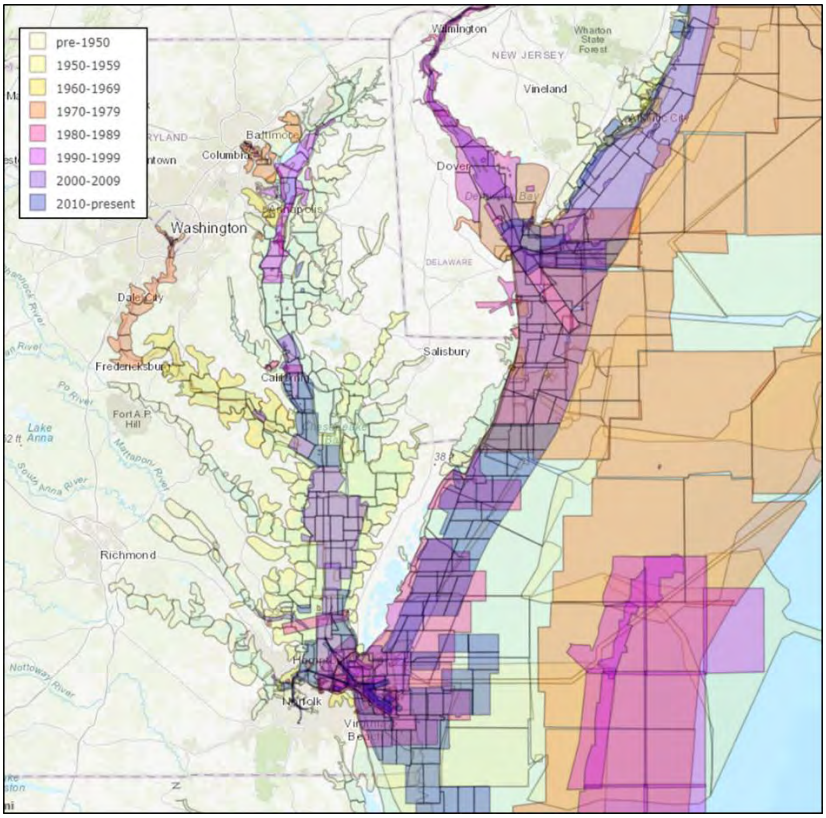

Figure 16: Areal coverage of NOAA hydrographic surveys for Chesapeake Bay and offshore Delmarva Peninsula colored by survey year.

The results of these studies indicate a coastal sediment influence on the far north side of the bay mouth and a riverine/terrestrial influence on the southern side of the bay mouth. Valle-Levinson and Lwiza (1995), Valle-Levinson *et al.* (2001), and Valle-Levinson *et al.* (2003) suggested an alternate circulation pattern for estuaries with channels. They argued that channel flows are opposite to the rest of the estuary and, depending on the wind direction, the bottom transport at the mouth of Chesapeake Bay can be in opposition at the north and southern ends. Quantifying the complex dynamics associated with estuarine-ocean interactions, their sediment transport patterns, and sediment pathways with numerical models could more accurately identify current and future survey priorities.

3.4 METHODS

HUG was implemented in ESRI ArcGIS version 10.5.1 along the central eastern coast of the United States between the New Jersey-Delaware and the Virginia-North Carolina borders as limits (Figure 16). This region was chosen for its high frequency survey and dredging activities that occur in response to consistent and significant sediment movement (USACE Norfolk Report and Environmental Assessment, 2017). By identifying the state of charted data in this area, it becomes possible for NOAA to limit their focus to specific problem areas within this region that exceed the allowable uncertainty.

Publicly available data from Marine Cadastre, the USGS, and many NOAA websites were used to calculate all terms in the HUG estimate (Appendix A). The most recent Electronic Navigation Charts (ENCs) were downloaded from NOAA Office of Coast Survey's (OCS) chart catalog[2]. The free ESRI S-57 Viewer version 2.2.0.9 was used to view ENC .000 files and a number of polygons were extracted from each ENC, primarily the MQUAL polygons. MQUAL (Meta: Quality of Data) polygons are required S-57 survey polygons that are attributed with the CATZOC level the survey met upon chart compilation and the survey start and end dates (IHO S-57, 2014). Various NOAA hydrographic surveys in the study area were downloaded from the National Centers for Environmental Information (NCEI – formerly the National Geographic Data Center or NGDC)[3]. Points, survey area polygons, and grids were created from these NOAA surveys (in ASCII XYZ format). A compilation 3 arc-second (~100 m) bathymetric grid of the study area was downloaded from NOAA's Coastal Relief Model (CRM)[4].

[2] NOAA Chart Catalog website: http://www.charts.noaa.gov/InteractiveCatalog/nrnc.shtml
[3] NOAA NCEI bathymetric database website: https://maps.ngdc.noaa.gov/viewers/bathymetry/
[4] NOAA Coastal Relief Model database website: https://www.ngdc.noaa.gov/mgg/coastal/crm.html

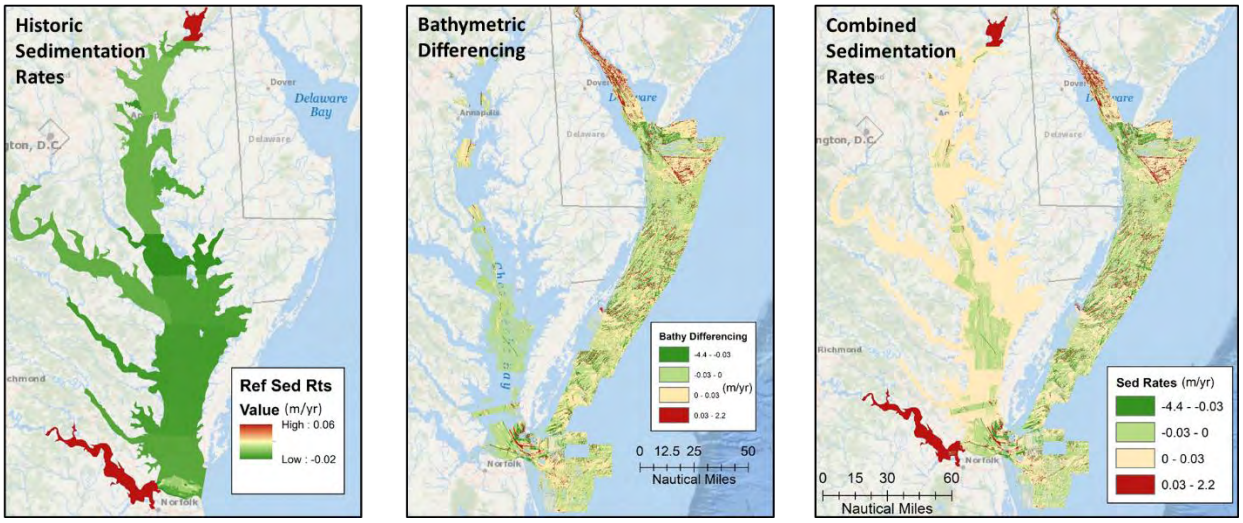

Figure 17: (Left) Sedimentation rates of Chesapeake Bay determined from a literature review (m/yr). (Center) Sedimentation rates determined from a bathymetric difference between overlapping surveys separated in time (m/yr). (Right) Combined sedimentation rates for the survey area (m/yr). Red indicates larger sedimentation rates across all three figures, yellow and green values are not as navigationally significant as they are either stable or erosional (negative).

To calculate the PSU ($\sigma_{present}$) term, the ISU ($\sigma_{initial}$) for each survey must first be determined. The standard procedure for addressing uncertainty requires CATZOC level assignment to the entire survey area regardless of full coverage. To quantify the uncertainty for the entire study area at greater accuracy and resolution including areas not fully covered in the surveys, all bathymetric data sets were downloaded and kriged to obtain a complete coverage bathymetric grid as well as an estimate of uncertainty based on the kriged variance output. Using AIS drafts, these uncertainties were constrained and mosaicked together with modern uncertainty-attributed BAG surveys to create a full coverage 40 m grid (a 10-fold improvement over current HHM outputs), finalizing the ISU term (Figure 10). A more complete outline of the AIS-based methods is discussed in Chapter 2.

To calculate the survey age, all NOAA survey polygons were attributed with a survey year and differenced from the current year (2018) in a new attribute field called ‘Survey Age’. The Survey Age was used to populate a new raster grid with a 40 m resolution.

Finally, the temporal variability components of the PSU were calculated. Chesapeake Bay proper has been thoroughly studied over the last forty years, making sedimentation rate estimates from a comprehensive literature review readily compiled (Figure 17- Left). Far less research has been conducted along the Delmarva Peninsula and into Delaware Bay. Therefore, sedimentation rates were acquired using another method. Here, a depth difference between older and more recent hydrographic surveys was performed using bathymetry obtained through kriging interpolation of bathymetric layers (Figure 17- Center; discussed in Chapter 2). The residuals were then divided by differences in acquisition years between these surveys to obtain rough estimates of sedimentation (in units of m/yr; Figure 17 – Right). Each component of the PSU term is a rasterized grid with a cell size of 40 m (Figure 18). The PSU calculation was performed using a simple raster calculation (Eq. 5) and a 40 m resolution was maintained. Note that sedimentation rates established through bathymetric differencing capture the changes observed over a certain amount of time and assumes it is constant, which may not be always true as some changes are oscillatory or migratory. While these estimates are better than nothing, more accurate estimates of change can come from numerical sediment transport modelling. However, future implementations should include methodologies to account for horizontal changes with no vertical changes; this is discussed further later.

The MAU is a user-defined variable meant to define a maximum uncertainty threshold for a specific desired CATZOC level. For this study MAU areas were defined based on NOAA's priorities included in their HHM estimates. To get the HHM desired survey score (DSS) grid into a usable format for HUG, a conversion table was created to go between the DSS values and CATZOC since the DSS values were based on coverages (outlined in Table 4). Using the uncertainty constants that align with the CATZOC levels and the NOAA coastal relief model

(CRM) as bathymetry, bathymetric TVU grids were established for the entire survey area. Areas with DSS values of 0, 30, 80, 100, and 110 were extracted individually from the HHM to make five grids that were used as masks to extract from their respective bathymetric TVU grids. These were later mosaicked together and resampled to a 40 m resolution final MAU grid (Figure 19).

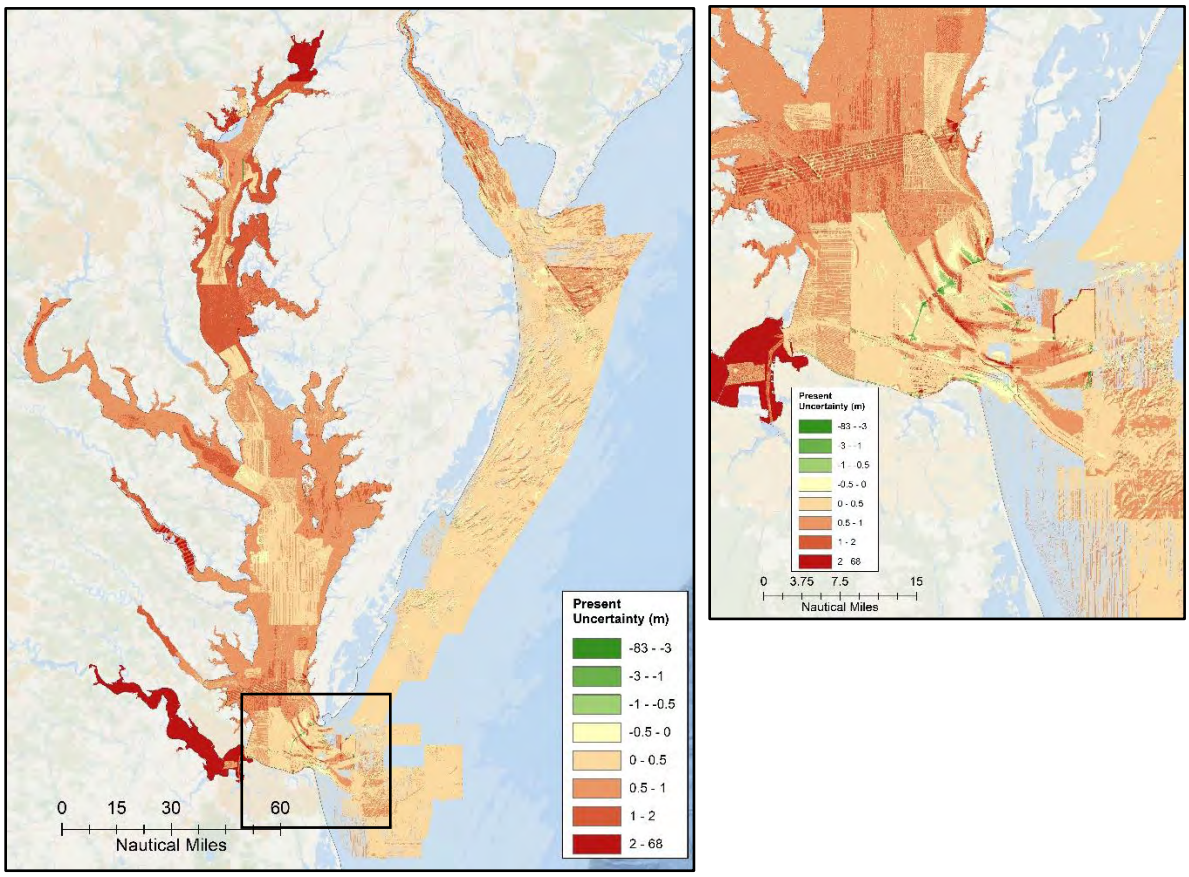

Figure 18: (Left) The final PSU calculation where areas shown in red indicate large uncertainties and areas shown in yellow and green are negative. (Right) A close up of the mouth of Chesapeake Bay, one of the most dynamic places in the study area.

HHM: DSS Value	HUG: MAU Level
10: Lesser Coverage	CATZOC D
30: Part Bottom Coverage	CATZOC C
80: Complete Coverage	CATZOC A2-B
100: Object Detection	CATZOC A1

Table 4: Conversion table for HHM DSS values and CATZOC levels.

The final PSU and MAU grids were differenced, so that positive values indicate that an area exceeds the maximum allowable uncertainty while negative values are within an allowable uncertainty. The final HUG grid has a 40 m resolution (Figure 20).

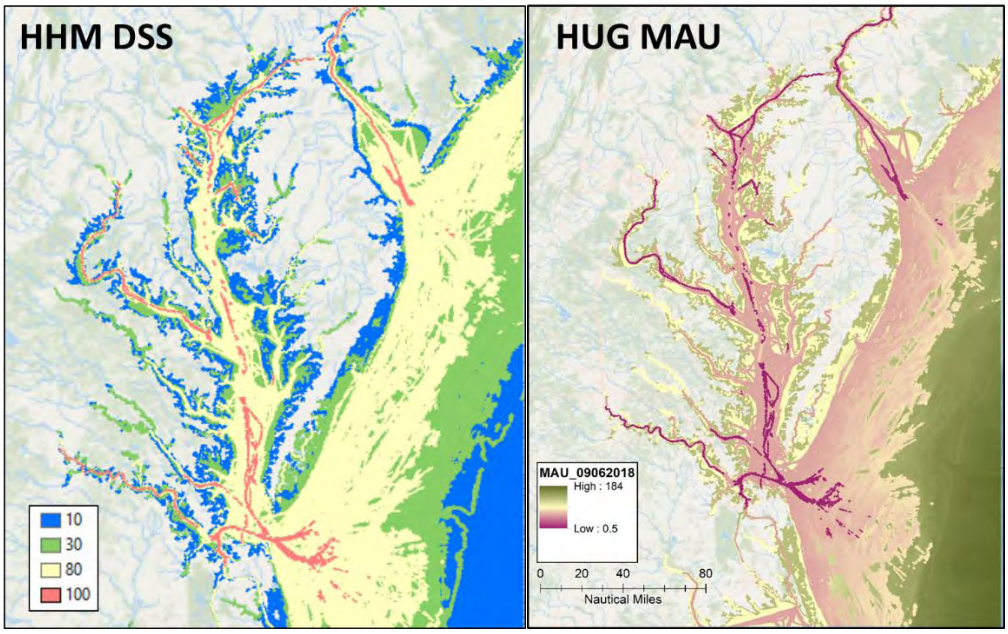

Figure 19: (Left) The Hydro Health Model Desired Survey Score (HHM DSS) output. (Right) Translation of the HHM DSS values to CATZOC confidence levels. Using the NOAA CRM as the depth component, the HUG maximum allowable uncertainties (MAU) were determined.

3.5 RESULTS

3.5.1 Sedimentation Rates

Sedimentation rates were estimated for the entire study area from bathymetric differencing and reported estimates, although bathymetric differencing was only available where repeat surveys exist. Combined, the average rate was +2.8 mm/yr and only 16% of the study area have rates over 10 mm/yr (Figure 21), the majority of which are found offshore and in Delaware Bay. The largest reported rates were observed at the Susquehanna and James Rivers within Chesapeake Bay and the largest rates from bathymetric differencing were found at the mouth of Chesapeake

Bay. The latter is consistent with the findings presented by Colman *et al*. (1988) where shoal sediments are worked into the bay by Fisherman's island and into the channels in a south-western progression. Similar patterns are observed at the mouth of Delaware Bay around Cape May.

Along offshore Delmarva, sedimentation rate patterns are consistent with sediment moving along the coast. The presence of positive values (or areas of deposition) contiguous with negative values (or areas of erosion) suggest movement from one location to the next. The rates along the coast generally fall between ± 20 mm/yr. A triangular region between the two approaching Delaware Bay channels more consistently shows depositional rates between 20-30 mm/yr (Figure 22). This is unlikely to be a natural feature, but more probably a product of bathymetric data error stemming from the modern coverage over the area as this region exactly aligns with the H10989 survey. However, it is possible the errors could stem from the surrounding surveys.

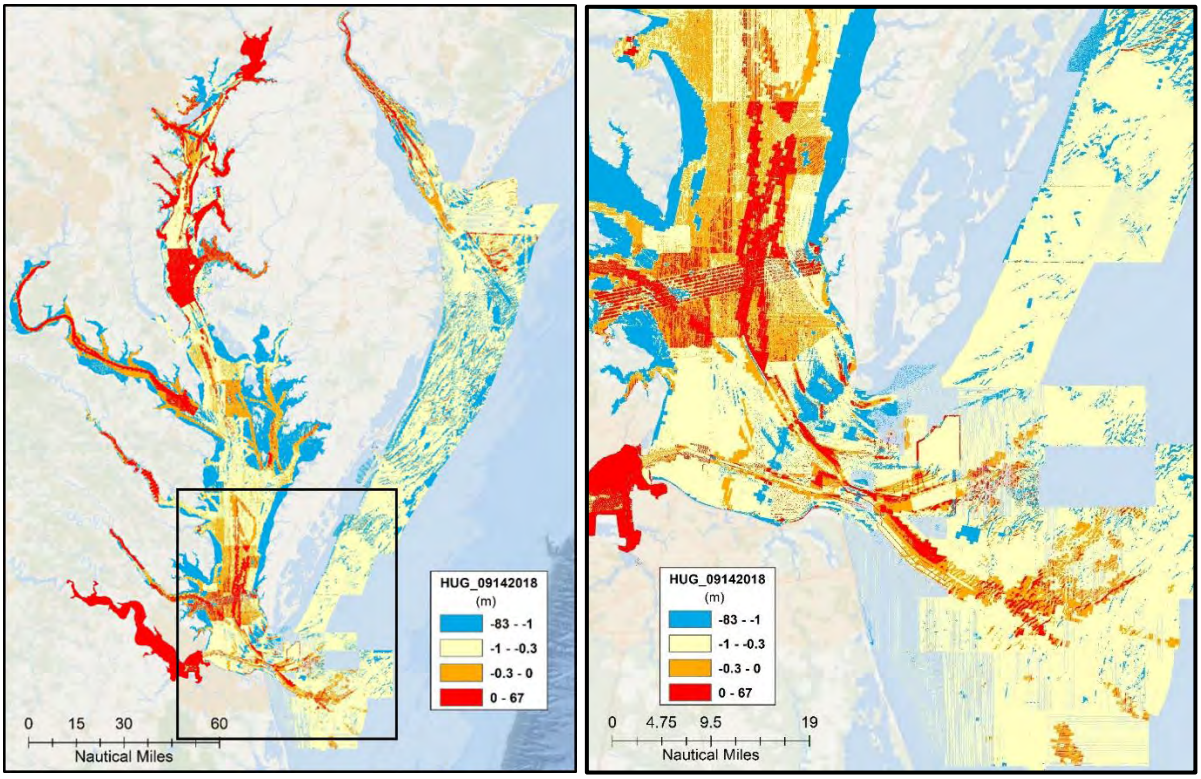

Figure 20: (Left) The HUG model output where red areas indicate areas that exceed the MAU and blues indicate areas that do not. (Right) Focus on the mouth of Chesapeake Bay.

3.5.2 Present Survey Uncertainty

The average present uncertainty is 0.66 m with a standard deviation of 0.87 m. Over 47% of the study area have present uncertainties larger than 0.5 m (Figure 23), but only 15% have uncertainties larger than 1 m and only 18% have uncertainties that are larger than 50% of the water depth. The largest uncertainties are found in and around the Susquehanna and James Rivers and result from large sedimentation rates and survey ages. The values around these rivers are extreme (> 10 m) and are likely not realistic but a product of not completely capturing the physical processes occurring due to a lack of bathymetric coverage, unrealistic sedimentation rates, and not accounting for dredging. It should be noted that all methodologies described in this work do not account for dredging operations that remove significant amounts of sediment from navigational channels. Nonetheless, these areas are still important as they call attention to a region of large change, or at the bare minimum, high uncertainty.

An area of particular interest is at the mouth of Chesapeake Bay where uncertainties fluctuate as a result of sedimentation rates and sediment movement. Even with more modern coverages and lower initial uncertainties, the larger sedimentation rates have a more significant influence on the uncertainty of this area. The opposite is observed in the majority of inner Chesapeake Bay. The bay uncertainties seem to more closely reflect survey age and the ISU, resulting in the preservation of survey area outlines.

3.5.3 Hydrographic Uncertainty Gap

The average HUG result is a gap of -0.57 m with a standard deviation of 0.92 m. The lowest values are observed primarily in the intertidal zones in central Chesapeake Bay. The maximum values are near navigational channels in both bays, upstream of the major rivers in Chesapeake Bay, and the mouth of Chesapeake Bay. Only 13% of the study area exceeds the MAU and are identified as survey priorities, which equates to ~2,700 km^2 (Figure 24). Eighty percent of these areas have HUG values that are less than 50% water depth, although a combined 121 km^2 in the Susquehanna and James Rivers have uncertainty values that exceed 50% water depth. As stated previously, the uncertainty values calculated in the Susquehanna and James Rivers are significantly skewed by the ages of their underlying data and assumptions with sedimentation rates. While these values can be more or less ignored, their relevance cannot. It is clear that the uncertainty of the seafloor in those locations is quite high and the area needs to be resurveyed.

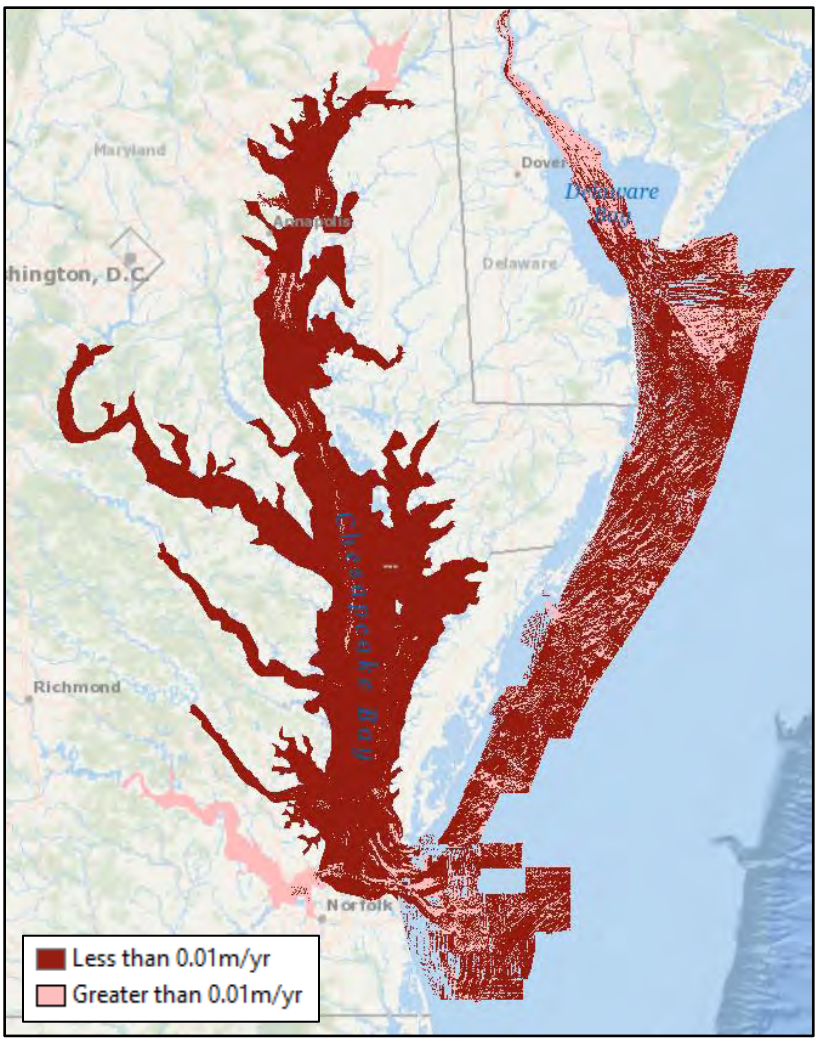

Figure 21: The locations in the study area where sedimentation rates are less than 0.01 m/yr (in red) and greater than 0.01 m/yr (in pink). Areas of large variability are located at the mouth of Chesapeake Bay and the Delmarva Peninsula.

A direct comparison with the current HHM hydrographic gap (H_{gap}) estimates is not easily accomplished due to the difference with which the changeability terms are calculated. However, H_{gap} values greater than 0 indicate hydrographic "needs" (Keown *et al*., 2016; Fandel *et al*., 2017; Hicks *et al*. 2017). With that in mind, ~52% of the H_{gap} estimates exceed the DSS (i.e.. are greater than 0). This is four times more than the survey priorities identified by the HUG methods presented here, potentially over-estimating risk and misdirecting priorities relative to the HUG values.

We also found that 14% of H_{gap} values exceeded a health rating of 50. This produces a more comparable quantity to the HUG priorities but lacks the consistent overlap (Figure 25). Only ~30% of the H_{gap} values over 50 overlap with HUG survey priorities, leaving almost 1000 km^2 of unique HUG survey priorities.

3.6 DISCUSSION

3.6.1 Sedimentation Rates

To capture and quantify temporal variability, sedimentation rates were estimated for the survey area. Sedimentation rates derived from bathymetry are inclusive of high-frequency changes like effects from tides, storms, and flooding. Estimating sedimentation rates through bathymetric differencing is not new and has been done before (Ludwick 1978; Donoghue, 1990; Hobbs *et al*., 1990; Van Der Wal and Pye, 2003). However, bathymetric differencing can lead to mis-predictions which includes those derived from migratory rates, ultimately resulting in deposition/erosion rate estimations that may only be valid for a given period of time. Similarly, this methodology assumes the bathymetric data used are without error, yet depth and position errors may propagate through the analysis and lead to misinterpretations (Van Der Wal and Pye, 2003; Jakobsson *et al.*, 2005). For example, offshore Delmarva has known sand waves that move along the shelf. Through bathymetric differencing, we identify the original location of a sand wave as having an erosion rate consistent with the appropriate rate to move the entire feature. However, a problem occurs when extrapolating these rates out several years, allowing the former location of the sand wave to continue eroding. These effects are similarly observed in the new location of the sand wave with a consistent rate of sediment deposition, rather than a migratory rate over the whole sand wave field. This can lead to larger (or smaller) estimates of

change than truly occur as sand bars are known to move horizontally shoreward and offshore depending on the wave energy (Gallagher *et al*., 1998).

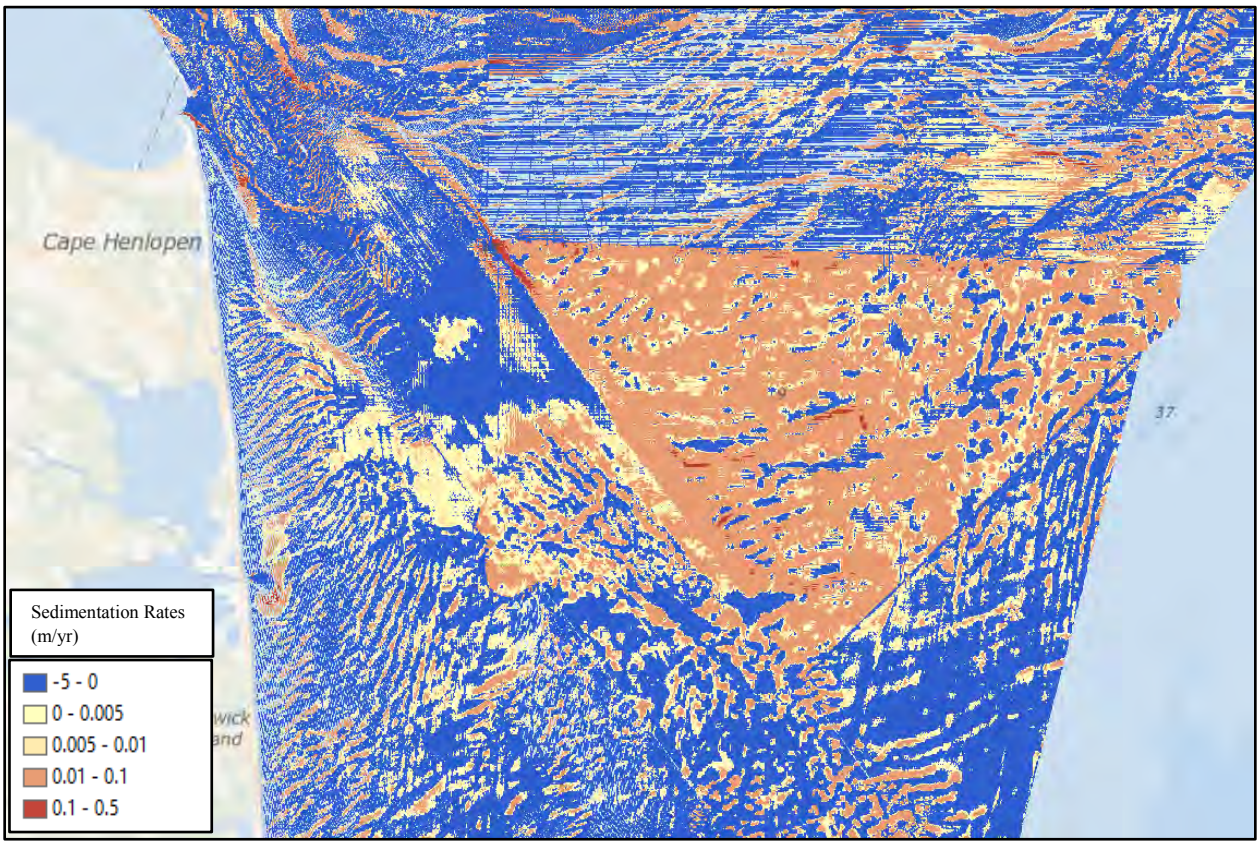

Figure 22: Close up of offshore Delmarva (approaching the mouth of Delaware Bay) sedimentation rates. Blue colors indicate erosional processes, and reds and oranges indicate sediment accumulation. The triangular-like high accumulation area shown is between two navigational channels.

Although the HUG estimates resulting from this approach may not quantify the true processes, they still capture areas of potential change (Van Der Wal and Pye, 2003). Future work should focus on more accurately accounting for migratory rates and patterns of known areas of change. Additionally, all sedimentation estimates could be further improved with outputs from a sediment transport model. The methodology discussed in this paper allows for sediment transport

model outputs to be directly included in the HUG ($\Delta Z/\Delta T$ in (5)) calculation and can ultimately be used to identify future survey priorities with more certainty as well as survey priorities under certain circumstances such as for extreme storm response.

3.6.2 Present Survey Uncertainty

The values observed in the PSU are a result of the most influential of the ISU, survey ages, and temporal variability estimates. Therefore, each value is unique to its location, geophysical processes, and data collection history. A few fundamental and known processes were captured through this estimation that give confidence in the results reported here. The larger uncertainties at the mouth of Chesapeake Bay surrounding the navigational channels is a known problem, and shows up despite modern data (lower survey ages and lower initial uncertainties) which highlights the energetic sediment dynamics in the area (Dalyander *et al*., 2013).

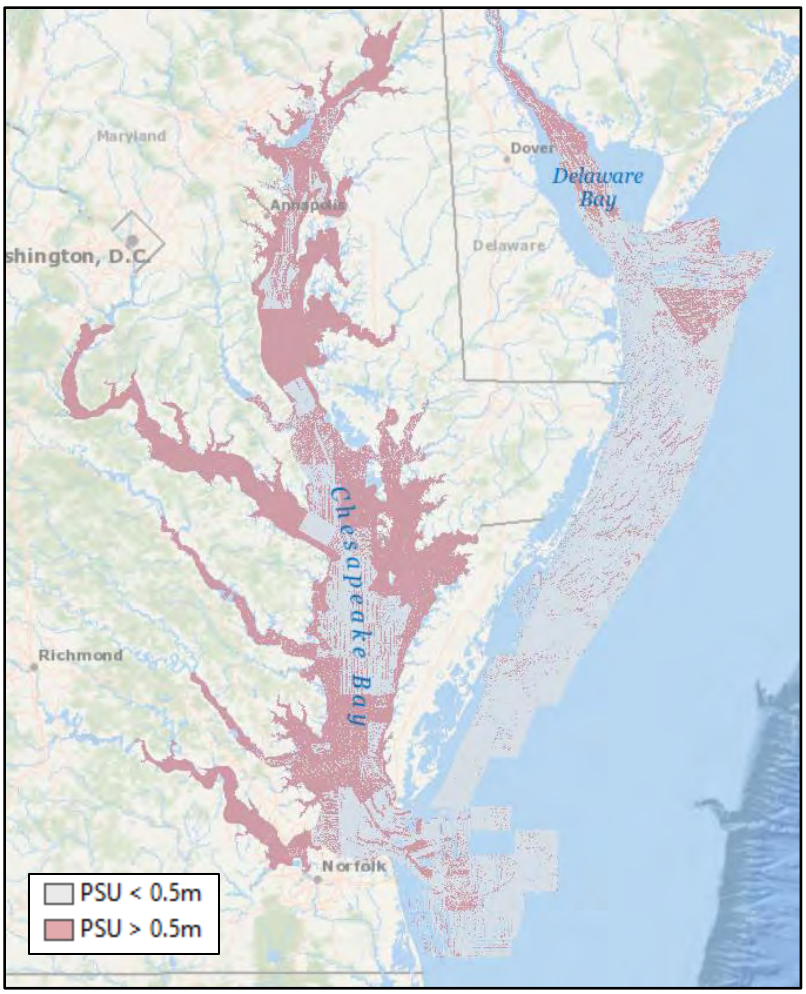

Figure 23: Areas where the PSU estimates are greater than 0.5 m (pink) and PSU estimates less than 0.5 m (grey).

The unrealistically large uncertainties calculated for the Susquehanna and James Rivers identify a serious lack of public knowledge or confidence in the currently charted bathymetry. It is possible that more modern datasets exist in this area (there is extensive naval activity near Norfolk, VA in the James River) that could improve chart health especially when dealing with lots of dredging and large vessels. Furthermore, hydrographic surveys are not the sole contributor to charted information. In recent years, the incorporation of more progressive data formats have been pushed in order to more frequently update charts. For example, bathymetric LiDAR (light detection and ranging) has begun to be used to fill in the upper intertidal regions

that are difficult to acquire with more traditional methods (Van Der Wal and Pye, 2003). The inclusion of all data formats would yield more accurate uncertainty assessments in all areas and should be reviewed for future estimations.

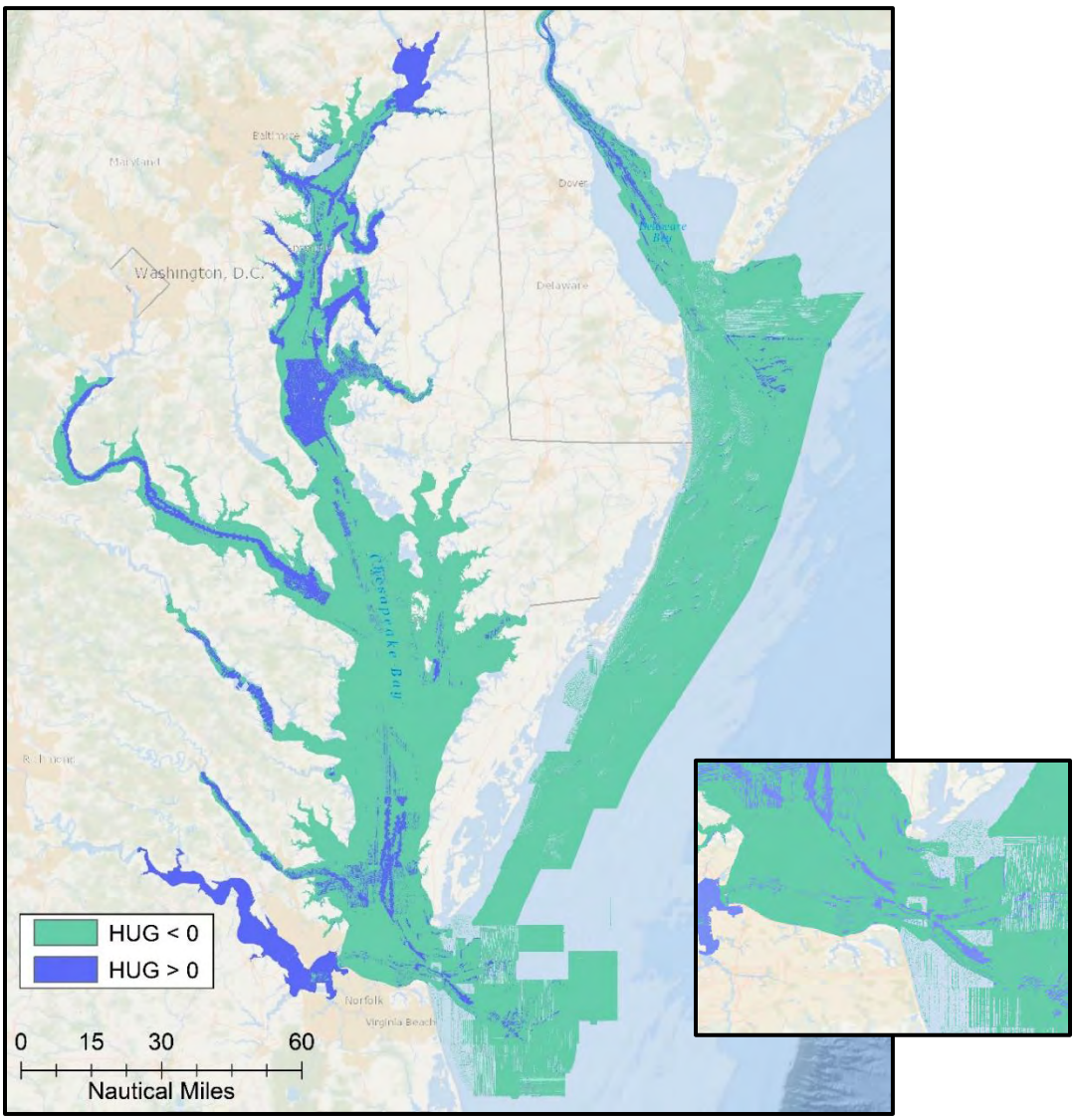

Figure 24: HUG model outputs. Values that exceed the MAU (or are greater than 0) are shown in purple and were identified as survey priorities. The remaining teal areas represent areas that are within the MAU limit (or final HUG model values less than 0). (Right) Subset of the larger image focusing on Thimble Shoal, Hampton Roads, and the Chesapeake Bay mouth navigation channels.

3.6.3 Hydrographic Uncertainty Gap

Final HUG estimates identified a significantly reduced number of survey priorities in comparison to the current H_{gap} hydrographic needs. Almost all the survey priorities identified by HUG are included in the hydrographic needs; however, once constrained to only areas of potential prioritization (HHM > 50), the H_{gap} correlation with HUG priorities lessened. This is particularly true for navigational channels and surrounding areas in both bays. While the H_{gap} does identify most of these areas as having exceeded the HHM DSS, they are not established as high priority areas. The reason for these differences comes from the calculation of the PSS.

In Chapter 2, we identified that 96% of our ISU estimates were smaller than the ISS equivalents. By underestimating the initial quality of data and with similar values for survey age and MAU/DSS, the HHM decay coefficient is left responsible for the differing results. A large number of the unique priorities identified by the HHM are found on the south western Virginia half of Chesapeake Bay, with few observed on the Fisherman's Island side. However, this area and the mouth of Chesapeake Bay are where the majority of unique priorities are observed in the HUG analysis and have been confirmed in geologic studies and dredging activities (USACE Norfolk Report and Environmental Assessment, 2017). The similarities between the two model outputs likely result from large survey ages and small user-defined maximums (MAU/DSS values).

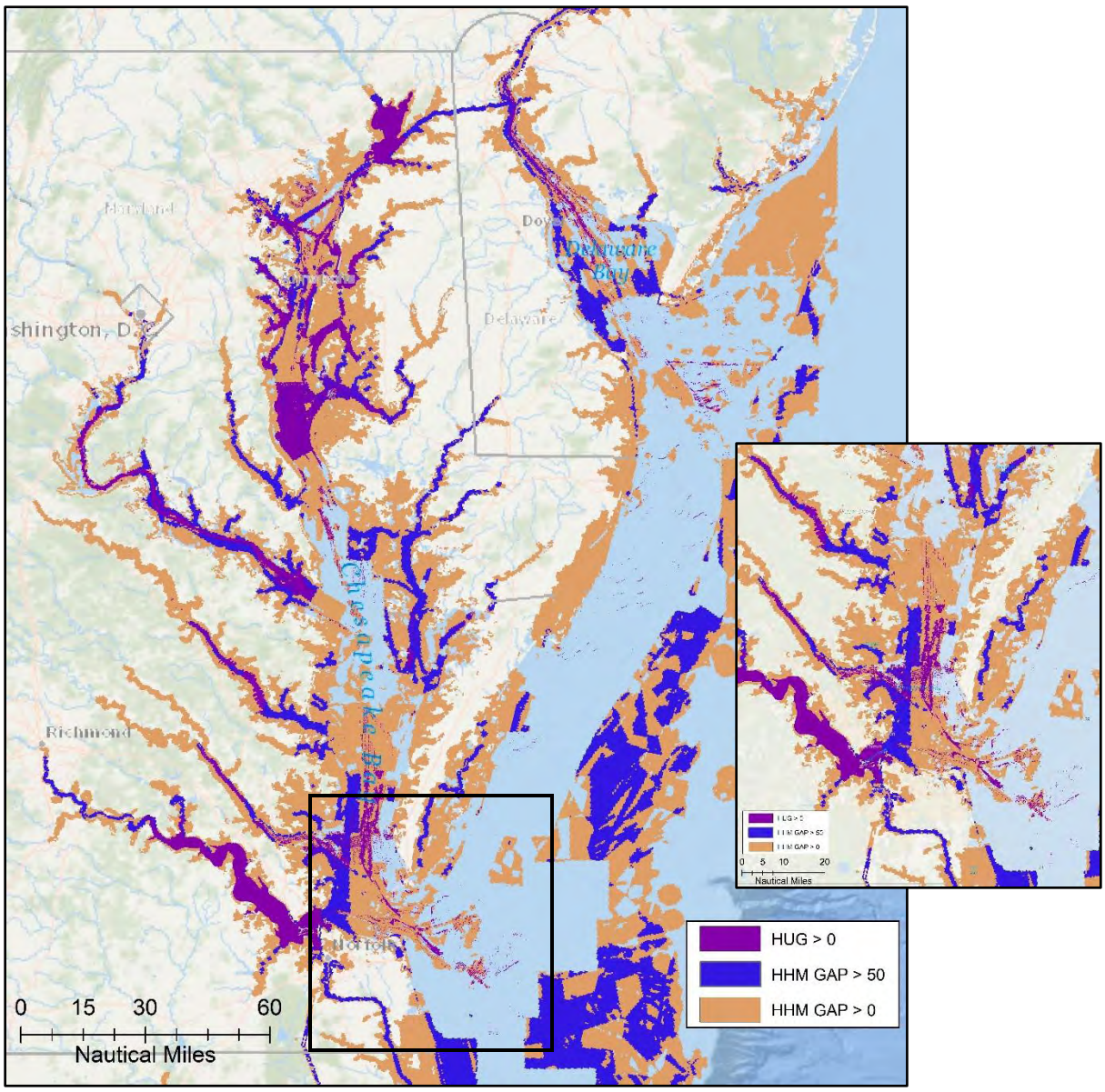

Figure 25: HUG and HHM output comparison. Purple areas are the HUG survey priorities (or areas that exceed the MAU). Blue indicate areas of the H_{gap} estimates that exceed the HHM DSS by more than 50. Tan areas are the H_{gap} survey needs, or all areas that exceed the HHM DSS (or values greater than 0). This figure shows both the overlapping priorities and the differences between the HHM and HUG model results which hint at the differences in the changeability calculations.

3.7 CONCLUSIONS

Through the work presented here, we outlined an alternative calculation for the hydrographic gap term within the HHM that incorporates quantifiable estimates of bathymetric change and uncertainty called the hydrographic uncertainty gap (HUG). The HUG model was implemented

in Chesapeake Bay and the Delmarva Peninsula where known depth-altering physical processes occur. We quantified change for the study area through sedimentation rates obtained from a literature review and bathymetric differencing. Additional confidence in the bathymetric differencing approach could come not only from incorporating a sediment migration component that allows for horizontal changes while flagging vertical changes, but also from physical validation of the rates we incorporated. Following (5), we estimated the present state of hydrographic uncertainty (PSU) and identified the James and Susquehanna Rivers as areas in need of more recent surveys. Over 47% of the PSU uncertainties are larger than 0.5 m, but with the incorporation of sediment transport model outputs and all forms of charted data, the confidence in this estimate would increase. Finally, we identified survey priorities by calculating the hydrographic uncertainty gap (HUG). Only 13% of the study area was identified as a survey priority, which is one fourth that identified by the current HHM H_{gap} output. This likely results from the specific calculation of the PSU and change terms.

It is possible, however, that the HUG model is underpredicting the number of survey priorities. Each variable within the HUG equation has an uncertainty to its estimated value which ultimately propagates through the model at each step in the calculation making the overall error hard to quantify. The best way to determine if these results are accurate (and calibrate the HUG model) would be to validate with new bathymetry.

Additionally, the HHM has model outputs that are at a 500 m grid resolution which is over an order of magnitude larger than the HUG output resolution of 40 m. This likely is a result of the model extent (for the entire coastal U.S.) and a limited computational power available. However, a resolution of that size may miss important seafloor characteristics and features increasing risk. Any implementation at a national scale should either incorporate a semi-variable resolution

output or adopt completely a finer output resolution. Future work should focus on resolving sedimentation rate and migration rates, incorporations of sediment transport model outputs, and validation of the results presented here.

CHAPTER 4
CONCLUSIONS AND RECOMMENDATIONS

Here we present a new methodology to quantify and constrain the vertical uncertainty of less-than full coverage hydrographic surveys to better and more economically present the true hydrographic health of Chesapeake Bay using recorded AIS vessel drafts and kriging. We also demonstrated an enhanced hydrographic gap calculation that incorporates the quantification of hydrodynamic components by analyzing bathymetric changes and their resulting uncertainty fluctuations. This work provides a proof-of-concept of a standard methodology for application to additional U.S. coastal areas, and more accurate predictive hydrographic assessment results.

Using a layered approach, all archive bathymetric data within the study area were interpolated using ESRI's ArcGIS Kriging implementation. Resulting uncertainty and bathymetry grids were compared to publicly available AIS vessel drafts. Through this process, over 420 km^2 (~2%) of the study area uncertainties were constrained. Further, 96% of the final constrained uncertainty grid was less than current uncertainty approximations.

The current HHM H_{gap} cannot incorporate measured bathymetric change estimates, whereas the proposed HUG model directly includes methodology to incorporate sedimentation rates and seabed change. Bathymetric change was quantified using sedimentation rates calculated from a literature review and actual bathymetric survey differencing. These estimates were used in conjunction with initial survey uncertainties to approximate the PSU. Differencing the PSU with the MAU identified 13% of the study area as current survey priorities, one fourth of the current HHM H_{gap} output.

Resolution and data size contribute significantly to the processing time needed to complete kriging interpolations. As discussed in Chapter 1, bathymetric datasets were broken up into layers based on age, then further segmented based on geographic location to allow for quicker processing times. Should kriging be implemented nationally, it is highly recommended that a similar approach be used. Further, the uncertainty outputs could also be incorporated into other aspects of charting and other NOAA uncertainty-based models like the National Bathymetric Database (NBD) that currently implements the HHM changeability calculation to determine a survey's supersession potential (Wyllie *et al*., 2015). Reusing the uncertainty outputs discussed in this thesis allow for the computational time to become more cost-effective.

The AIS draft analysis relies heavily on accurate AIS data which often does not exist, since user errors related to input units are well-established in publicly available datasets (Schultz, 2015). A multi-step filtering process was performed to account for these errors, removing a significant number of unreliable data points from each AIS dataset. Erroneous data likely still made it into the analysis but within the acceptable limits of each vessel category. Gaining access to additional AIS datasets and accounting for tides would produce more accurate results and likely alter the final percentage of the study area constrained through this procedure.

Quantifying sedimentary change over time can be done in a number of ways and provide differing "resolutions", two of which were outlined in this thesis: estimating sedimentation rates through bathymetric differencing and a literature review. A literature review provides a coarse estimate, where point observations are utilized regionally. Bathymetric differencing provides a finer definition of change. However, is only possible where repeat surveys exist. Further, it can lead to misinterpretations as it does not account for continual sediment migration. An even finer resolution may be obtained by incorporating hydrodynamic sediment transport model outputs.

Sediment transport models do not have to be run or implemented by NOAA but could come from known and verified models run by outside sources. The HUG model allows for all three to be utilized simultaneously and all necessary estimates should be included for a national implementation. Though it is recommended that sedimentation rates and HUG model outputs be validated for future use and model calibration.

The HUG output has a resolution of 40 m while the HHM output has a resolution of 500 m. The resolution difference is attributed to computational necessity based on the extent of each model output: the HHM is a national model and covers the entirety of US coastal water. Important bathymetric features are missed entirely with grid sizes this large, and bathymetric differencing can cause serious errors related to cell overlap locations. A semi-variable resolution or altogether finer resolution approach could resolve these issues and should be implemented for a national-scale model.

REFERENCES

Adams, K.T., 1942, Hydrographic Manual, U.S. Department of Commerce, Coast and Geodetic Survey, Special Publication No. 143.

Amante, C.J., and Eakins, B.W., 2019, Accuracy of Interpolated Bathymetry in Digital Elevation Models: Journal of Coastal Research, v. 76, p. 123-133.

Bailly, J., Le Coarer, Y., Languille, P., Stigermark, C., and Allouis, T., 2010, Geostatistical estimations of bathymetric LiDAR errors on rivers: Earth Surface Processes and Landforms, v. 35, p. 1199-1210.

Brush, G.S., 1984, Patterns of Recent Sediment Accumulation in Chesapeake Bay (Virginia-Maryland, U.S.A.) Tributaries: Chemical Geology, v. 44, p. 227-242.

Calder, B., 2006, On the Uncertainty of Archive Hydrographic Data Sets: IEEE Journal of Oceanic Engineering, v. 31, no. 2, p. 249-265.

Calder, B., 2015, On Risk-Based Expression of Hydrographic Uncertainty: Marine Geodesy, v. 38, p. 99-127.

Calder, B., 2016, Risk Models and Survey Completeness (or, “Are We There Yet?”), *in* Canadian Hydrographic Conference: Halifax, Nova Scotia, Canada, p. 1-12.

Chenier, R., Abado, L., and Martin, H., 2018, CHS Priority Planning Tool (CPPT) - A GIS Model for defining hydrographic survey and charting priorities: International Journal of Geo-Information, v. 7, p. 240-234.

Colman, S., Berquist Jr., C.R., and Hobbs, C.H., 1988, Structure, Age and Origin of the Bay-Mouth Shoal Deposits, Chesapeake Bay, Virginia: Marine Geology, v. 83, p. 95-113.

Cressie, N., 1990, The origins of Kriging: Mathematical Geology, v. 22, no. 3, p. 239-252.

Dalyander, P.S., Butman, B., Sherwood, C.R., Signell, R.P., and Wilkin, J., 2013, Characterizing wave- and current- induced bottom shear stress: U.S. middle Atlantic continental shelf: Continental Shelf Research, v. 52, p. 73-86.

Department of Commerce, NOAA Hydrographic Survey Specifications and Deliverables, April 2018.

Donoghue, J.F., 1990, Trends in Chesapeake Bay Sedimentation Rates during the Late Holocene: Quaternary Research, v. 34, p. 33-46.

Elmore, P., Fabre, D.H., Sawyer, R.T., and Ladner, R.W., 2009, Uncertainty Estimation of Historical Bathymetric Data from Bayesian Networks, *in* OCEANS 2009: Biloxi, MS, USA, IEEE, p. 1-8.

Fandel, C., Allen, C., Gallagher, B., Gonsalves, M., Hick, L., and Keown, P., 2017, Desire, decay, and risk: Establishing survey priorities through the assessment of hydrographic health, *in* NOAA Field Procedures Workshop: Virginia Beach, VA, USA, NOAA.

Gallagher, E.L., Elgar, S., and Guza, R.T., 1998, Observations of sand bar evolution on a natural beach: Journal of Geophysical Research, v. 103, no. C2, p. 3203-3215.

Gonsalves, M., Brunt, D., Fandel, C., and Keown, P., 2015, A Risk-based Methodology of Assessing the Adequacy of Charting Products in the Arctic Region: Identifying the Survey Priorities of the Future, *in* U.S. Hydrographic Conference 2015: National Harbor, MD, USA, p. 1-20.

Grenier, M., and Hally, P., 1991, Model for determination of cartographic and hydrographic priorities, *in* Canadian Hydrographic Conference 1991, International Hydrographic Review, p. 1-19.

Haidvogel, D.B., Arango, H.G., Budgell, W.P., *et al*., 2008, Ocean forecasting in terrain-following coordinates: Formulation and skill assessment of the Regional Ocean Modeling System: Journal of Computational Physics, v. 227, p. 3595-3624.

Hawley, J.H., 1931, Hydrographic Manual, U.S. Department of Commerce, U.S. Coast and Geodetic Survey, Special Publication No. 143.

Hick, L., Gonsalves, M., Allen, C., Fandel, C., Gallagher, B., and Keown, P., 2017, Incorporating vessel traffic in an assessment of hydrographic health, *in* Environmental Data Management Workshop: Silver Spring, MD, USA, NOAA.

Hobbs, C.H., Halka, J.P., Kerhin, R.T., and Carron, M.J., 1992, Chesapeake Bay Sediment Budget: Journal of Coastal Research, v. 8, no. 2, p. 292-300.

Hobbs, C.H., Halka, J.P., Kerhin, R.T., and Carron, M.J., 1990, A 100-Year Sediment Budget for Chesapeake Bay: A Special Report in Applied Marine Science and Ocean Engineering: 307, 1 p.

Hoffman, M., Miyoshi, T., Haine, T.W.N., Ide, K., Brown, C., and Murtuguddle, R., 2012, An Advanced Data Assimilation System for the Chesapeake Bay: Performance Evaluation: Journal of Atmospheric and Oceanic Technology, v. 29, p. 1542-1557.

IHO Hydrographic Dictionary Part 1 Volume 1, Special Publication 32, 5th Edition 1994: Monaco.

IHO Standards for Hydrographic Surveys, Special Publication 44, 5th Edition 2008: Monaco.

The IHO Transfer Standard for Digital Hydrographic Data: Supplementary Information for the Encoding of S-57 Edition 3.1 ENC Data June 2014: International Hydrographic Bureau Monaco S-57 Supplement No. 3, 1-4 p.

IHO Universal Hydrographic Data Model, Special Publication 100, 2nd Edition 2015: Monaco.

Jakobsson, M., Calder, B., and Mayer, L., 2002, On the effect of random errors in gridded bathymetric compilations: Journal of Geophysical Research, v. 107, no. B12, p. 1-11.

Jakobsson, M., Armstrong, A., Calder, B., Huff, L., and Mayer, L., 2005, On the Use of Historical Bathymetric Data to Determine Changes in Bathymetry: An Analysis of Errors and Application to Great Bay Estuary, NH: International Hydrographic Review, no.1016.

Keown, P., Gonsalves, M., Allen, C., Fandel, C., Gallagher, B., and Hick, L., 2016, A risk-based approach to determine hydrographic survey priorities using GIS, *in* 2016 ESRI Ocean GIS Forum: Redlands, California, USA.

Krige, D., 1951, A statistical approach to some basic mine valuation problems on the Witwatersrand: Journal of the Chemical Metallurgical & Mining Society of South Africa, v. 52, no. 6, p. 119-138.

Ladner, R.W., Elmore, P., Perkins, A.L., Bourgeois, B., and Avera, W., 2017, Automated cleaning and uncertainty attribution of archival bathymetry based on a priori knowledge: Marine Geophysical Research, no. 38, p. 291-301.

Ludwick, J.C., 1981, Bottom sediments and depositional rates near Thimble Shoal Channel, lower Chesapeake Bay, Virginia: GSA Bulletin, v. 92, no. 1, p. 496-506.

Ludwick, J.C., 1978, Coastal Currents and an Associated Sand Stream off Virginia Beach, Virginia: Journal of Geophysical Research, v. 83, no. C5, p. 2365-2372.

Maa, J.P., and Lee, C.-., 1997, Variation of the Resuspension Coefficients in the Lower Chesapeake Bay: Journal of Coastal Research, v. 25, p. 36-74.

Maa, J., and Hobbs, C.H., 1998, Physical Impact of Waves on Adjacent Coasts Resulting from Dredging at Sandbridge Shoal, Virginia: Journal of Coastal Research, v. 14, no. 2, p. 525-536.

Maa, J., Hobbs, C.H., Kim, S., and Wei, E., 2004, Potential Impacts of Sand Mining Offshore of Maryland and Delaware: Part 1: Impacts on Physical Oceanographic Processes: Journal of Coastal Research, v. 20, no. 1, p. 44-60.

Masetti, G., Faulkes, T., Kastrisios, C., 2018, Automated Identification of Discrepancies between Nautical Charts and Survey Soundings: International Journal of Geo-Information, v. 7, p1-19.

National Geophysical Data Center, 1999. U.S. Coastal Relief Model - Southeast Atlantic. National Geophysical Data Center, NOAA. doi:10.7289/V53R0QR5

Oliver, M.A., and Webster, R., 2014, A tutorial guide to geostatistics: Computing and modelling variograms and kriging: Catena, v. 113, p. 56-69.

Perillo, G.M.E., and Ludwick, J.C., 1984, Geomorphology of a Sand Wave in Lower Chesapeake Bay, Virginia, USA: Geo-Marine Letters, v. 4, p. 105-112.

Sanford, L.P., 2008, Modeling a dynamically varying mixed sediment bed with erosion, deposition, bioturbation, consolidation, and armoring: Computers & Geosciences, v. 34, p. 1263-1283.

Sanford, L.P., 1994, Wave-forced resuspension of upper Chesapeake Bay muds: Estuaries, v. 17, no. 1B, p. 148-165.

Sanford, L.P., and Halka, J.P., 1993, Assessing the paradigm of mutually exclusive erosion and deposition of mud, with examples from upper Chesapeake Bay: Marine Geology, v. 114, p. 37-57.

Sanford, L.P., Panageotou, W., and Halka, J.P., 1991, Tidal resuspension of sediments in northern Chesapeake Bay: Marine Geology, v. 97, p. 87-103.

Sanford, L.P., Suttles, S.E., and Halka, J.P., 2001, Reconsidering the physics of the Chesapeake Bay estuarine turbidity maximum: Estuaries, v. 24, no. 5, p. 655-669.

Schultz, C., 2015, Crowdsourced Maritime Data: Examining the feasibility of using under keel clearance data from AIS to identify hydrographic survey priorities, University of Southern California: GIS and Technology.

Skrabal, S., 1991, Clay mineral distributions and source discrimination of upper Quaternary sediments, lower Chesapeake Bay, Virginia: Estuaries, v. 14, no. 1, p. 29-37.

Stumpf, R.P., 1988, Sediment Transport in Chesapeake Bay during Floods: Analysis Using Satellite and Surface Observations: Journal of Coastal Research, v. 4, no. 1, p. 1-15.

Taylor, J.R., 1982, An Introduction to Error Analysis: The Study of Uncertainties in Physical Measurements (Second Edition), University Science Books, 1-327 p.

U.S. Army Corps of Engineers, Norfolk District, 2017, Norfolk Harbor Navigation Improvements: DRAFT General Reevaluation Report and Environmental Assessment, p. 1-295.

Valle-Levinson, A., and Lwiza, K.M.M., 1995, The effects of channels and shoals on exchange between the Chesapeake Bay and the adjacent ocean: Journal of Geophysical Research, v. 100, no. C9, p. 551-563.

Valle-Levinson, A., Reyes, C., and Sanay, R., 2003, Effects of Bathymetry, Friction, and Rotation on Estuary-Ocean Exchange: Journal of Physical Oceanography, v. 33, p. 2375-2393.

Valle-Levinson, A., Wong, K., and Bosley, K.T., 2001, Observations of the wind-induced exchange at the entrance to Chesapeake Bay: Journal of Marine Research, v. 59, p. 391-416.

Van Der Wal, D., and Pye, K., 2003, The use of historical bathymetric charts in a GIS to assess morphological change in estuaries: The Geographical Journal, v. 169, no. 1, p. 21-31.

Ward, L., 1985, The Influence of Wind Waves and Tidal Currents on Sediment Resuspension in Middle Chesapeake Bay: Geo-Marine Letters, v. 5, p. 71-75.

Willard, D.A., Cronin, T.M., and Verardo, S., 2003, Late-Holocene climate and ecosystem history from Chesapeake Bay sediment cores, USA: The Holocene, v. 13, no. 2, p. 201-214.

Wong, A.M., Campagnoli, J.G., and Cole, M.A., 2007, Assessing 155 Years of Hydrographic Survey Data for High Resolution Bathymetry Grids, *in* OCEANS 2007: Vancouver, BC, Canada, IEEE, p. 1-8.

Wright, L.D., Kim, C.S., Hardaway, C.S., Kimball, S.M., and Green, M.O., 1987, Shoreface and Beach Dynamics of the Coastal Region from Cape Henry to False Cape, Virginia: https://doi.org/10.21220/V5ZD87.

Wyllie, K., Cole, M., Froelich, G., Wilson, M., and Nelson, K., 2017, Developing a method to validate the navigational bathymetric database, *in* U.S. Hydro 2017, p. 1-14.

APPENDIX A: DATA

SUMMARY

The follow sections outline the publicly-available datasets utilized in the analyses discussed in this thesis.

NOAA ELECTRONIC CHARTS

ENC	Chart	Scale	Date Downloaded	Version	Date Edited	What I Used	What they were used for
US4DE11M	12214	1:80,000	01/23/2018	34	01/11/2018	MQUAL, FAIRWY, DRGARE, TWRTPT, TSSLPT, TSEZNE	CATZOC level analysis, MAU designation,
US4DE12M	12304	1:80,000	01/23/2018	22	12/13/2017	MQUAL, FAIRWY, DRGARE	CATZOC level analysis, MAU designation,
US4VA50M	12211	1:80,000	01/23/2018	24	01/10/2018	MQUAL, FAIRWY, DRGARE, TSSLPT	CATZOC level analysis, MAU designation,
US4VA70M	12210	1:80,000	01/23/2018	19	12/14/2017	MQUAL, FAIRWY, DRGARE	CATZOC level analysis, MAU designation,
US5DE13M	12311	1:80,000	01/23/2018	31	10/20/2017	MQUAL, FAIRWY, DRGARE	CATZOC level analysis, MAU designation,
US5MD1AM	12266	1:40,000	01/23/2018	3	01/12/2018	MQUAL, FAIRWY, DRGARE	CATZOC level analysis, MAU designation,
US5MD12M	12278	1:40,000	01/23/2018	42	12/14/2017	MQUAL, FAIRWY, DRGARE	CATZOC level analysis, MAU designation,
US5MD13M	12270	1:40,000	01/23/2018	26	01/10/2018	MQUAL, FAIRWY, DRGARE	CATZOC level analysis, MAU designation,
US5MD14M	12274	1:40,000	01/23/2018	23	01/10/2018	MQUAL, FAIRWY, DRGARE	CATZOC level analysis, MAU designation,
US5MD15M	12277	1:20,000	01/23/2018	30	10/06/2017	MQUAL, FAIRWY, DRGARE	CATZOC level analysis, MAU designation,
US5MD16M	12266	1:40,000	01/23/2018	28	09/27/2017	MQUAL, FAIRWY, DRGARE	CATZOC level analysis, MAU designation,
US5MD17M	12270	1:40,000	01/23/2018	17	01/10/2018	MQUAL, FAIRWY, DRGARE	CATZOC level analysis, MAU designation,
US5MD21M	12264	1:40,000	01/23/2018	24	11/30/2017	MQUAL, FAIRWY, DRGARE	CATZOC level analysis, MAU designation,
US5MD22M	12282	1:25,000	01/23/2018	11	07/21/2017	MQUAL, FAIRWY, DRGARE	CATZOC level analysis, MAU designation,
US5MD32M	12283	1:10,000	01/23/2018	17	10/13/2017	MQUAL, FAIRWY, DRGARE	CATZOC level analysis, MAU designation,
US5VA10M	12226	1:40,000	01/23/2018	24	11/14/2017	MQUAL, FAIRWY, DRGARE	CATZOC level analysis, MAU designation,
US5VA14M	12224	1:40,000	01/23/2018	31	12/14/2017	MQUAL, FAIRWY, DRGARE	CATZOC level analysis, MAU designation,
US5VA15M	12245	1:20,000	01/23/2018	49	01/17/2018	MQUAL, FAIRWY, DRGARE	CATZOC level analysis, MAU designation,
US5VA16M	12228	1:40,000	01/23/2018	35	01/10/2018	MQUAL, FAIRWY, DRGARE, TSSLPT, TSEZNE	CATZOC level analysis, MAU designation,
US5VA19M	12254	1:20,000	01/23/2018	32	01/17/2018	MQUAL, FAIRWY, DRGARE	CATZOC level analysis, MAU designation,
US5VA20M	12256	1:20,000	01/23/2018	17	12/14/2017	MQUAL, FAIRWY, DRGARE	CATZOC level analysis, MAU designation,
US5VA21M	12231	1:40,000	01/23/2018	20	01/09/2018	MQUAL, FAIRWY, DRGARE	CATZOC level analysis, MAU designation,
US5VA22M	12233	1:40,000	01/23/2018	27	12/19/2017	MQUAL, FAIRWY, DRGARE	CATZOC level analysis, MAU designation,
US5VA24M	12238	1:40,000	01/23/2018	26	12/14/2017	MQUAL, FAIRWY, DRGARE	CATZOC level analysis, MAU designation,
US5VA27M	12233	1:40,000	01/23/2018	23	09/12/2017	MQUAL, FAIRWY, DRGARE	CATZOC level analysis, MAU designation,
US5VA41M	12235	1:40,000	01/23/2018	39	12/05/2017	MQUAL, FAIRWY, DRGARE	CATZOC level analysis, MAU designation,
US5VA13M	12222	1:40,000	01/23/2018	38	01/17/2018	MQUAL, FAIRWY, DRGARE, TSSLPT	CATZOC level analysis, MAU designation,
US5VA11M	12208	1:50,000	01/23/2018	23	01/16/2018	MQUAL, TSSLPT	CATZOC level analysis, MAU designation,
US4VA12M	12221	1:80,000	01/23/2018	33	12/19/2017	MQUAL, FAIRWY, DRGARE, TSSLPT	CATZOC level analysis, MAU designation,
US4VA1AM	12221	1:80,000	01/23/2018	4	11/15/2017	MQUAL, FAIRWY, DRGARE	CATZOC level analysis, MAU designation,
US3EC08M	12280	1:200,000	01/23/2018	26	11/20/2017	MQUAL, FAIRWY, DWRTPT, TSSLPT, TSEZNE	CATZOC level analysis, MAU designation,
US4NC32M	12207	1:80,000	01/23/2018	14	01/11/2018	MQUAL, FAIRWY, DRGARE	CATZOC level analysis, MAU designation,
US4MD40M	12285	1:80,000	02/19/2018	17	01/31/2018	MQUAL, FAIRWY, DRGARE	CATZOC level analysis, MAU designation,
US5VA51M	12251	1:40,000	02/19/2018	22	02/07/2018	MQUAL, FAIRWY, DRGARE	CATZOC level analysis, MAU designation,
US5VA25M	12248	1:40,000	02/19/2018	27	02/08/2018	MQUAL, FAIRWY, DRGARE	CATZOC level analysis, MAU designation,
US5VA60M	12241	1:20,000	02/19/2018	19	12/13/2017	MQUAL, FAIRWY, DRGARE	CATZOC level analysis, MAU designation,
US5VA61M	12243	1:40,000	02/19/2018	6	02/14/2018	MQUAL, FAIRWY, DRGARE	CATZOC level analysis, MAU designation,
US5VA63M	12237	1:40,000	02/19/2018	16	11/20/2017	MQUAL, FAIRWY, DRGARE	CATZOC level analysis, MAU designation,
US5MD23M	12261	1:40,000	02/19/2018	16	11/30/2017	MQUAL, FAIRWY, DRGARE	CATZOC level analysis, MAU designation,

Figure 26: NOAA electronic navigation charts (ENCs) that were used in HUG calculations.

NOAA HYDROGRAPHIC SURVEYS

Area	Survey	Year	Data Type
Central Chesapeake	T00813	1860	XYZ
Lower Chesapeake, Mouth	H01721	1886	XYZ
Upper Chesapeake	H02335	1897	XYZ
Upper Chesapeake	H02347	1897	XYZ
Central Chesapeake	H03003A	1909	XYZ
Central Chesapeake	H03003	1909	XYZ
Central Chesapeake	H03029	1909	XYZ
Central Chesapeake	H03003B	1910	XYZ
Central Chesapeake	H03009	1910	XYZ
Central Chesapeake	H03010	1910	XYZ
Central Chesapeake	H03011	1910	XYZ
Central Chesapeake	H03311	1911	XYZ
Central Chesapeake	H03343	1912	XYZ
Lower Chesapeake	H04084	1919	XYZ
Lower Chesapeake	H05000	1929	XYZ
Central Chesapeake	H05228	1932	XYZ
Upper Chesapeake	H05197	1932	XYZ
Upper Chesapeake	H05198	1932	XYZ
Upper Chesapeake	H05237	1932	XYZ
Upper Chesapeake	H05295	1933	XYZ
Upper Chesapeake	H05327	1933	XYZ
Upper Chesapeake	H05328	1933	XYZ
Upper Chesapeake	H05329	1933	XYZ
Upper Chesapeake	H05374	1933	XYZ
Upper Chesapeake	H05403	1933	XYZ
Upper Chesapeake	H05416	1933	XYZ
Upper Chesapeake	H05432	1933	XYZ
Upper Chesapeake	H05501	1933	XYZ
Lower Chesapeake	H05968	1934	XYZ
Lower Chesapeake	H05969	1934	XYZ
Offshore Delmarva	H05703	1934	XYZ
Offshore Delmarva	H05715	1934	XYZ
Offshore Delmarva	H05771	1934	XYZ
Offshore Delmarva	H05988	1934	XYZ
Offshore Delmarva, Mouth	H05989	1934	XYZ
Offshore Delmarva, Mouth	H05990	1935	XYZ
Offshore Delmarva	H05991	1935	XYZ
Offshore Delmarva	H05992	1935	XYZ
Upper Chesapeake	H06360	1938	XYZ

Upper Chesapeake	H06362	1938	XYZ
Upper Chesapeake	H06363	1938	XYZ
Upper Chesapeake	H06364	1938	XYZ
Upper Chesapeake	H06365	1938	XYZ
Upper Chesapeake	H06366	1938	XYZ
Upper Chesapeake	H06367	1938	XYZ
Upper Chesapeake	H06368	1938	XYZ
Upper Chesapeake	H06369	1938	XYZ
Upper Chesapeake	H06370	1938	XYZ
Upper Chesapeake	H06371	1938	XYZ
Upper Chesapeake	H06372	1938	XYZ
Upper Chesapeake	H06373	1938	XYZ
Upper Chesapeake	H06374	1938	XYZ
Upper Chesapeake	H06375	1938	XYZ
Upper Chesapeake	H06376	1938	XYZ
Lower Chesapeake, Mouth	H06595	1940	XYZ
Upper Chesapeake	H06597	1940	XYZ
Upper Chesapeake	H06598	1940	XYZ
Upper Chesapeake	H06599	1940	XYZ
Upper Chesapeake	H06600	1940	XYZ
Upper Chesapeake	H06601	1940	XYZ
Upper Chesapeake	H06602	1940	XYZ
Upper Chesapeake	H06603	1940	XYZ
Upper Chesapeake	H06604	1940	XYZ
Upper Chesapeake	H06605	1940	XYZ
Upper Chesapeake	H06683	1941	XYZ
Central Chesapeake	H06775	1942	XYZ
Central Chesapeake	H06776	1942	XYZ
Central Chesapeake	H06779	1942	XYZ
Lower Chesapeake	H06729	1942	XYZ
Central Chesapeake	H06878	1943	XYZ
Lower Chesapeake	H06812	1943	XYZ
Lower Chesapeake	H06832	1943	XYZ
Upper Chesapeake	H06950	1943	XYZ
Upper Chesapeake	H06951	1943	XYZ
Central Chesapeake	H06876	1944	XYZ
Central Chesapeake	H06877	1944	XYZ
Central Chesapeake	H06966	1944	XYZ
Lower Chesapeake	H06928	1944	XYZ
Lower Chesapeake	H06930	1944	XYZ
Lower Chesapeake, Mouth	H06962	1944	XYZ

Lower Chesapeake	H07021	1944	XYZ
Upper Chesapeake	H06599	1944	XYZ
Upper Chesapeake	H06952	1944	XYZ
Upper Chesapeake	H06954	1944	XYZ
Upper Chesapeake	H06955	1944	XYZ
Upper Chesapeake	H06956	1944	XYZ
Upper Chesapeake	H06958	1944	XYZ
Upper Chesapeake	H07002	1944	XYZ
Upper Chesapeake	H07003	1944	XYZ
Upper Chesapeake	H07010	1944	XYZ
Upper Chesapeake	H07011	1944	XYZ
Central Chesapeake	H07022	1945	XYZ
Lower Chesapeake	H07025	1945	XYZ
Upper Chesapeake	H06953	1945	XYZ
Upper Chesapeake	H07001	1945	XYZ
Upper Chesapeake	H07009	1945	XYZ
Upper Chesapeake	H07027	1945	XYZ
Upper Chesapeake	H07032	1945	XYZ
Upper Chesapeake	H07043	1945	XYZ
Upper Chesapeake	H07047	1945	XYZ
Upper Chesapeake	H07064	1945	XYZ
Upper Chesapeake	H07065	1945	XYZ
Upper Chesapeake	H07075	1945	XYZ
Central Chesapeake	H07091	1946	XYZ
Central Chesapeake	H07092	1946	XYZ
Central Chesapeake	H07094	1946	XYZ
Central Chesapeake	H07154	1946	XYZ
Central Chesapeake	H07155	1946	XYZ
Central Chesapeake	H07156	1946	XYZ
Central Chesapeake	H07157	1946	XYZ
Lower Chesapeake	H07087	1946	XYZ
Lower Chesapeake, Mouth	H07089	1946	XYZ
Central Chesapeake	H07175	1947	XYZ
Central Chesapeake	H07181	1947	XYZ
Lower Chesapeake	H07160	1947	XYZ
Lower Chesapeake	H07162	1947	XYZ
Lower Chesapeake, Mouth	H07171	1947	XYZ
Lower Chesapeake, Mouth	H07185	1947	XYZ
Lower Chesapeake	H07174	1948	XYZ
Lower Chesapeake	H07610	1948	XYZ
Lower Chesapeake	H07641	1948	XYZ

Lower Chesapeake	H07642	1948	XYZ
Lower Chesapeake, Mouth	H07703	1948	XYZ
Central Chesapeake	H07680	1949	XYZ
Central Chesapeake	H07722	1949	XYZ
Central Chesapeake	H07778	1949	XYZ
Central Chesapeake	H07779	1949	XYZ
Central Chesapeake	H07780	1949	XYZ
Central Chesapeake	H07781	1949	XYZ
Central Chesapeake	H07782	1949	XYZ
Lower Chesapeake, Mouth	H07721	1949	XYZ
Lower Chesapeake, Mouth	H07783	1949	XYZ
Lower Chesapeake, Mouth	H07791	1949	XYZ
Central Chesapeake, Mouth	H07750	1950	XYZ
Central Chesapeake	H07879	1950	XYZ
Central Chesapeake	H07880	1950	XYZ
Central Chesapeake	H07881	1950	XYZ
Central Chesapeake	H07882	1950	XYZ
Central Chesapeake	H07883	1950	XYZ
Central Chesapeake	H07884	1950	XYZ
Central Chesapeake	H07885	1950	XYZ
Lower Chesapeake, Mouth	H07823	1950	XYZ
Lower Chesapeake, Mouth	H07824	1950	XYZ
Lower Chesapeake	H07910	1950	XYZ
Central Chesapeake	H07942	1951	XYZ
Central Chesapeake	H07943	1951	XYZ
Central Chesapeake	H07944	1951	XYZ
Central Chesapeake	H07945	1951	XYZ
Central Chesapeake	H07946	1951	XYZ
Central Chesapeake	H08069	1951	XYZ
Lower Chesapeake	H07894	1951	XYZ
Central Chesapeake	H07955	1952	XYZ
Central Chesapeake	H07956	1952	XYZ
Central Chesapeake	H07957	1952	XYZ
Central Chesapeake	H07958	1952	XYZ
Central Chesapeake	H07960	1952	XYZ
Central Chesapeake	H08012	1952	XYZ
Lower Chesapeake	H07959	1952	XYZ
Central Chesapeake	H07952	1953	XYZ
Central Chesapeake	H07953	1953	XYZ
Central Chesapeake	H08078	1953	XYZ
Central Chesapeake	H08079	1953	XYZ

Central Chesapeake	H08080	1953	XYZ
Central Chesapeake	H08081	1953	XYZ
Central Chesapeake	H08083	1953	XYZ
Lower Chesapeake	H07954	1953	XYZ
Central Chesapeake	H07911	1954	XYZ
Central Chesapeake	H08082	1954	XYZ
Central Chesapeake	H08185	1954	XYZ
Central Chesapeake	H08186	1954	XYZ
Central Chesapeake	H08187	1954	XYZ
Central Chesapeake	H08188	1954	XYZ
Central Chesapeake	H08189	1954	XYZ
Lower Chesapeake, Mouth	H08217	1954	XYZ
Lower Chesapeake, Mouth	H08218	1954	XYZ
Offshore Delmarva	H08218	1954	XYZ
Central Chesapeake	H08190	1955	XYZ
Central Chesapeake	H08191	1955	XYZ
Central Chesapeake	H08276	1955	XYZ
Central Chesapeake	H08277	1955	XYZ
Central Chesapeake	H08278	1955	XYZ
Central Chesapeake	H08280	1955	XYZ
Central Chesapeake	H08283	1956	XYZ
Central Chesapeake	H08347	1956	XYZ
Central Chesapeake	H08435	1956	XYZ
Central Chesapeake	H08405	1957	XYZ
Central Chesapeake	H08406	1957	XYZ
Central Chesapeake	H08407	1957	XYZ
Central Chesapeake	H08408	1957	XYZ
Central Chesapeake	H08445	1958	XYZ
Central Chesapeake	H08447	1958	XYZ
Central Chesapeake	H08448	1958	XYZ
Central Chesapeake	H08279	1959	XYZ
Central Chesapeake	H08494	1959	XYZ
Central Chesapeake	H08495	1959	XYZ
Central Chesapeake	H08496	1959	XYZ
Central Chesapeake	H08505	1959	XYZ
Central Chesapeake	H08506	1959	XYZ
Central Chesapeake	H08507	1959	XYZ
Central Chesapeake	H08547	1960	XYZ
Central Chesapeake	H08548	1960	XYZ
Central Chesapeake	H08549	1960	XYZ
Central Chesapeake	H08550	1960	XYZ

Central Chesapeake	H08551	1960	XYZ
Central Chesapeake	H08552	1960	XYZ
Central Chesapeake	H08553	1960	XYZ
Central Chesapeake	H08446	1961	XYZ
Central Chesapeake	H08610	1961	XYZ
Central Chesapeake	H08611	1961	XYZ
Central Chesapeake	H08612	1961	XYZ
Central Chesapeake	H08613	1961	XYZ
Central Chesapeake	H08614	1961	XYZ
Central Chesapeake	H08702	1962	XYZ
Central Chesapeake	H08703	1962	XYZ
Central Chesapeake	H08704	1962	XYZ
Central Chesapeake	H08705	1962	XYZ
Central Chesapeake	H08706	1962	XYZ
Lower Chesapeake, Mouth	H08724	1963	XYZ
Upper Chesapeake	H08859	1965	XYZ
Upper Chesapeake	H08860	1965	XYZ
Mid Layer	H08859	1965	XYZ
Mid Layer	H08860	1965	XYZ
Lower Chesapeake	H08878	1966	XYZ
Upper Chesapeake	H08874	1966	XYZ
Lower Chesapeake, Mouth	H09098	1969	XYZ
Offshore Delmarva	H09136	1970	XYZ
Offshore Delmarva	H09154	1970	XYZ
Offshore Delmarva	H09175	1970	XYZ
Offshore Delmarva	H09176	1970	XYZ
Delaware Bay	H09202	1971	XYZ
Delaware Bay	H09241	1971	XYZ
Offshore Delmarva	H09153	1971	XYZ
Central Chesapeake	H09301	1972	XYZ
Central Chesapeake	H09321	1972	XYZ
Central Chesapeake	H09322	1972	XYZ
Offshore Delmarva	H09311	1972	XYZ
Offshore Delmarva	H09312	1972	XYZ
Central Chesapeake	H09292	1973	XYZ
Central Chesapeake	H09324	1973	XYZ
Central Chesapeake	H09349	1974	XYZ
Central Chesapeake	H09479	1974	XYZ
Upper Chesapeake	H09453	1974	XYZ
Upper Chesapeake	H09454	1974	XYZ
Mid Layer	H09453	1974	XYZ

Mid Layer	H09454	1974	XYZ
Upper Chesapeake	H09582	1975	XYZ
Delaware Bay	H09533	1975	XYZ
Offshore Delmarva	H09578	1975	XYZ
Offshore Delmarva	H09579	1975	XYZ
Upper Chesapeake	H09562	1976	XYZ
Upper Chesapeake	H09563	1976	XYZ
Upper Chesapeake	H09564	1976	XYZ
Upper Chesapeake	H09566	1976	XYZ
Upper Chesapeake	H09643	1976	XYZ
Offshore Delmarva	H09629	1976	XYZ
Offshore Delmarva	H09639	1976	XYZ
Offshore Delmarva	H09640	1976	XYZ
Lower Chesapeake, Mouth	H09693	1977	XYZ
Offshore Delmarva	H09693	1977	XYZ
Offshore Delmarva	H09699	1977	XYZ
Offshore Delmarva	H09700	1977	XYZ
Offshore Delmarva	H09714	1977	XYZ
Offshore Delmarva	H09723	1977	XYZ
Offshore Delmarva	H09727	1977	XYZ
Offshore Delmarva	H09759	1978	XYZ
Offshore Delmarva	H09764	1978	XYZ
Offshore Delmarva	H09780	1978	XYZ
Offshore Delmarva	H09788	1978	XYZ
Offshore Delmarva	H09796	1978	XYZ
Lower Chesapeake	H09814	1980	XYZ
Lower Chesapeake, Mouth	H09901	1980	XYZ
Lower Chesapeake	H09910	1980	XYZ
Offshore Delmarva	H09901	1980	XYZ
Offshore Delmarva, Mouth	H09905	1980	XYZ
Offshore Delmarva, Mouth	H09919	1980	XYZ
Offshore Delmarva, Mouth	H09922	1980	XYZ
Mid Layer	H09880	1980	XYZ
Mid Layer	H09901	1980	XYZ
Mid Layer,	H09905	1980	XYZ
Mid Layer	H09910	1980	XYZ
Mid Layer	H09919	1980	XYZ
Mid Layer	H09922	1980	XYZ
Offshore Delmarva	H09948	1981	XYZ
Offshore Delmarva	H09955	1981	XYZ
Offshore Delmarva, Mouth	H09959	1981	XYZ

Offshore Delmarva, Mouth	H09961	1981	XYZ
Offshore Delmarva	H09962	1981	XYZ
Offshore Delmarva	H09969	1981	XYZ
Offshore Delmarva	H09970	1981	XYZ
Offshore Delmarva	H09972	1981	XYZ
Offshore Delmarva	H09978	1981	XYZ
Offshore Delmarva	H09980	1981	XYZ
Mid Layer	H09955	1981	XYZ
Offshore Delmarva	H09981	1982	XYZ
Offshore Delmarva	H10034	1982	XYZ
Offshore Delmarva	H10044	1982	XYZ
Offshore Delmarva	H10045	1982	XYZ
Offshore Delmarva	H10046	1982	XYZ
Offshore Delmarva	H10066	1982	XYZ
Delaware Bay	H10079	1983	XYZ
Delaware Bay	H10084	1983	XYZ
Delaware Bay	H10092	1983	XYZ
Delaware Bay	H10112	1983	XYZ
Mid Layer	H10116	1983	XYZ
Mid Layer	H10212	1983	XYZ
Delaware Bay	H10167	1984	XYZ
Mid Layer	H10127	1984	XYZ
Mid Layer	D00052	1985	XYZ
Delaware Bay	H10199	1986	XYZ
Delaware Bay	H10200	1986	XYZ
Delaware Bay	H10217	1986	XYZ
Mid Layer	H10193	1986	XYZ
Delaware Bay	D00081	1987	XYZ
Delaware Bay	H10255	1987	XYZ
Offshore Delmarva, Mouth	H10340	1990	XYZ
Offshore Delmarva, Mouth	H10341	1990	XYZ
Offshore Delmarva, Mouth	H10343	1990	XYZ
Offshore Delmarva, Mouth	H10356	1990	XYZ
Mid Layer	H10343	1990	XYZ
Mid Layer	H10356	1990	XYZ
Offshore Delmarva	H10439	1992	XYZ
Offshore Delmarva	H10444	1993	XYZ
Offshore Delmarva	H10446	1993	XYZ
Offshore Delmarva	H10464	1993	XYZ
Offshore Delmarva	H10475	1993	XYZ
Mid Layer	H10476	1993	XYZ

Mid Layer	H10518	1993	XYZ
Delaware Bay	H10234	1994	XYZ
Delaware Bay	H10537	1994	XYZ
Offshore Delmarva	H10241	1994	XYZ
Offshore Delmarva	H10476	1994	XYZ
Offshore Delmarva	H10533	1994	XYZ
Mid Layer	F00387	1994	XYZ
Mid Layer	H10622	1995	XYZ
Upper Chesapeake	H10691	1996	XYZ
Mid Layer	H10691	1996	XYZ
Upper Chesapeake	H10688	1997	XYZ
Mid Layer	H10652	1997	XYZ
Mid Layer	H10688	1997	XYZ
Mid Layer	H10752	1997	XYZ
Upper Chesapeake	H10703	1998	XYZ
Upper Chesapeake	H10757	1998	XYZ
Offshore Delmarva	D00129	1998	XYZ
Mid Layer	D00129	1998	XYZ
Mid Layer	H10703	1998	XYZ
Mid Layer	H10790	1998	XYZ
Mid Layer	H10823	1998	XYZ
Offshore Delmarva	H10854	1999	XYZ
Offshore Delmarva	H10931	1999	XYZ
Mid Layer	H10854	1999	XYZ
Mid Layer	H10859	1999	XYZ
Mid Layer	H10905	1999	XYZ
Mid Layer	H10926	1999	XYZ
Mid Layer	H10931	1999	XYZ
Mid Layer	H10934	2000	XYZ
Mid Layer	H10952	2000	XYZ
Mid Layer	H10989	2000	XYZ
Delaware Bay	H11022	2001	XYZ
Delaware Bay	H11023	2001	XYZ
Delaware Bay	H11070	2001	XYZ
Mid Layer	H11027	2001	XYZ
Upper Chesapeake	H11026	2002	XYZ
Delaware Bay	H11081	2002	XYZ
Mid Layer	F00474	2002	XYZ
Mid Layer	H11028	2002	XYZ
Mid Layer	H11104	2002	XYZ
Upper Layer	H11196	2002	XYZ

Upper Layer	H11302	2003	BAG
Mid Layer	H10945	2004	XYZ
Mid Layer	H11088	2004	XYZ
Upper Layer	H11207	2005	BAG
Upper Layer	H11301	2005	BAG
Upper Layer	H11401	2005	BAG
Upper Layer	H11402	2005	BAG
Upper Layer	H11407	2005	BAG
Upper Layer	H11450	2005	BAG
Upper Layer	H11205	2006	BAG
Upper Layer	H11206	2006	BAG
Upper Layer	H11303	2006	BAG
Upper Layer	H11323	2006	BAG
Upper Layer	H11503	2006	BAG
Upper Layer	H11504	2006	BAG
Upper Layer	H11505	2006	BAG
Upper Layer	H11529	2006	BAG
Upper Layer	H11535	2006	BAG
Upper Layer	H11554	2006	BAG
Upper Layer	H11555	2006	BAG
Upper Layer	H11568	2006	BAG
Upper Layer	H11598	2006	BAG
Upper Layer	H11295	2007	BAG
Upper Layer	H11530	2007	BAG
Upper Layer	H11603	2007	BAG
Upper Layer	H11647	2007	BAG
Upper Layer	H11648	2007	BAG
Upper Layer	H11649	2007	BAG
Upper Layer	H11650	2007	BAG
Upper Layer	H11651	2007	BAG
Upper Layer	H11652	2007	BAG
Upper Layer	H11653	2007	BAG
Upper Layer	H11655	2007	BAG
Upper Layer	H11656	2007	BAG
Upper Layer	H11657	2007	BAG
Upper Layer	H11788	2008	BAG
Upper Layer	H11789	2008	BAG
Upper Layer	H11872	2008	BAG
Upper Layer	H11873	2008	BAG
Upper Layer	H11874	2008	BAG
Upper Layer	H11918	2008	BAG

Upper Layer	H11992	2008	BAG
Upper Layer	D00151	2009	BAG
Upper Layer	H12001	2009	BAG
Upper Layer	H12002	2009	BAG
Upper Layer	H12003	2009	BAG
Upper Layer	H12037	2009	BAG
Upper Layer	H12038	2009	BAG
Upper Layer	H12039	2009	BAG
Upper Layer	H12040	2009	BAG
Upper Layer	H12041	2009	BAG
Upper Layer	H12042	2009	BAG
Upper Layer	H12043	2009	BAG
Upper Layer	H12044	2009	BAG
Upper Layer	H12045	2009	BAG
Upper Layer	H12091	2009	BAG
Upper Layer	H12100	2009	BAG
Upper Layer	F00583	2010	BAG
Upper Layer	F00586	2010	BAG
Upper Layer	H12092	2010	BAG
Upper Layer	H12093	2010	BAG
Upper Layer	H12094	2010	BAG
Upper Layer	H12161	2010	BAG
Upper Layer	H12180	2010	BAG
Upper Layer	H12181	2010	BAG
Upper Layer	H12200	2010	BAG
Upper Layer	H12201	2010	BAG
Upper Layer	H12202	2010	BAG
Upper Layer	H12203	2010	BAG
Upper Layer	H12238	2010	BAG
Upper Layer	H12239	2010	BAG
Upper Layer	H12240	2010	BAG
Upper Layer	H12241	2010	BAG
Upper Layer	H12160	2011	BAG
Upper Layer	H12267	2011	BAG
Upper Layer	H12277	2011	BAG
Upper Layer	H12286	2011	BAG
Upper Layer	H12306	2011	BAG
Upper Layer	H12307	2011	BAG
Upper Layer	H12309	2011	BAG
Upper Layer	H12315	2011	BAG
Upper Layer	H12316	2011	BAG

Upper Layer	H12321	2011	BAG
Upper Layer	H12336	2011	BAG
Upper Layer	H12337	2011	BAG
Upper Layer	H12338	2011	BAG
Upper Layer	H12339	2011	BAG
Upper Layer	H12341	2011	BAG
Upper Layer	H12342	2011	BAG
Upper Layer	H12343	2011	BAG
Upper Layer	H12346	2011	BAG
Upper Layer	F00622	2012	BAG
Upper Layer	H12304	2012	BAG
Upper Layer	H12367	2012	BAG
Upper Layer	H12394	2012	BAG
Upper Layer	H12395	2012	BAG
Upper Layer	H12396	2012	BAG
Upper Layer	H12397	2012	BAG
Upper Layer	H12421	2012	BAG
Upper Layer	H12423	2012	BAG
Upper Layer	H12503	2012	BAG
Upper Layer	H12305	2013	BAG
Mid Layer	H12559	2013	XYZ
Upper Layer	H12560	2013	BAG
Upper Layer	H12561	2013	BAG
Upper Layer	H12568	2013	BAG
Upper Layer	H12569	2013	BAG
Upper Layer	H12570	2013	BAG
Upper Layer	H12571	2013	BAG
Upper Layer	H12572	2013	BAG
Upper Layer	H12573	2013	BAG
Upper Layer	H12575	2013	BAG
Upper Layer	H12605	2013	BAG
Upper Layer	H12666	2014	BAG
Upper Layer	H12667	2014	BAG
Upper Layer	H12668	2014	BAG
Upper Layer	H12674	2014	BAG
Upper Layer	W00331	2014	BAG
Upper Layer	H12786	2015	BAG
Upper Layer	H12854	2015	BAG
Upper Layer	H12856	2015	BAG
Upper Layer	H12866	2016	BAG

Table 5: NOAA NOS downloaded hydrographic surveys from NCEI

APPENDIX B: AIS TRACKLINE MATLAB CODE

The AIS data used in the Chapter 2 analysis underwent a filtering process performed in MATLAB to limit the amount of erroneous data used. Each trackline for each year includes a mandatory vessel category number and a draft measurement in meters. As mentioned previously, significant errors can occur from submitted measurements with incorrect units (feet instead of meters). To fix these, vessel categories were used as a validity reference. For example, a vessel with a draft input of 20 m and a vessel category of 37 would almost never realistically occur. Using a combined knowledge of vessel classes and the depth of the study area, a table of maximum drafts for each vessel category was created and compared using MATLAB to the recorded drafts.

AIS DATA COMPOSITION AND PERCENTAGES

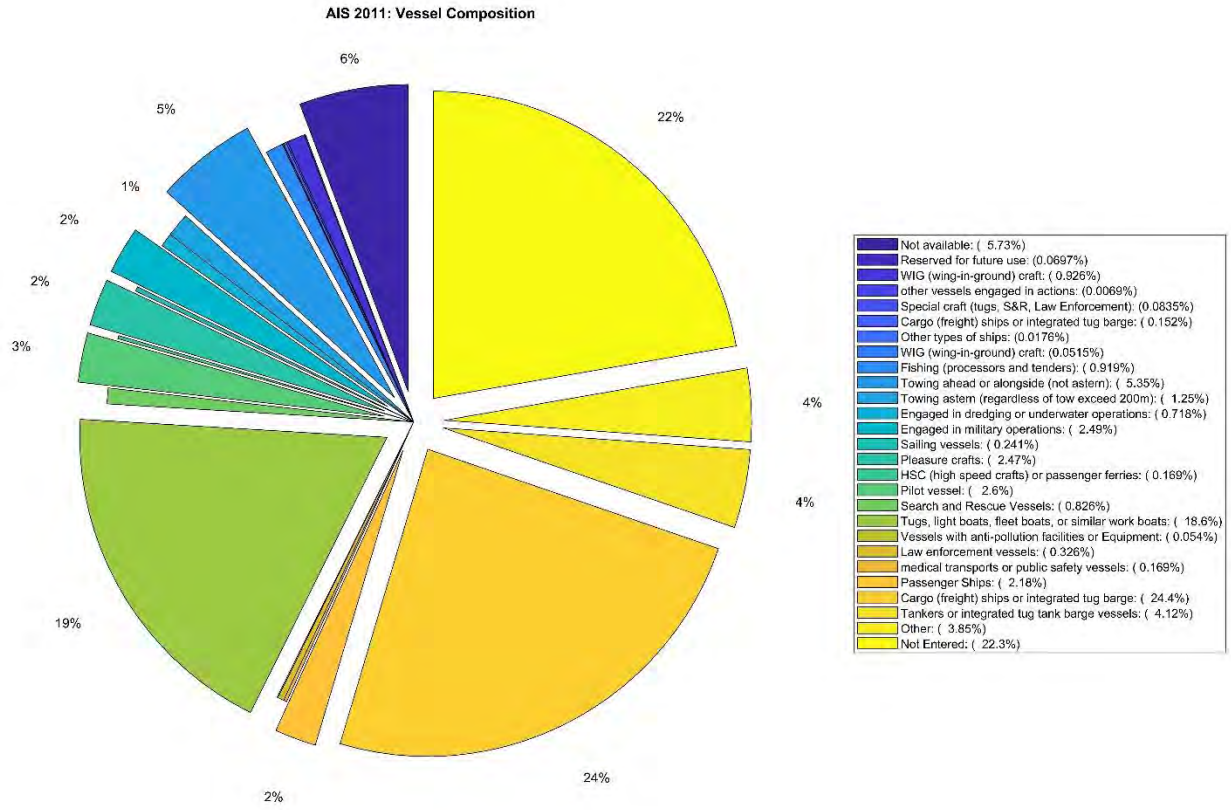

Figure 27: Original vessel composition of 2011 AIS tracklines.

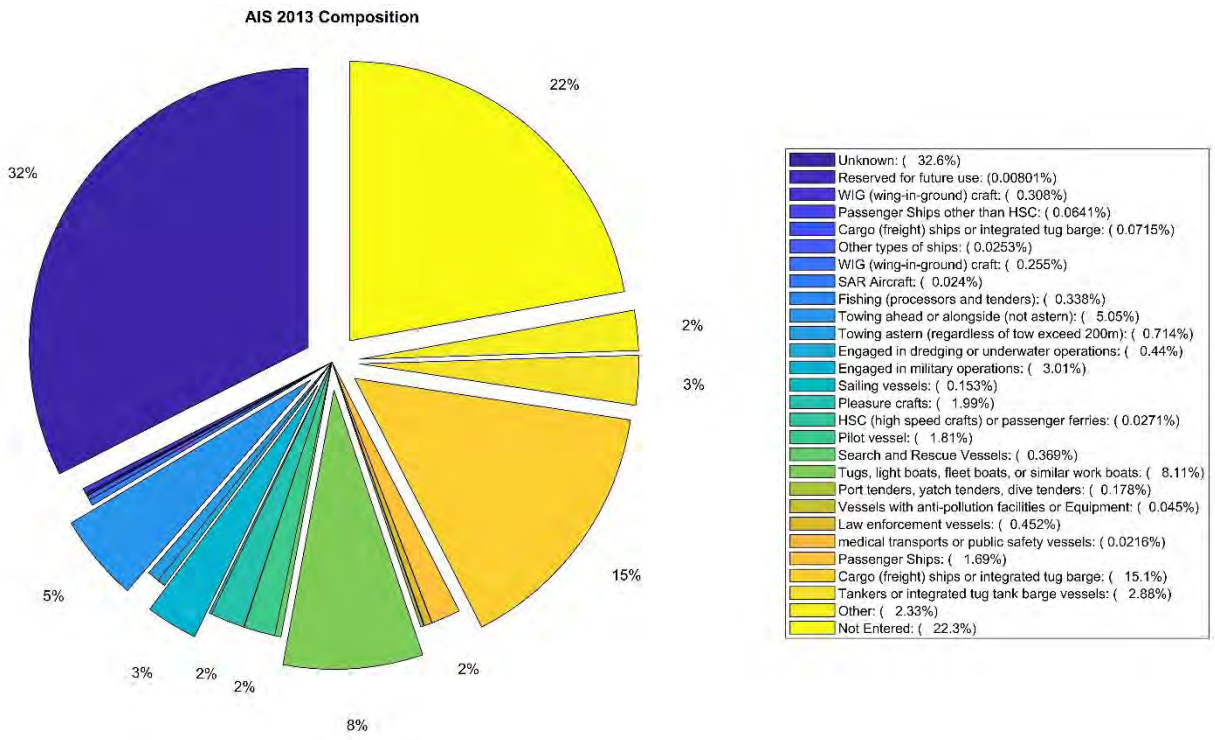

Figure 28: Original vessel composition for 2013 AIS tracklines.

AIS VESSEL DRAFT CORRECTION REFERENCE

The following values were used as a reference of maximum draft values for each AIS vessel category (number) in order to correct for errors with the metric-system conversion.

Number	Ship_type	Max_size (m)
0	Unknown	16
1	Reserved for future use	3
2	WIG (wing-in-ground) craft	3
3	other vessels engaged in actions	6.5
4	HSC (high speed crafts) or passenger ferries	6
5	Special craft (tugs, S&R, Law Enforcement)	7
6	Passenger Ships other than HSC	10
7	Cargo (freight) ships or integrated tug barge	16
8	Tankers or integrated tug tank barge vessels	16
9	Other types of ships	16
10-19	Reserved for future use	3
20-28	WIG (wing-in-ground) craft	3
29	SAR Aircraft	1
30	Fishing (processors and tenders)	8
31	Towing ahead or alongside (not astern)	6.5
32	Towing astern (regardless of tow exceed 200m)	6.5
33	Engaged in dredging or underwater operations	16
34	Engaged in diving operations	8.5
35	Engaged in military operations	16
36	Sailing vessels	10
37	Pleasure crafts	8
38-39	Reserved for future use	3
40-49	HSC (high speed crafts) or passenger ferries	6
50	Pilot vessel	3
51	Search and Rescue Vessels	7
52	Tugs, light boats, fleet boats, or similar work boats	9.5
53	Port tenders, yacht tenders, dive tenders	3
54	Vessels with anti-pollution facilities or Equipment	5
55	Law enforcement vessels	3
56-57	local vessels	3
58	medical transports or public safety vessels	10
59	ships according to RR Resolution No.18	10
60-69	Passenger Ships	10
70-79	Cargo (freight) ships or integrated tug barge	16
80-89	Tankers or integrated tug tank barge vessels	16
90-255	Other	16

Table 6: List of AIS vessel types and assigned maximum draft limits

Table 6 was turned into a MATLAB .mat file named AIS_Vessel.mat.

Both AIS2011.mat and AIS2013.mat have the following structure:

Figure 29: AIS trackline MATLAB structure formats.

CODE

AIS_validation.m

```
%% AIS DATA RECTIFICATION

% The follow code outlines the steps taken to ensure the vessel draft values % for each entry are recorded in meters, and not feet.

%Load data
load('AIS2011.mat'); %Load previously parsed 2011 Chesapeake Bay (and surrounding areas) AIS trackline metadata
load('AIS2013.mat'); %Load previously parsed 2013 Chesapeake Bay (and surrounding areas) AIS trackline metadata
load('AIS_vessel.mat'); %Load maximum draft measurements (in meters) by vessel category

%feet per meter
meter= 3.28084; %feet to meter conversion

%% AIS 2011 tracklines

%allocate space to record number of edits per category
edit=zeros(length(Vessel.type),3);

% function does not account for NAN values
[AIS2011.draft2,edit]=AIS_analyze(Vessel.type, AIS2011.vessel, AIS2011.draft, Vessel.draft, meter); %AIS 2011 analysis

AIS2011.draft2=AIS2011.draft2'; %flip output

%validate results
true(1,1)=length(AIS2011.vessel)-(sum(edit(:,3))+sum(isnan(AIS2011.vessel)));


%% AIS 2013 tracklines

%allocate space to record number of edits per category
edit13=zeros(length(Vessel.type),3);

% function does not account for NAN values
[AIS2013.draft2,edit13]=AIS_analyze(Vessel.type, AIS2013.vessel, AIS2013.draft, Vessel.draft, meter); %AIS 2013 analysis

AIS2013.draft2=AIS2013.draft2'; %flip output

%validate results
true(1,2)=length(AIS2013.vessel)-(sum(edit13(:,3))+sum(isnan(AIS2013.vessel)));
```

AIS_analyze.m

```
function [output, edit]= AIS_analyze(vessel_type, AIS_vessel, AIS_draft, Vessel_draft, unit)

for i=1:length(vessel_type)

    %attribute r with vessel category
    r=vessel_type(i);

    %determine where the vessel type matches and where the recorded draft
    %exceeds allowable vessel draft for the category
    true=find(AIS_vessel==r & AIS_draft>Vessel_draft(i));

    %pull the recorded AIS drafts
    f=AIS_draft(true);

    %divide into meters
    f(:,2)=f(:,1)./unit;

    %add the edited values back into new vector
    output(true)=f(:,2);

    %grab the other values for this category
    false=find(AIS_vessel==r & AIS_draft<=Vessel_draft(i));

    %place these values into the new vector
    output(false)=AIS_draft(false);

    edit(i,1)=length(true); %record the number of edited draft values for each category
    edit(i,2)=length(false); %record the number of UNEDITED draft values
    edit(i,3)=sum(AIS_vessel==r); %total sum of values in each category
end

end
```

APPENDIX C: GEOSTATISTICAL ANALYSIS

SUMMARY

Archive hydrographic survey data are sparse, making comparison with modern datasets difficult (Calder, 2006; Dorst, 2009; Wong *et al*., 2013). Traditionally, these sparse data are interpolated into coarse-resolution surfaces that unintentionally omit navigationally significant bathymetric features for such comparisons and can ultimately lead to misinterpretations of bathymetric change (Van Der Wal and Pye, 2003). Errors for these types of calculations depends not only the uncertainty with the data, but also with interpolation technique (Elmore *et al*., 2009; Aykut *et al*., 2013; Amante and Eakins, 2016). As most of these archive surveys lack paired bathymetry and uncertainty, the uncertainty is hard to estimate (Calder, 2006; Calder, 2015; Ladner *et al*., 2017), allowing for large uncertainties to develop in end-products.

There are a number of interpolation techniques, but kriging is particularly popular in the remote sensing and ocean mapping world. Kriging is an iterative geostatisical interpolation technique first developed by Daniel Krige (1951) that uses spatial weighting and linear regression to determine the optimal value and its certainty for a given location (Cressie, 1990; Oliver and Webster, 2014). Specifically, kriging uses statistical models to compare each data point with surrounding data in order to better predict the voids. Since the data are statistically compared, estimates of accuracy are possible for the resulting surface (Calder, 2006; Oliver and Webster, 2014; ESRI: How Kriging Works Doc), making kriging ideal for uncertainty-based products like those outlined in this thesis.

As this study was almost entirely performed in ESRI ArcGIS 10.5.1., it is important to understand the kriging implementation. The general equation is: $\hat{Z}(s_0) = \sum_{i=1}^{N} \lambda_i Z(s_i)$ (ESRI: How Kriging Works Doc). Where $Z(s_i)$ is the measured value at the ith location, λ_i is an

unknown weight for the measured value at the ith location, s_0 is the prediction location, and N is the number of measured values.

Appropriate kriging and variogram parameters must be specified a priori. Each of these parameters contributes to λ_i, can influence the output surface, and can be changed to fit the purpose of the analysis. These parameters include:

- **Kriging method**: Ordinary or Universal
- **Semivariogram Model**: Gaussian, Linear, Exponential, Circular, Spherical
- **Lag Size**: distance with which data pairs exist
- **Major range**: The x-axis distance to where the model evens out
- **Nugget**: Where the semivariogram model meets the y-axis
- **Partial Sill**: The y-axis values above the nugget to the y-value where the model evens out
- **Output Cell Size**: Determines resolution of surface output

For this study, we used ESRI's ArcGIS 'Geostatistical Wizard' tool in the Geostatistcal Analyst toolbox. Each data group were run through the Wizard, and optimal settings were determined (Table 2, Chapter 2). As is standard practice, the Wizard uses z-value residuals to calculate the semivariogram graph. Additionally, the Wizard automatically optimizes the parameters for processing speed. In situations where the automatic values are not necessarily optimal for a user's specific needs, the user-interface becomes necessary.

For each of the following sub-sections in this Appendix, a figure of four subplots show the empirical semivariogram graph and chosen model, the covariance graph and model, the predicted vs. measurement errors graph, and standard error graphs, all vital to choosing the kriging

parameters. A table of the data extent and prediction errors determined by the Wizard are also included for each subsection. After the parameters were determined (Table 2, Chapter 2), each group was interpolated using the ESRI ArcGIS 'Kriging' tool in the Spatial Analyst toolbox. All data were interpolated using Ordinary Kriging methods. As kriging does not necessarily maintain the true measured data points (Amante and Eakins, 2016), a final interpolated vs. measurement depth graph is included to show the errors in the final interpolated depths at each known location.

It is important to note that there are other methods and parameters to choose for the kriging of each subgroup, and the methods and parameters outlined in this thesis may in fact be inferior to those other choices. That said, the purpose of this work was to outline potential improvements to existing procedures and to provide a proof of concept. Future work could and should focus on determining and validating the best possible kriging parameters for the data.

DELAWARE BAY

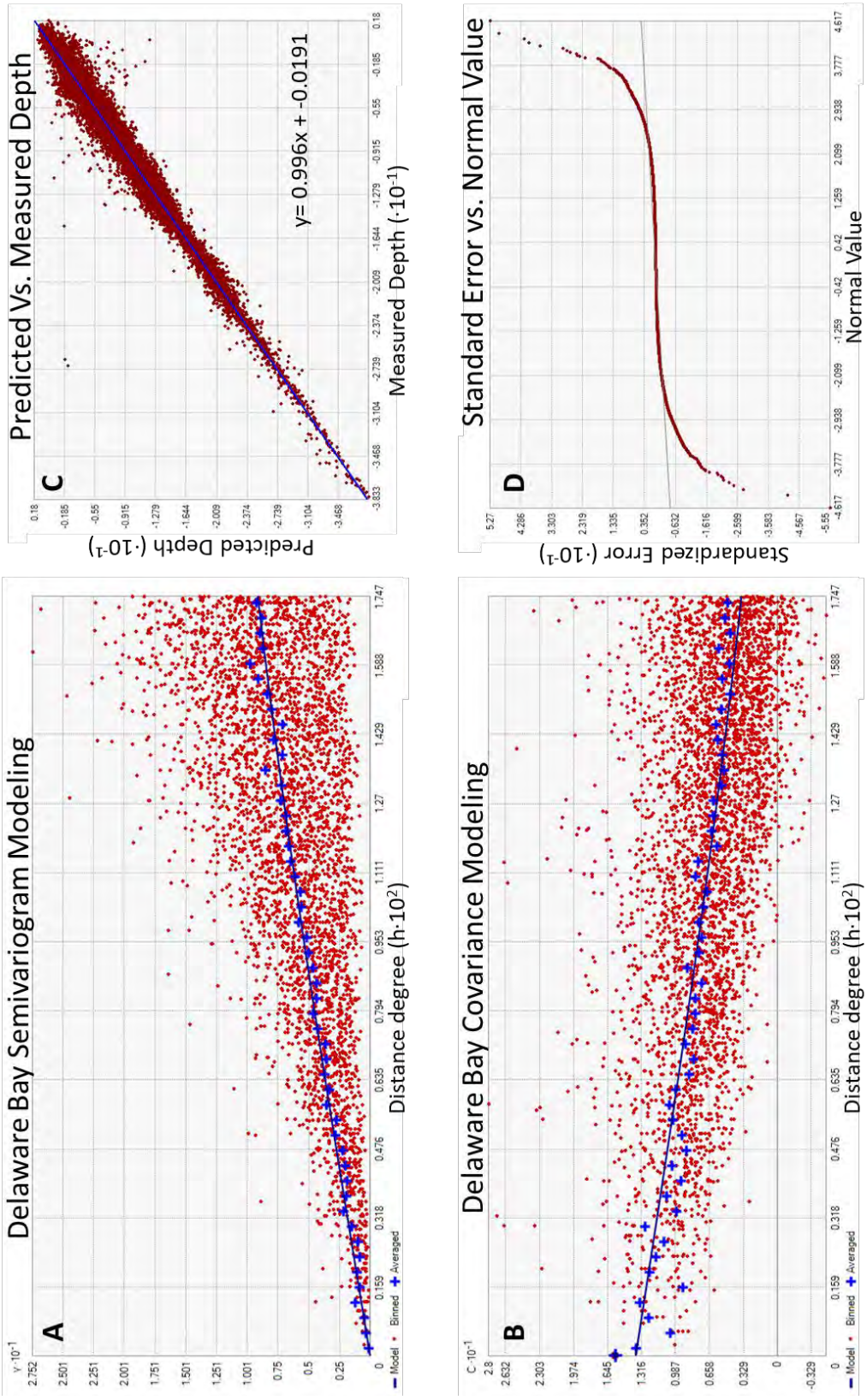

Figure 30: Lower-layer Delaware Bay graphs used to determine kriging parameters. (A) Empirical Semivariogram Spherical Model comparison. (B) Covariance Spherical Model comparison. Plots (A) and (B) incorporate binned (red dots) and average values (blue crosses) of the data within the set lag size to help the user determine which statistical model (solid blue line) fits the each data set the best. (C) Predicted depth vs. measured depth graph with trend line equation that shows how much error could occur at known data points using the parameters chosen. (D) Standardized error vs. normal value graph.

Location	**Delaware Bay**
Northeast Extent	39.6603 N, 74.887 W
Southwest Extent	38.7887 N, 75.619 W
Number of Points	256,744
Predicted Errors	
Mean	0.001918
Root-Mean-Square	0.341532
Mean Standardized	0.002061
RMS Standardized	0.847683
Average Standard Error	0.563800

Table 7: Lower-level Delaware Bay extent and kriging bathymetry prediction errors.

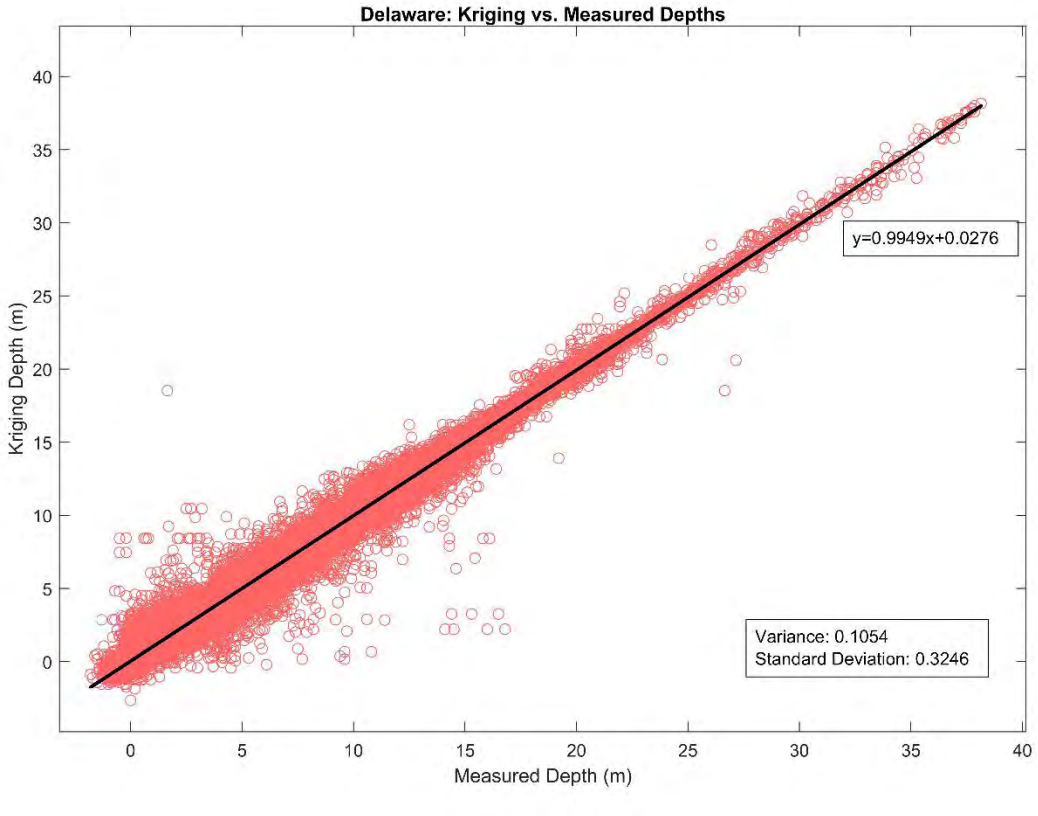

Figure 31: Delaware Bay trend between kriging interpolated depth and measured depths.

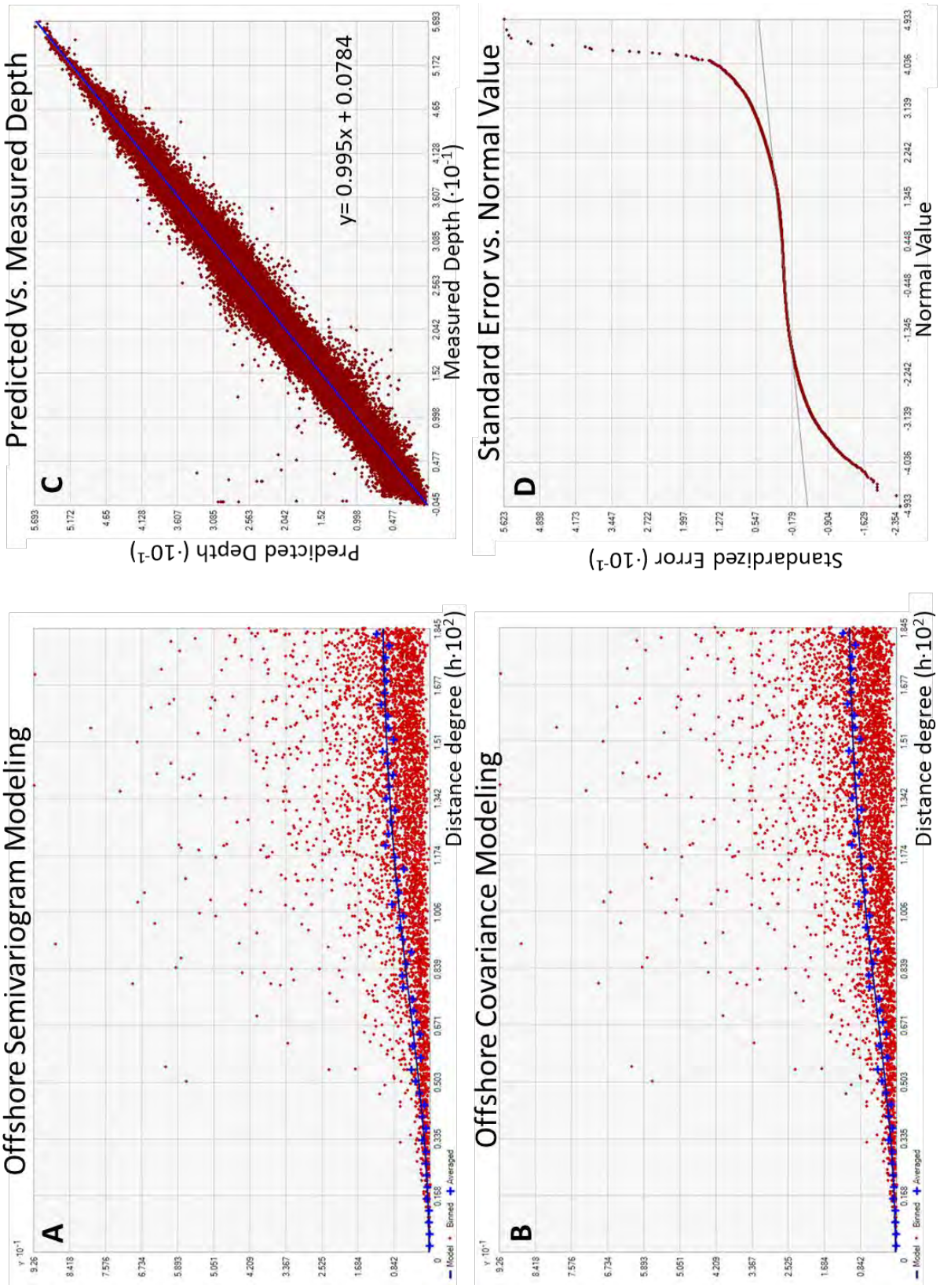
A
Offshore Semivariogram Modeling
Distance degree (h·10²)
B
Offshore Covariance Modeling
Distance degree (h·10²)
C
Predicted Vs. Measured Depth
y= 0.995x + 0.0784
Measured Depth (·10⁻¹)
Predicted Depth (·10⁻¹)
D
Standard Error vs. Normal Value
Normal Value
Standardized Error (·10⁻¹)

Figure 32: Lower-layer Offshore graphs used to determine kriging parameters. (A) Empirical Semivariogram Gaussian Model comparison. (B) Covariance Gaussian Model comparison. Plots (A) and (B) incorporate binned (red dots) and average values (blue crosses) of the data within the set lag size to help the user determine which statistical model (solid blue line) fits the each data set the best. (C) Predicted depth vs. measured depth graph with trend line equation that shows how much error could occur at known data points using the parameters chosen. (D) Standardized error vs. normal value graph.

Location	**Offshore**
Northeast Extent	39.01624 N, 74.1591 W
Southwest Extent	36.4954 N, 76.1197 W
Number of Points	1,233,936
Predicted Errors	
Mean	0.0021021
Root-Mean-Square	0.5921259
Mean Standardized	0.0039846
RMS Standardized	1.0636332
Average Standard Error	0.5538353

Table 8: Lower-layer Offshore region extents and kriging bathymetry prediction errors.

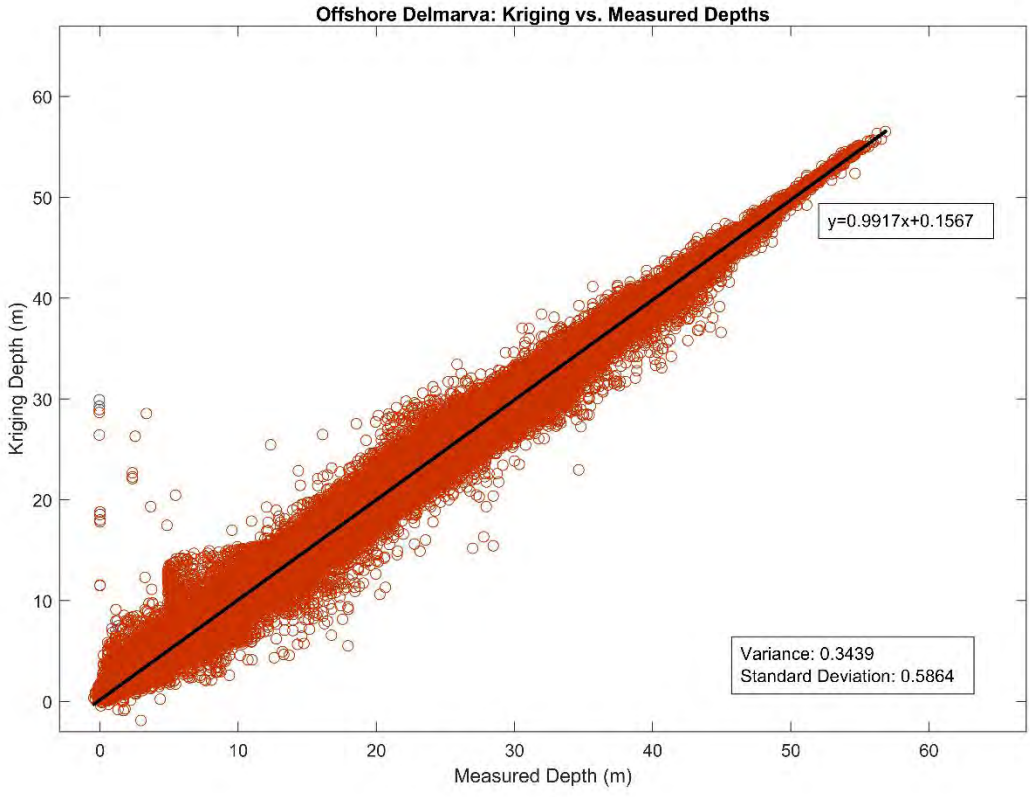

Figure 33: Offshore region estimated kriging trend between interpolated depths and measured depths.

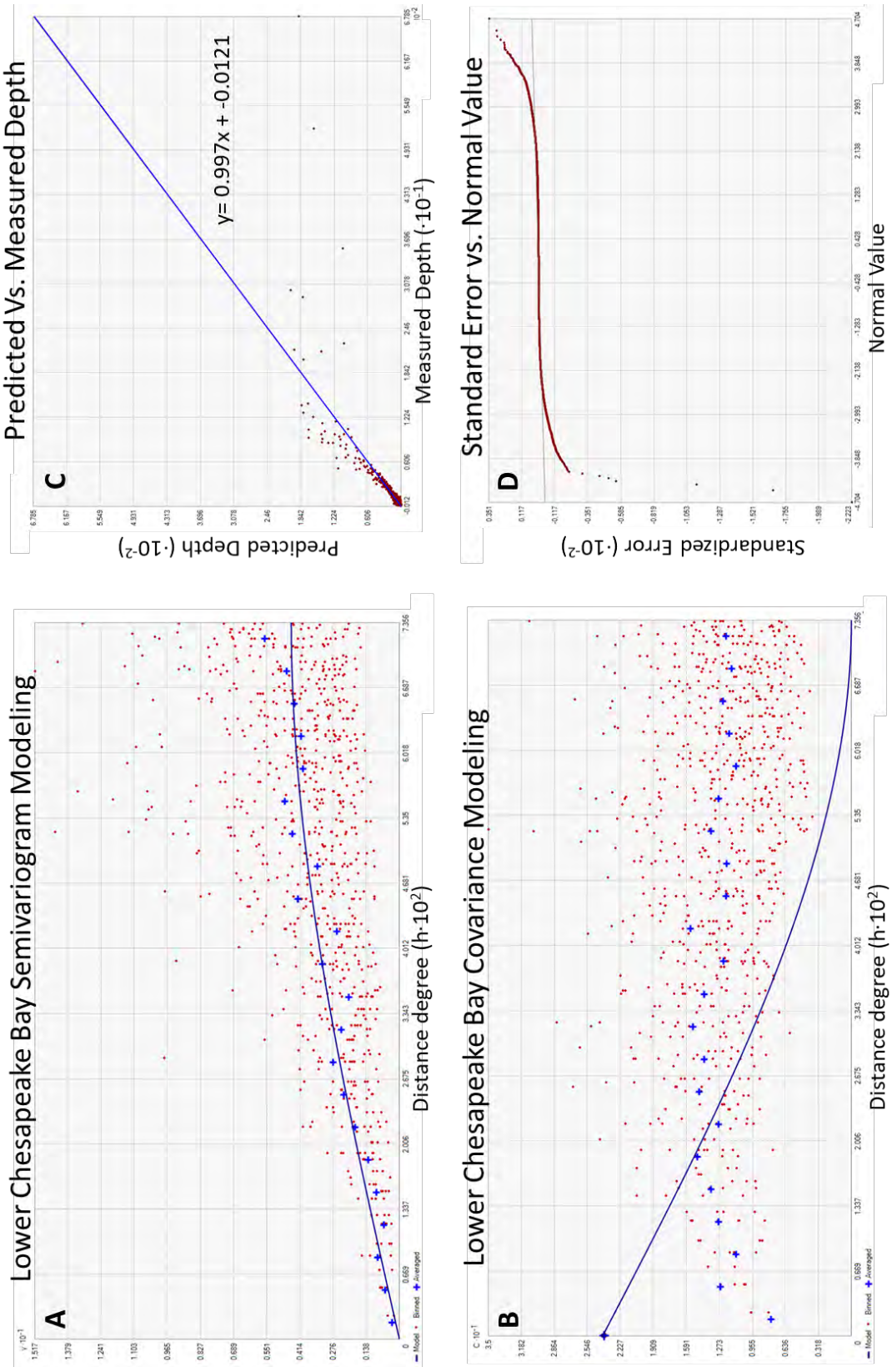
A
Lower Chesapeake Bay Semivariogram Modeling
Distance degree (h-10²)
B
Lower Chesapeake Bay Covariance Modeling
Distance degree (h-10²)
C
Predicted Vs. Measured Depth
y= 0.997x + -0.0121
Predicted Depth (·10-2)
Measured Depth (·10-1)
D
Standard Error vs. Normal Value
Standardized Error (·10-2)
Normal Value

Figure 34: Lower-layer Lower Chesapeake Bay graphs used to determine kriging parameters. (A) Empirical Semivariogram Spherical Model comparison. (B) Covariance Spherical Model comparison. (Plots (A) and (B) incorporate binned (red dots) and average values (blue crosses) of the data within the set lag size to help the user determine which statistical model (solid blue line) fits the each data set the best. (C) Predicted depth vs. measured depth graph with trend line equation that shows how much error could occur at known data points using the parameters chosen. (D) Standardized error vs. normal value graph.

Location	**Lower Chesapeake Bay**
Northeast Extent	37.31198 N, 75.70812 W
Southwest Extent	36.7893 N, 77.03376 W
Number of Points	391,881
Predicted Errors	
Mean	-0.0009533
Root-Mean-Square	1.21097041
Mean Standardized	-0.0007441
RMS Standardized	0.91606101
Average Standard Error	0.57710673

Table 9: Lower-layer Lower Chesapeake Bay extent and kriging bathymetry prediction errors.

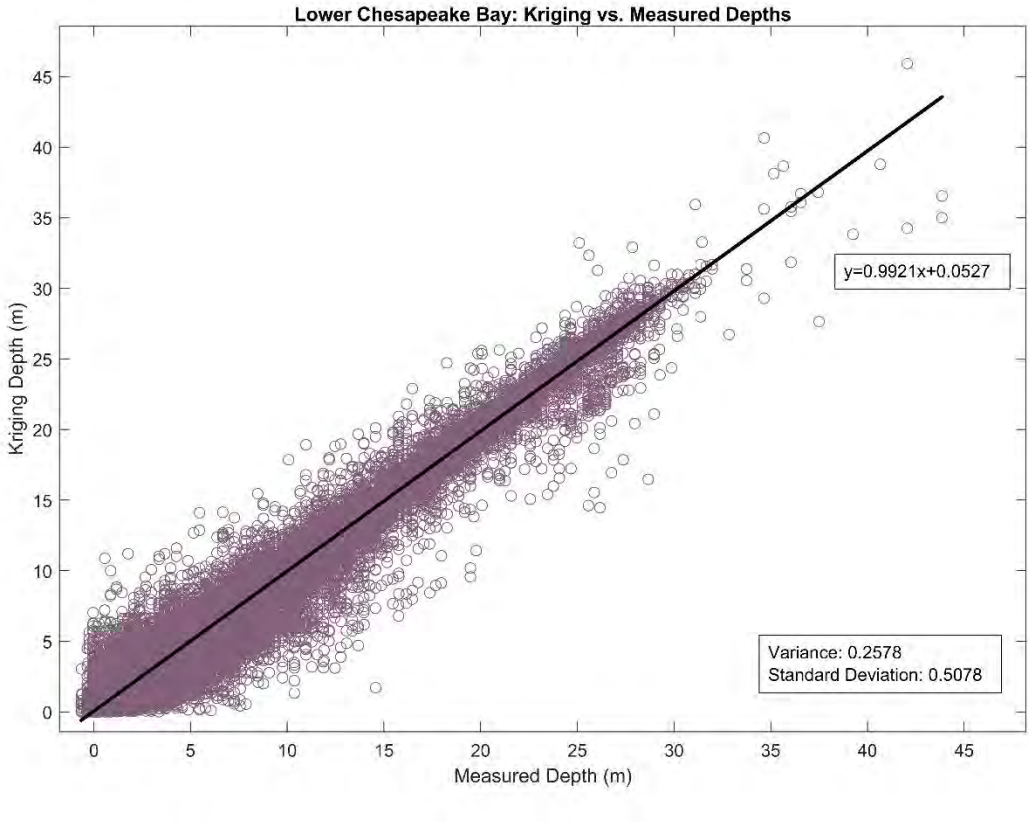

Figure 35: Lower Chesapeake Bay interpolated depths vs. measured depths.

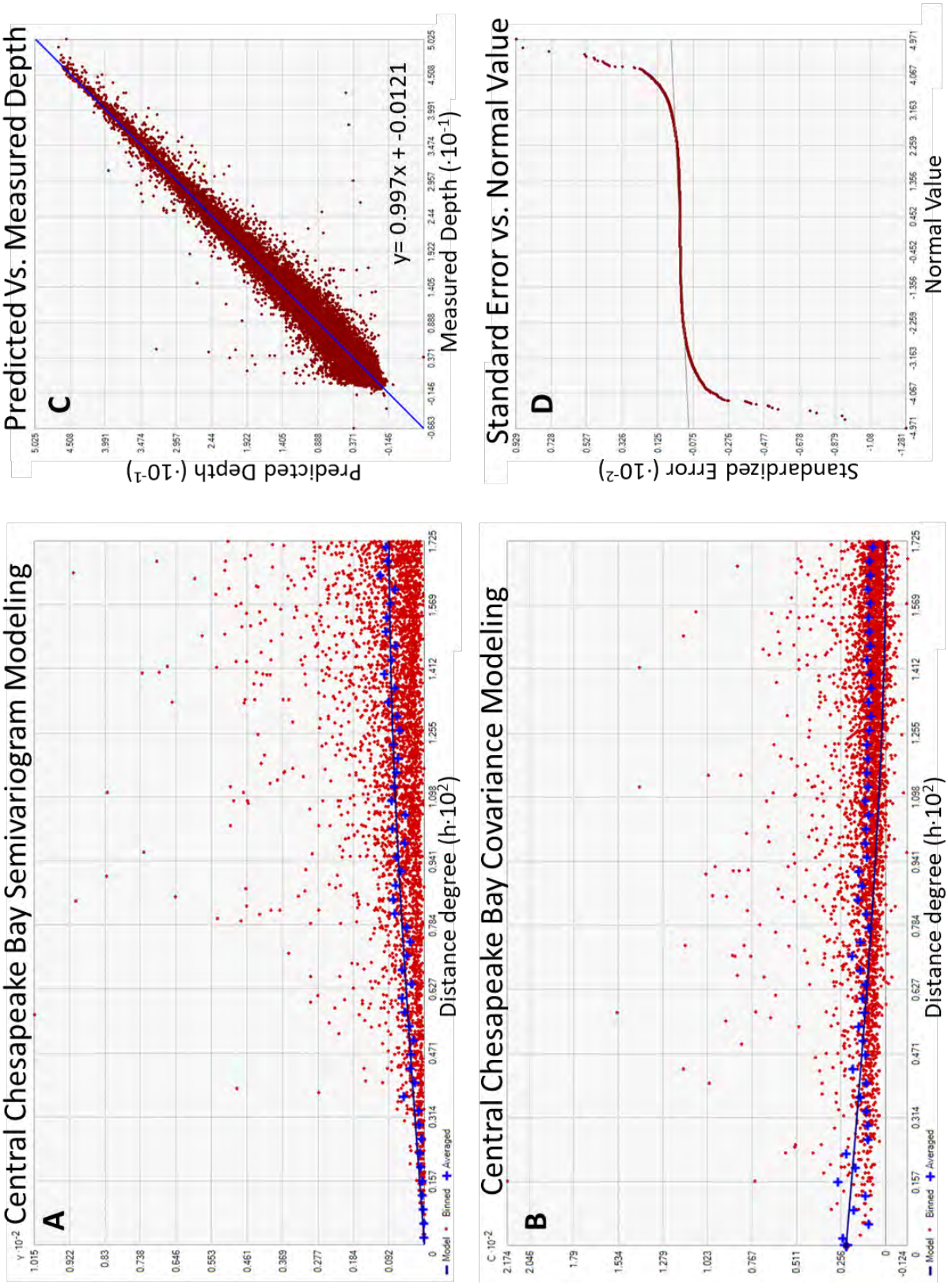
A
Central Chesapeake Bay Semivariogram Modeling
Distance degree (h·10²)
Model
Binned
Averaged
B
Central Chesapeake Bay Covariance Modeling
Distance degree (h·10²)
Model
Binned
Averaged
C
Predicted Vs. Measured Depth
y= 0.997x + -0.0121
Measured Depth (·10⁻¹)
Predicted Depth (·10⁻¹)
D
Standard Error vs. Normal Value
Normal Value
Standardized Error (·10⁻²)

Figure 36: Lower-layer Central Chesapeake Bay graphs used to determine kriging parameters. (A) Empirical Semivariogram Spherical Model comparison. (B) Covariance Spherical Model comparison. Plots (A) and (B) incorporate binned (red dots) and average values (blue crosses) of the data within the set lag size to help the user determine which statistical model (solid blue line) fits the each data set the best. (C) Predicted depth vs. measured depth graph with trend line equation that shows how much error could occur at known data points using the parameters chosen. (D) Standardized error vs. normal value graph.

Location	**Central Chesapeake Bay**
Northeast Extent	38.7932 N, 75.5712 W
Southwest Extent	36.9239 N, 77.3877 W
Number of Points	1,498,565
Predicted Errors	
Mean	6.3576838e-005
Root-Mean-Square	0.3459982
Mean Standardized	-9.0026693e-005
RMS Standardized	0.7200176
Average Standard Error	0.5843674

Table 10: Lower-layer Central Chesapeake Bay extent and kriging bathymetry prediction errors.

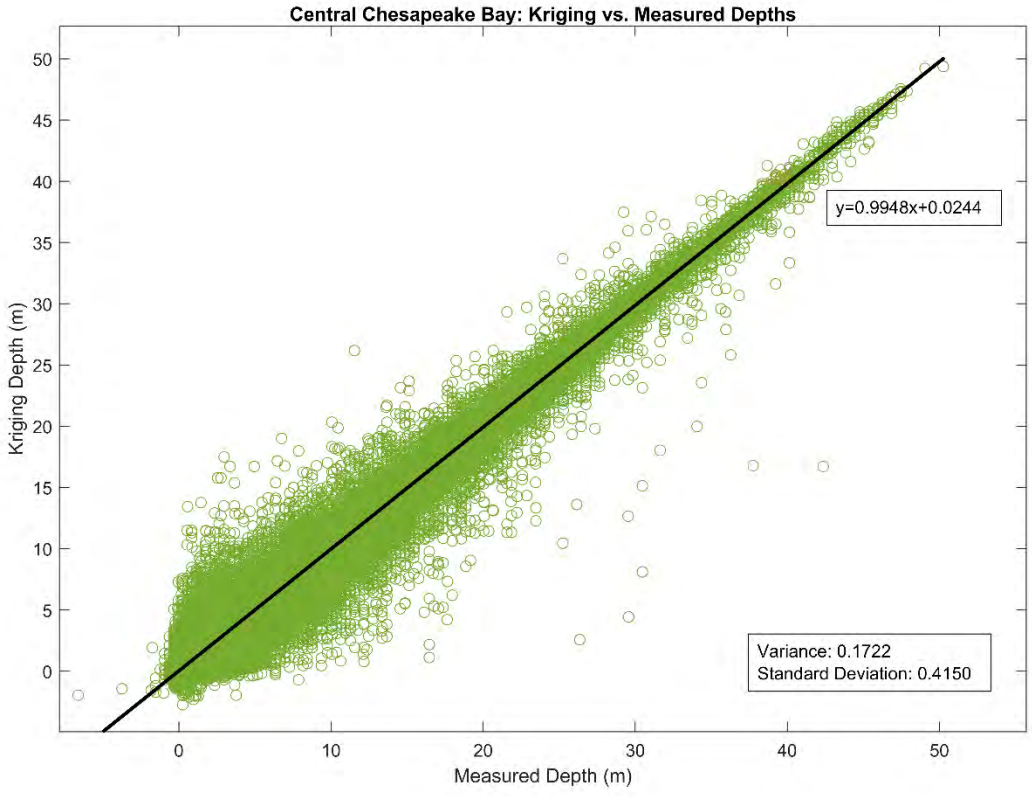

Figure 37: Central Chesapeake Bay kriging interpolated depths versus measured depths.

UPPER CHESAPEAKE BAY

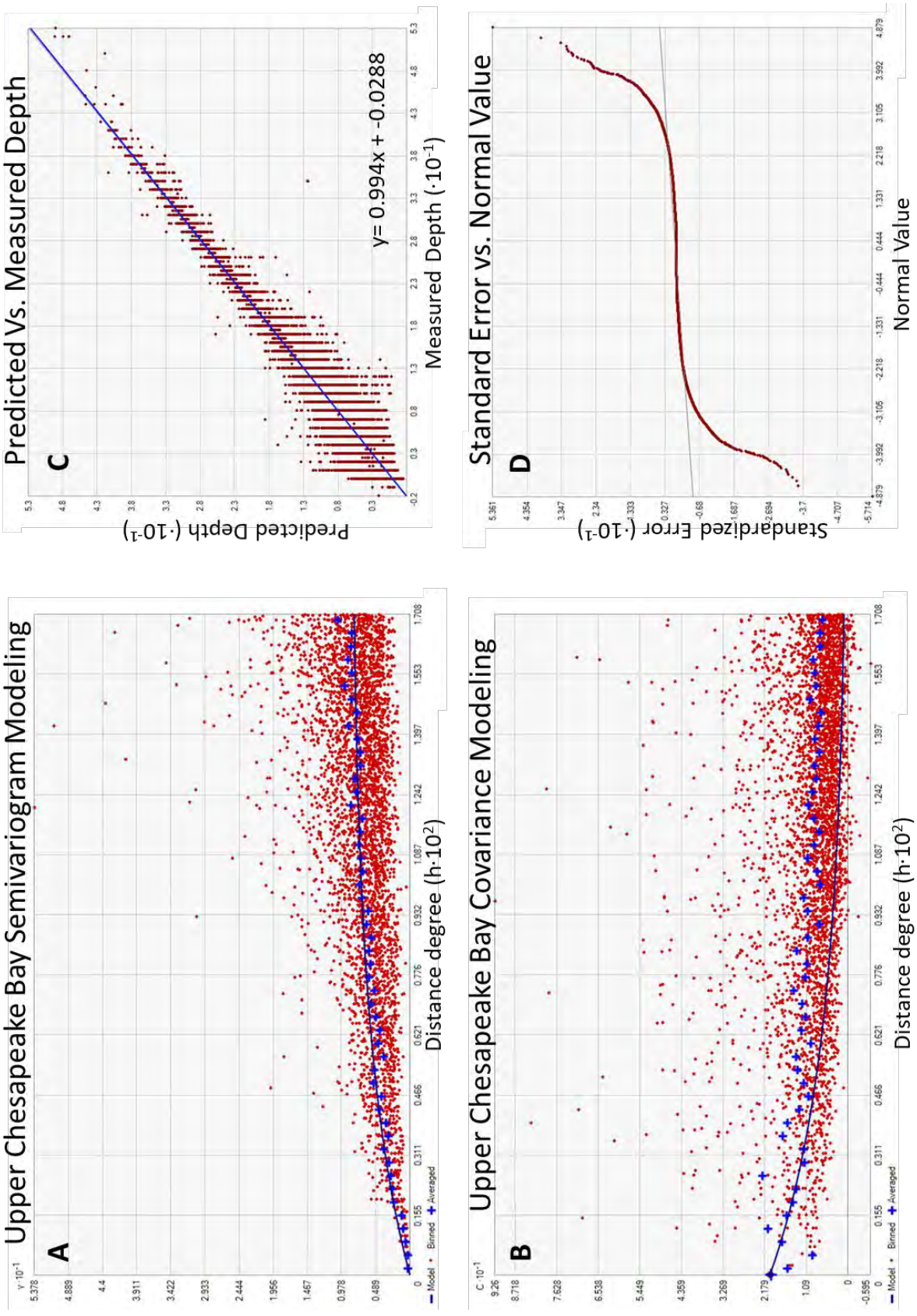

Figure 38: Lower-layer Upper Chesapeake Bay graphs used to determine kriging parameters. (A) Empirical Semivariogram Exponential Model comparison. (B) Covariance Exponential Model comparison. Plots (A) and (B) incorporate binned (red dots) and average values (blue crosses) of the data within the set lag size to help the user determine which statistical model (solid blue line) fits the each data set the best. (C) Predicted depth vs. measured depth graph with trend line equation that shows how much error could occur at known data points using the parameters chosen. (D) Standardized error vs. normal value graph.

Location	**Upper Chesapeake Bay**
Northeast Extent	39.6128 N, 75.8074 W
Southwest Extent	38.3596 N, 76.632 W
Number of Points	937,990
Predicted Errors	
Mean	0.0003233
Root-Mean-Square	0.4628166
Mean Standardized	0.0001100
RMS Standardized	0.8191227
Average Standard Error	0.6978359

Table 11: Lower-layer Upper Chesapeake Bay extent and kriging bathymetry prediction errors.

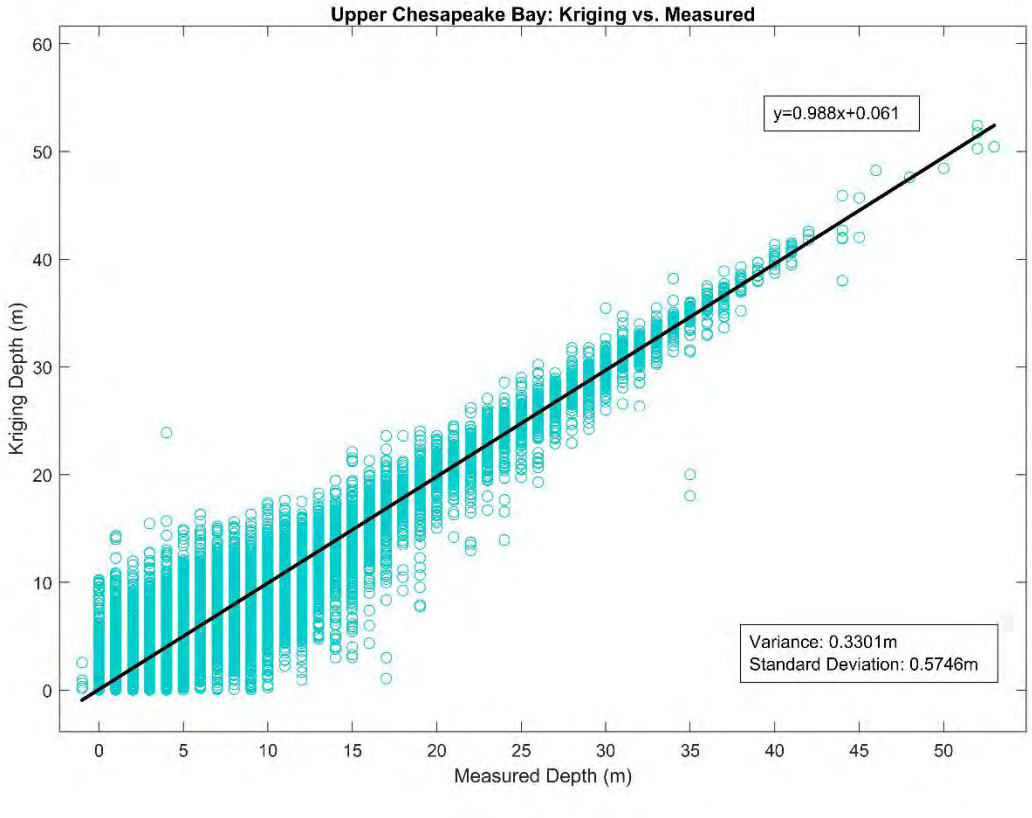

Figure 39: Upper Chesapeake Bay kriging interpolated depths versus measured depths.

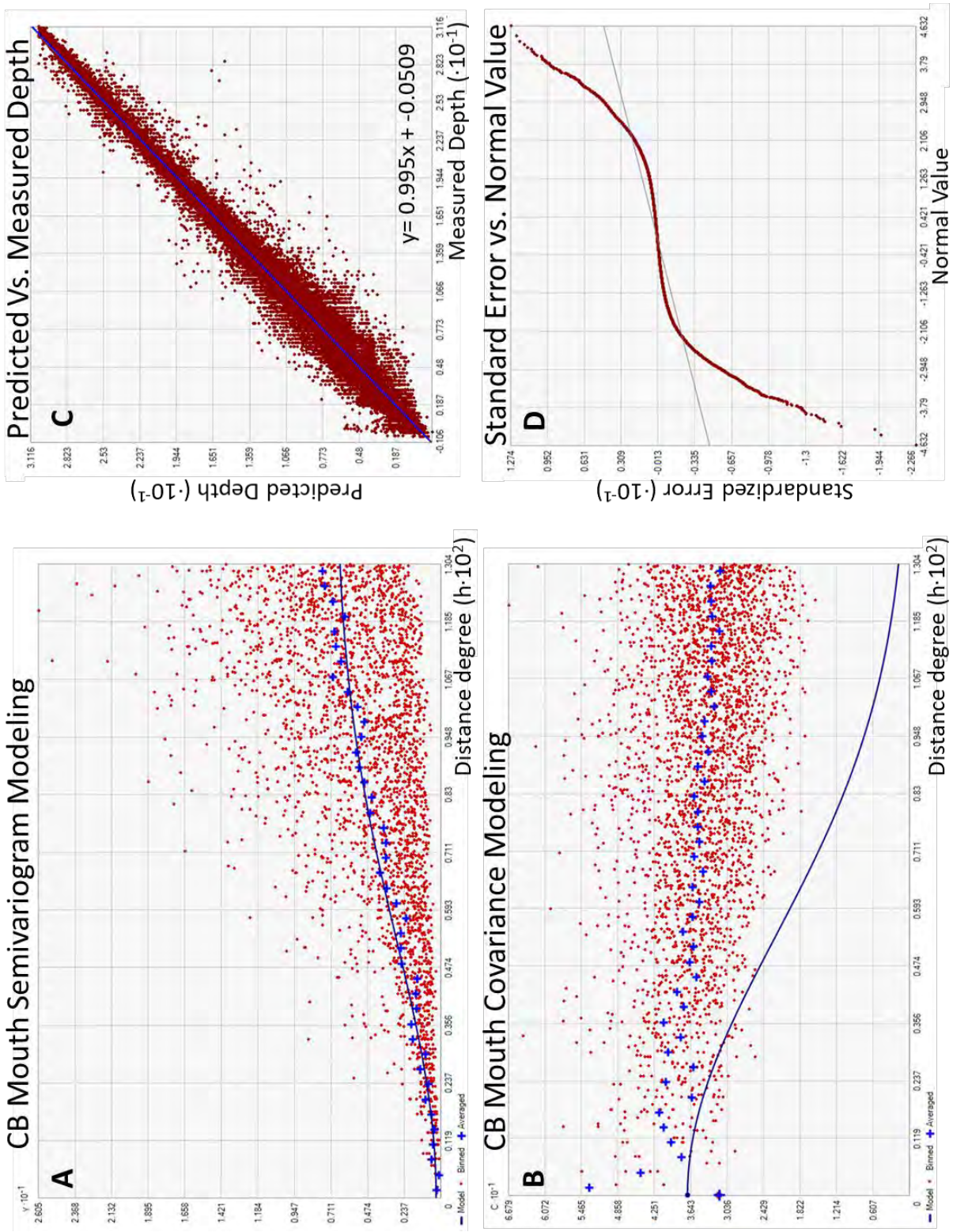

Figure 40: Lower-layer Chesapeake Bay Mouth graphs used to determine kriging parameters. (A) Empirical Semivariogram Guassian Model comparison. (B) Covariance Guassian Model comparison. Plots (A) and (B) incorporate binned (red dots) and average values (blue crosses) of the data within the set lag size to help the user determine which statistical model (solid blue line)

fits the each data set the best. (C) Predicted depth vs. measured depth graph with trend line equation that shows how much error could occur at known data points using the parameters chosen. (D) Standardized error vs. normal value graph.

Location	**Mouth Chesapeake Bay**
Northeast Extent	37.1960 N, 75.7114 W
Southwest Extent	36.8162 N, 76.2601 W
Number of Points	276,734
Predicted Errors	
Mean	-0.00248597
Root-Mean-Square	0.47344879
Mean Standardized	-0.00444149
RMS Standardized	0.83314642
Average Standard Error	0.56902197

Table 12: Lower-layer Mouth of Chesapeake Bay extent and kriging bathymetry prediction errors.

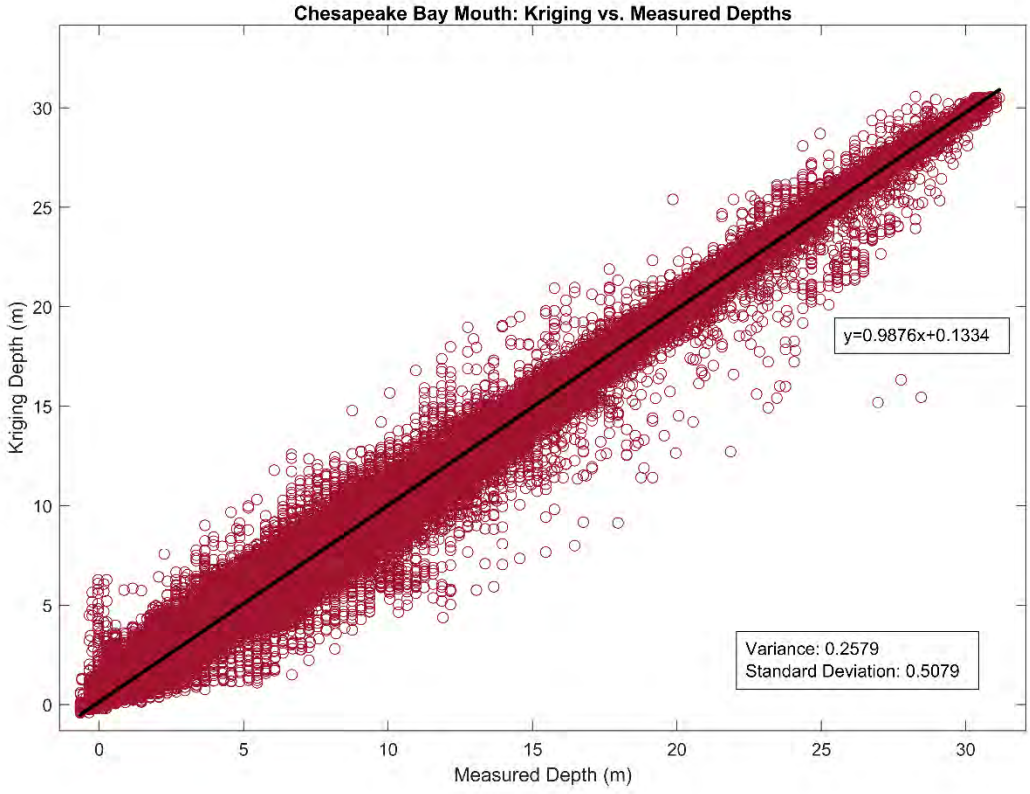

Figure 41: Mouth of Chesapeake Bay kriging interpolated depths versus measured depths.

MID-LAYER: LOWER CHESAPEAKE BAY

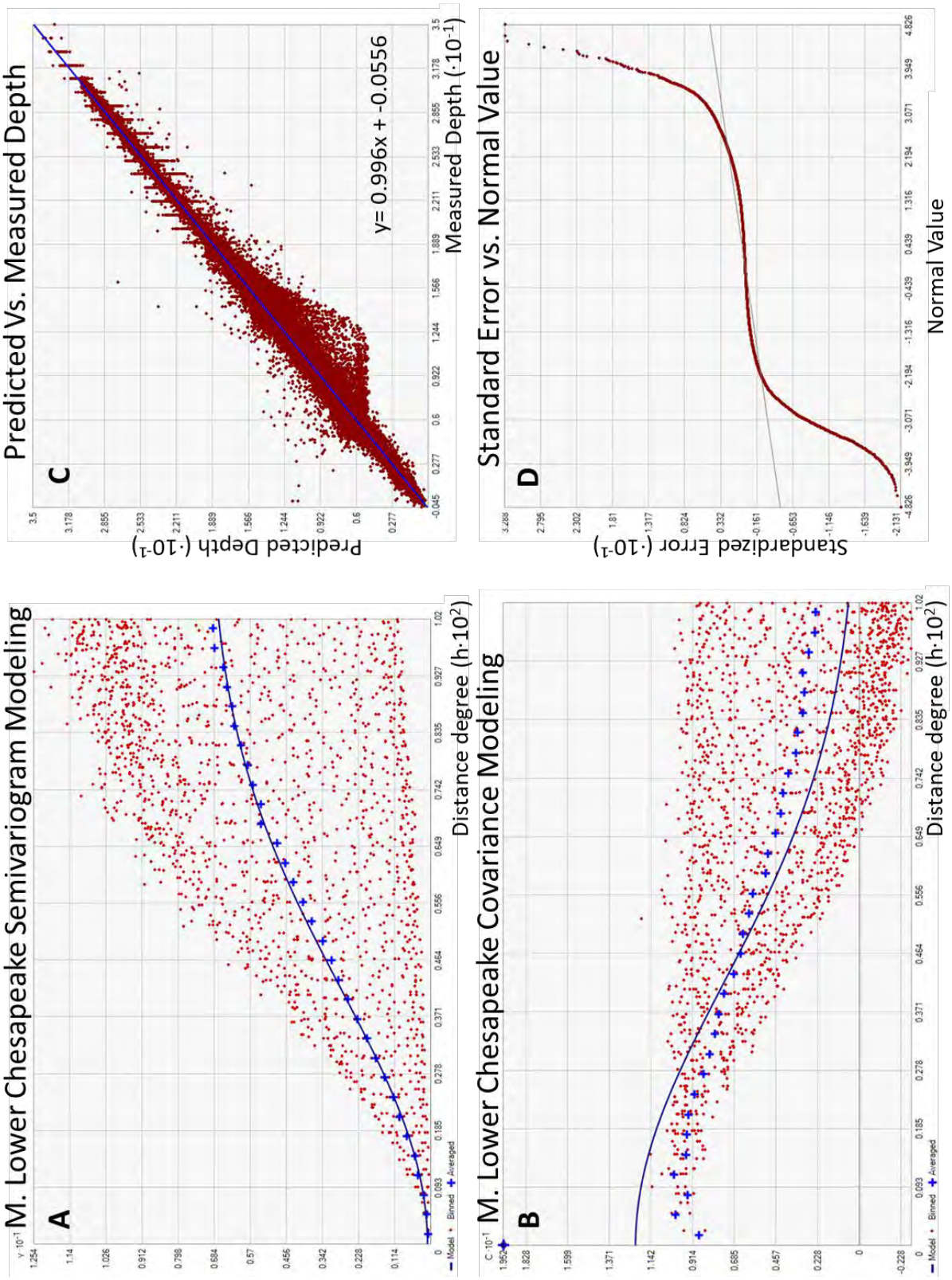

Figure 42: Mid-layer Lower Chesapeake Bay graphs used to determine kriging parameters. (A) Empirical Semivariogram Gaussian Model comparison. (B) Covariance Gaussian Model comparison. Plots (A) and (B) incorporate binned (red dots) and average values (blue crosses) of the data within the set lag size to help the user determine which statistical model (solid blue line) fits the each data set the best. (C) Predicted depth vs. measured depth graph with trend line equation that shows how much error could occur at known data points using the parameters chosen. (D) Standardized error vs. normal value graph.

Location	**M. Lower Chesapeake Bay**
Northeast Extent	37.1850 N, 75.4335 W
Southwest Extent	36.7875 N, 76.2148 W
Number of Points	718,462
Prediction Errors	
Mean	0.0005590368
Root-Mean-Square	0.3095545
Mean Standardized	0.00173856
RMS Standardized	0.8989027
Average Standard Error	0.3435862

Table 13: Mid-layer Lower Chesapeake Bay extent and kriging bathymetry prediction errors.

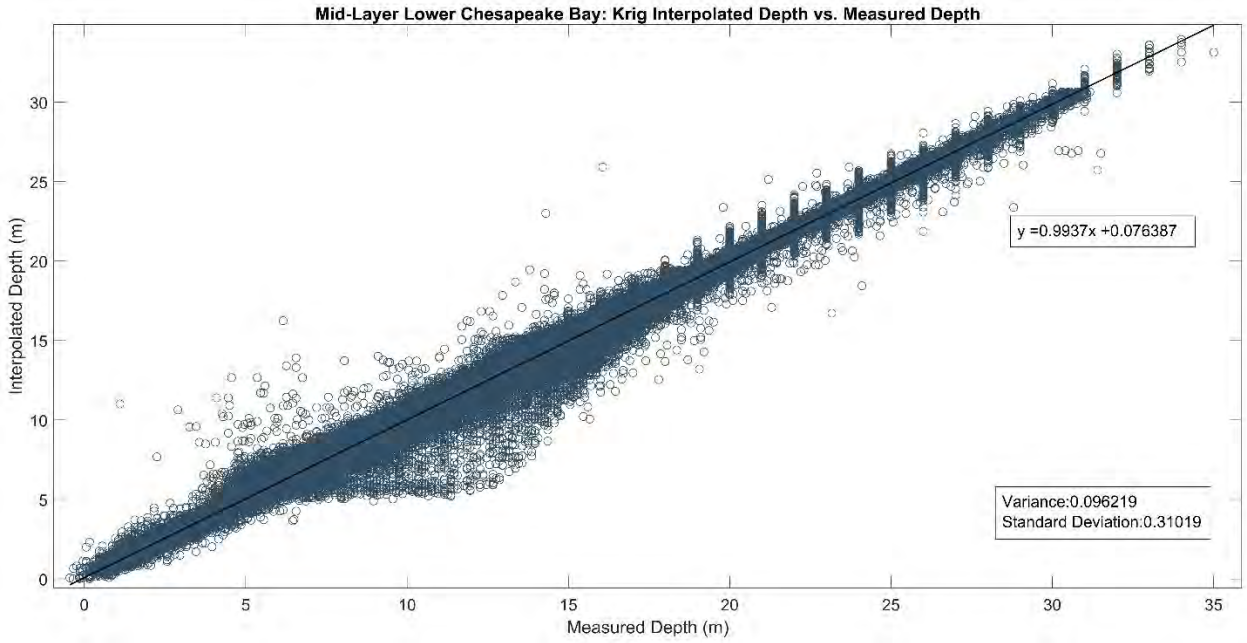

Figure 43: Mid-Layer Lower Chesapeake Bay kriging interpolated depths versus measured depths.

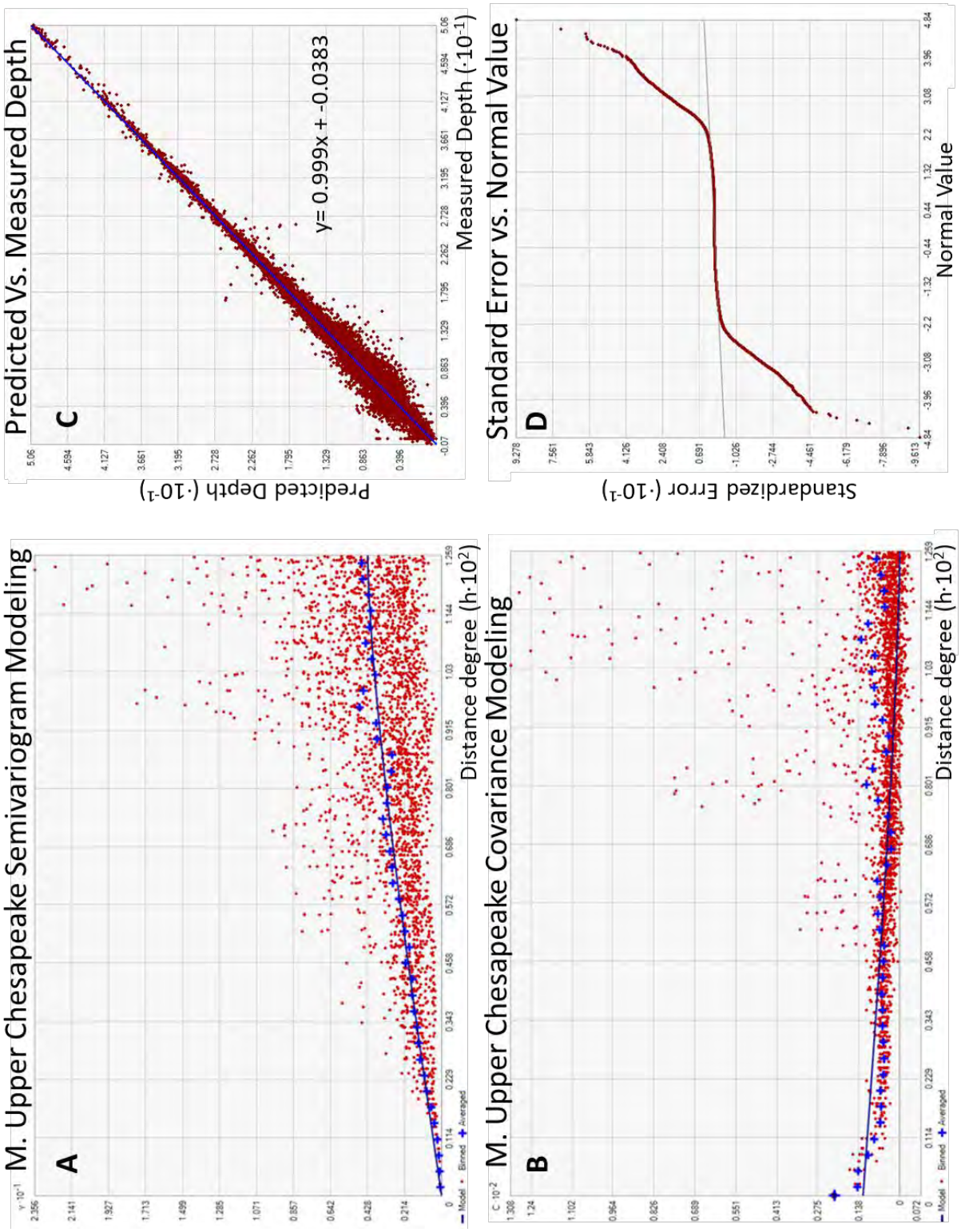

Figure 44: Mid-layer Upper Chesapeake Bay graphs used to determine kriging parameters. (A) Empirical Semivariogram Circular Model comparison. (B) Covariance Circular Model comparison. Plots (A) and (B) incorporate binned (red dots) and average values (blue crosses) of the data within the set lag size to help the user determine which statistical model (solid blue line) fits the each data

set the best. (C) Predicted depth vs. measured depth graph with trend line equation that shows how much error could occur at known data points using the parameters chosen. (D) Standardized error vs. normal value graph.

Location	M. Upper Chesapeake Bay
Northeast Extent	39.4120 N, 76.0955 W
Southwest Extent	38.6844 N, 76.5617 W
Number of Points	770,427
Prediction Errors	
Mean	-0.001021986
Root-Mean-Square	0.21382
Mean Standardized	-0.004245591
RMS Standardized	2.120599
Average Standard Error	0.2196721

Table 14: Mid-layer Upper Chesapeake Bay extent and kriging bathymetry prediction errors.

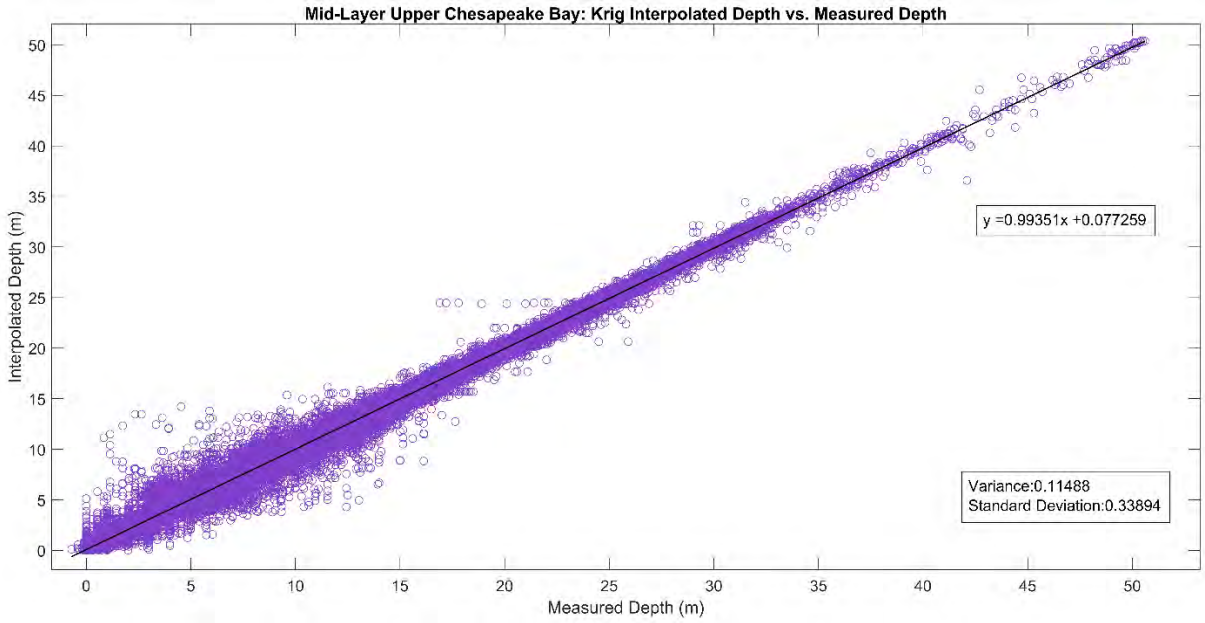

Figure 45: Mid-layer Upper Chesapeake Bay kriging interpolated depths versus measured depths.

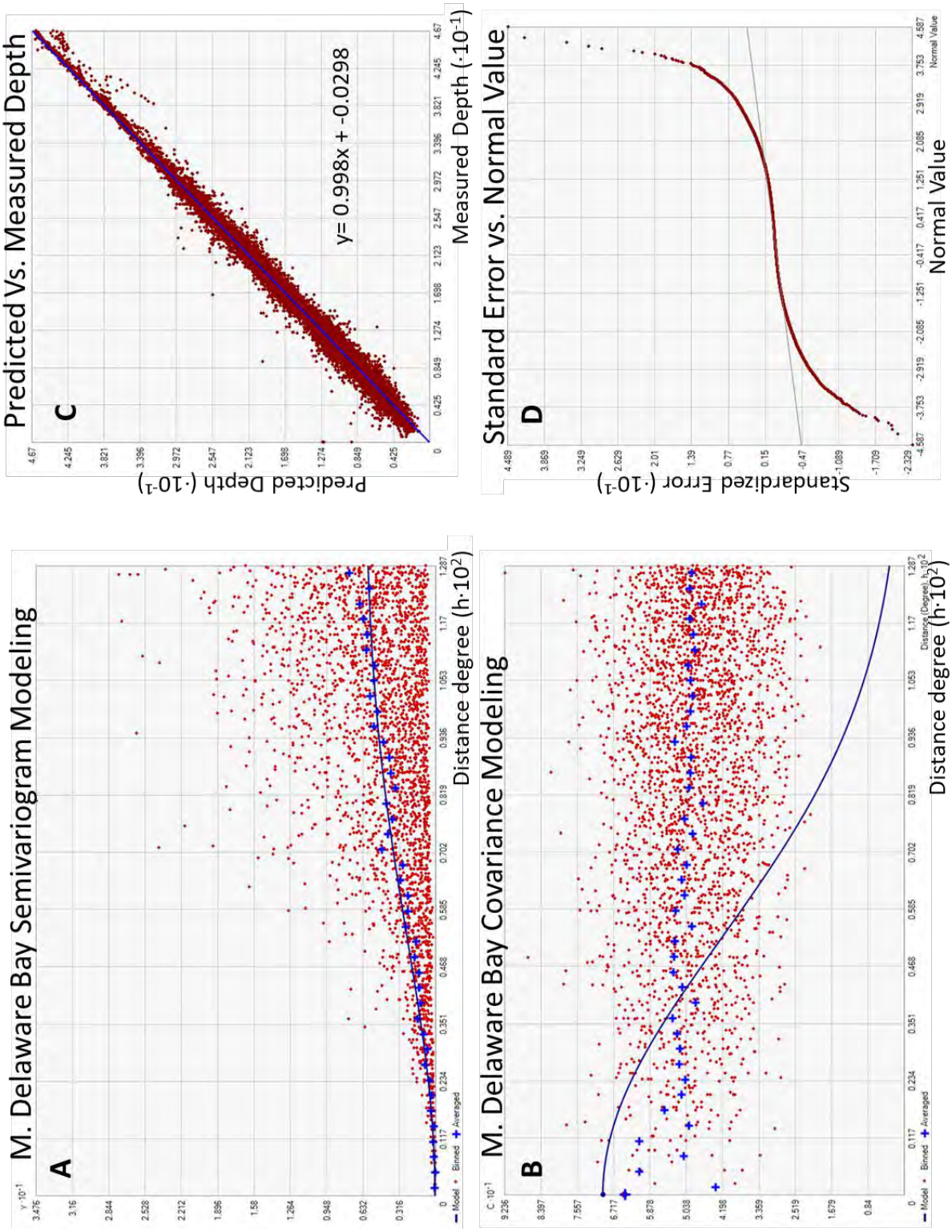

Figure 46: Mid-layer Delaware Bay graphs used to determine kriging parameters. (A) Empirical Semivariogram Gaussian Model comparison. (B) Covariance Gaussian Model comparison. Plots (A) and (B) incorporate binned (red dots) and average values (blue crosses) of the data within the set lag size to help the user determine which statistical model (solid blue line) fits the each data set

the best. (C) Predicted depth vs. measured depth graph with trend line equation that shows how much error could occur at known data points using the parameters chosen. (D) Standardized error vs. normal value graph.

Location	**M. Delaware Bay**
Northeast Extent	39.6600 N, 74.5507 W
Southwest Extent	38.4671 N, 75.6048 W
Number of Points	222,031
Prediction Errors	
Mean	-0.002153824
Root-Mean-Square	0.3637845
Mean Standardized	-0.007495826
RMS Standardized	1.239448
Average Standard Error	0.2915771

Table 15: Mid-layer Delaware Bay extent and kriging bathymetry prediction errors.

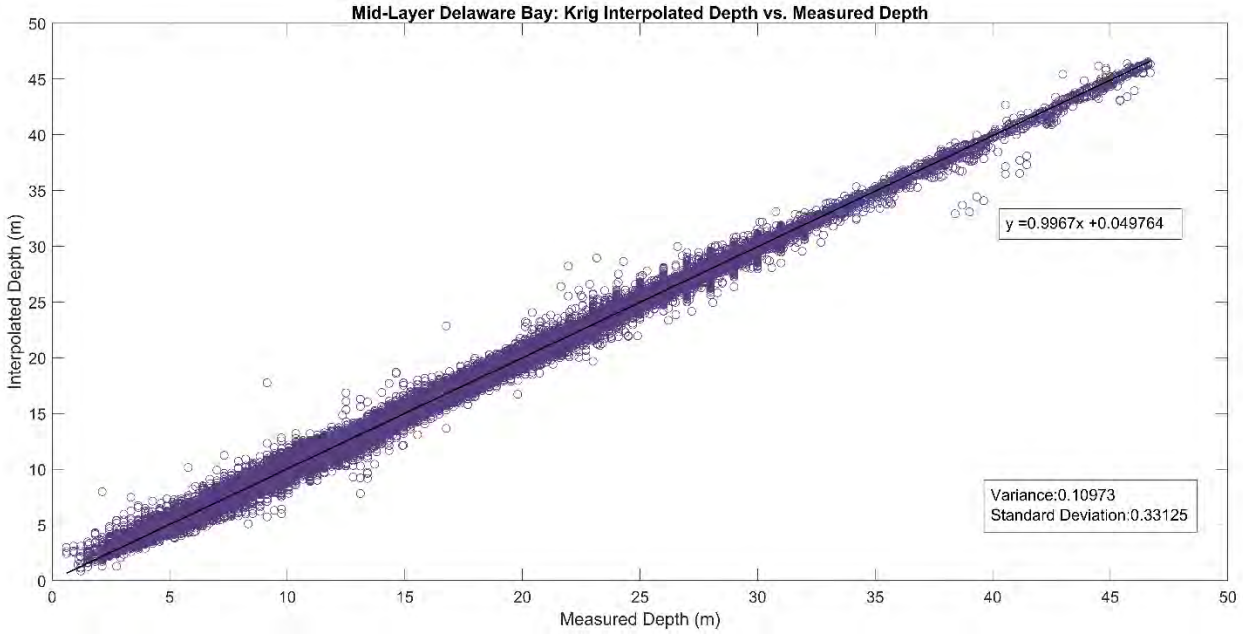

Figure 47: Mid-Layer Delaware Bay kriging interpolated depths versus measured depths.

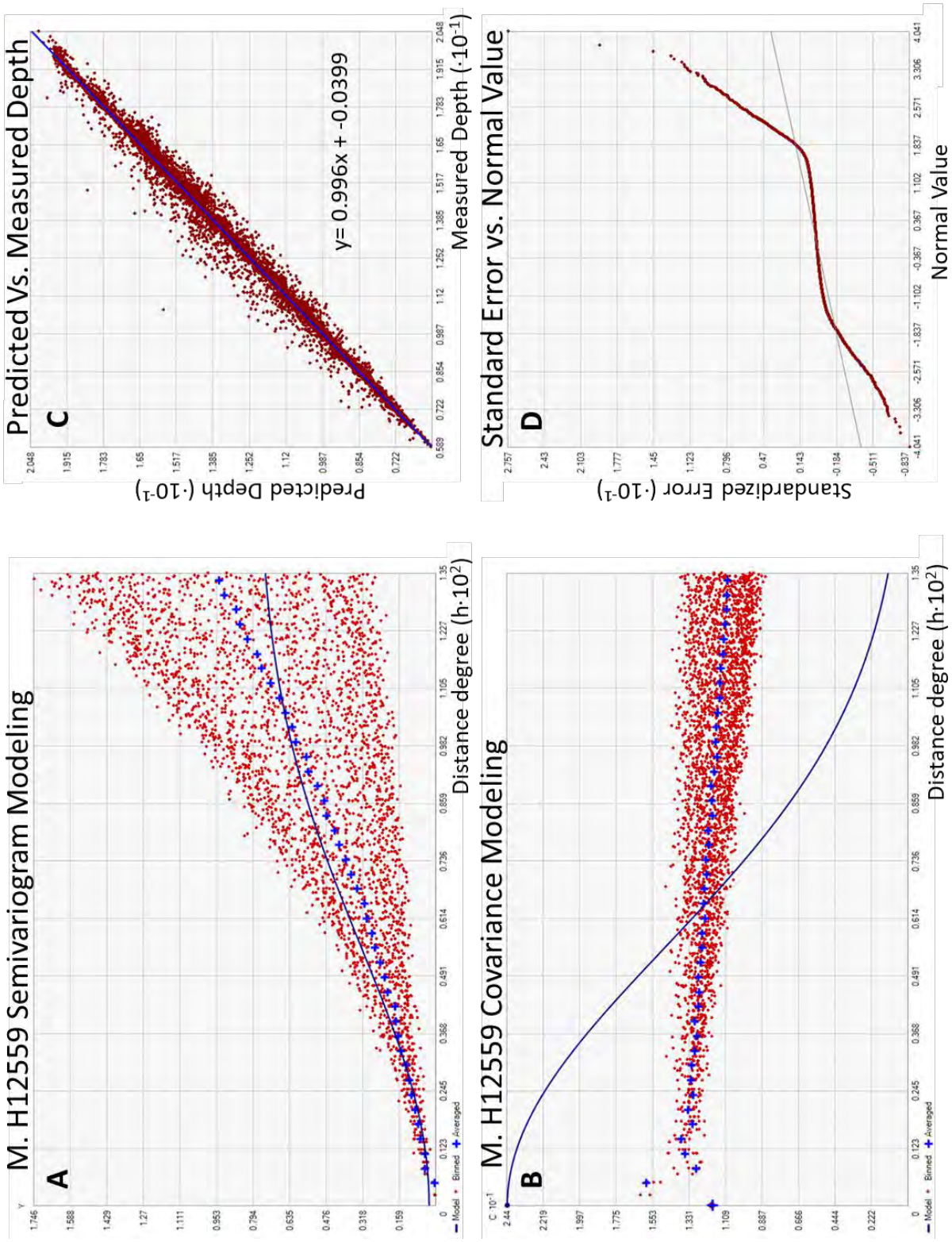

Figure 48: Mid-layer H12559 graphs used to determine kriging parameters. (A) Empirical Semivariogram Gaussian Model comparison. (B) Covariance Gaussian Model comparison. Plots (A) and (B) incorporate binned (red dots) and average values (blue

crosses) of the data within the set lag size to help the user determine which statistical model (solid blue line) fits the each data set the best. (C) Predicted depth vs. measured depth graph with trend line equation that shows how much error could occur at known data points using the parameters chosen. (D) Standardized error vs. normal value graph.

Location	**M. H12559**
Northeast Extent	37.3474 N, 75.5556 W
Southwest Extent	37.2478 N, 75.7352 W
Number of Points	18,775
Prediction Errors	
Mean	-0.00009242529
Root-Mean-Square	0.221048
Mean Standardized	-0.0004141973
RMS Standardized	1.225284
Average Standard Error	0.1794785

Table 16: Mid-layer H12559 extent and kriging bathymetry prediction errors.

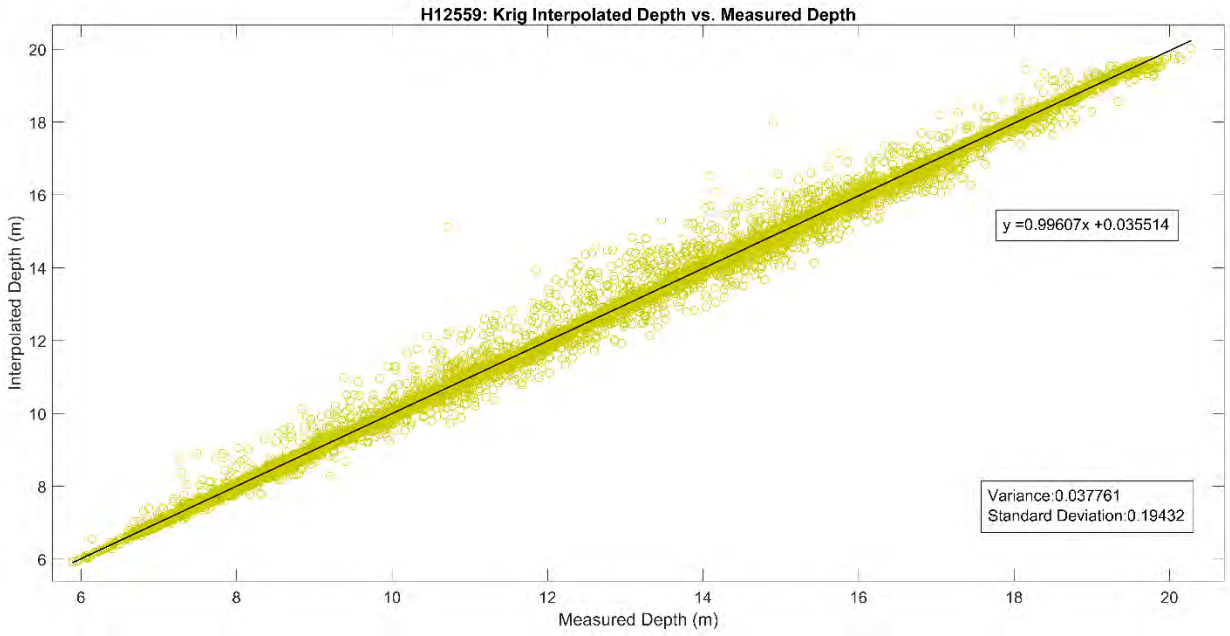

Figure 49: Mid-Layer H12559 kriging interpolated depths versus measured depths.

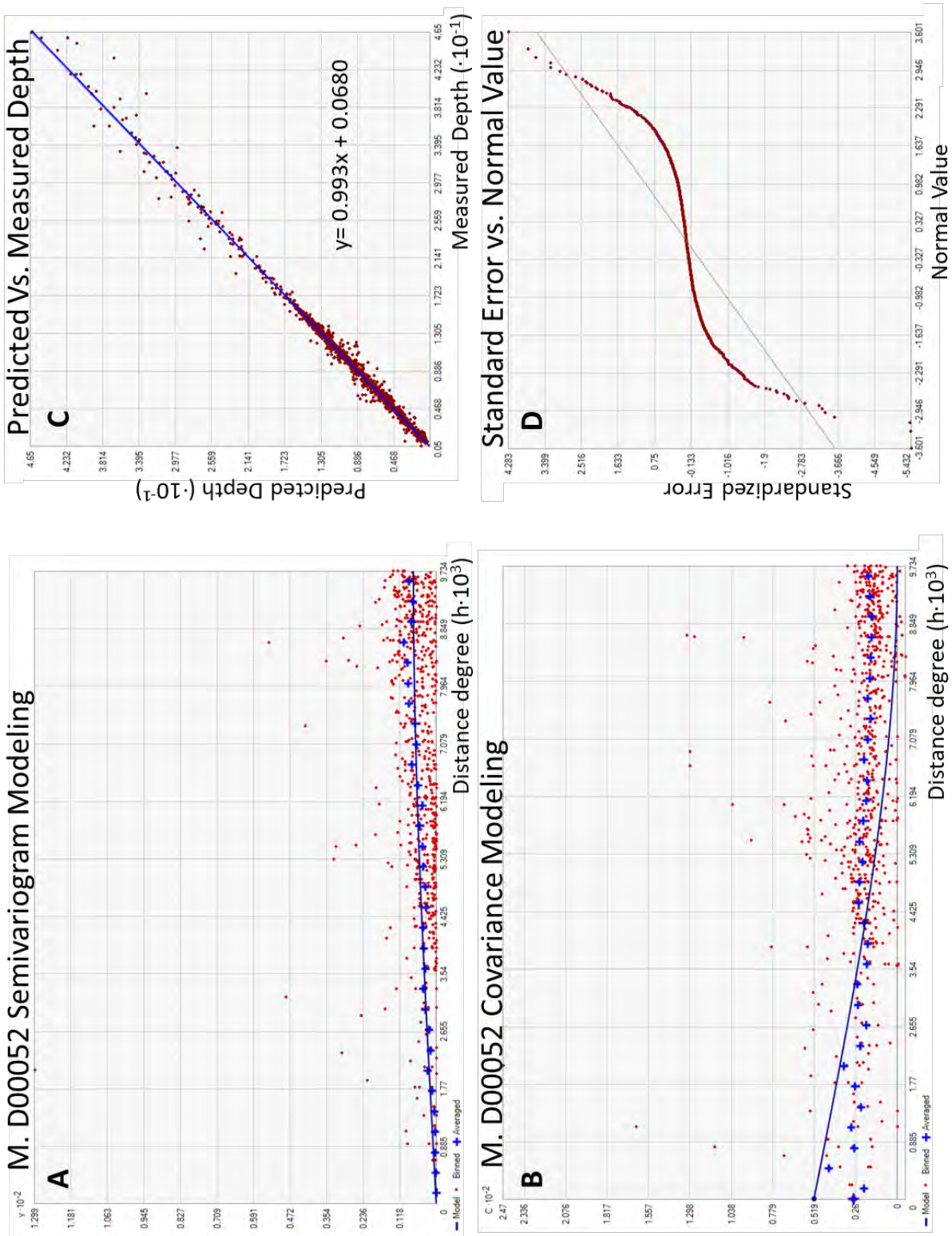

Figure 50: Mid-layer D00052 graphs used to determine kriging parameters. (A) Empirical Semivariogram Spherical Model comparison. (B) Covariance Spherical Model comparison. Plots (A) and (B) incorporate binned (red dots) and average values (blue crosses) of the data within the set lag size to help the user determine which statistical model (solid blue line) fits the each data set

the best. (C) Predicted depth vs. measured depth graph with trend line equation that shows how much error could occur at known data points using the parameters chosen. (D) Standardized error vs. normal value graph.

Location	**M. D00052**
Northeast Extent	37.2709 N, 76.0246 W
Southwest Extent	37.1729 N, 76.3913 W
Number of Points	3,149
Prediction Errors	
Mean	-0.001441357
Root-Mean-Square	0.4521762
Mean Standardized	-0.001180366
RMS Standardized	0.4650055
Average Standard Error	1.058081

Table 17: Mid-layer D00052 extent and kriging bathymetry prediction errors.

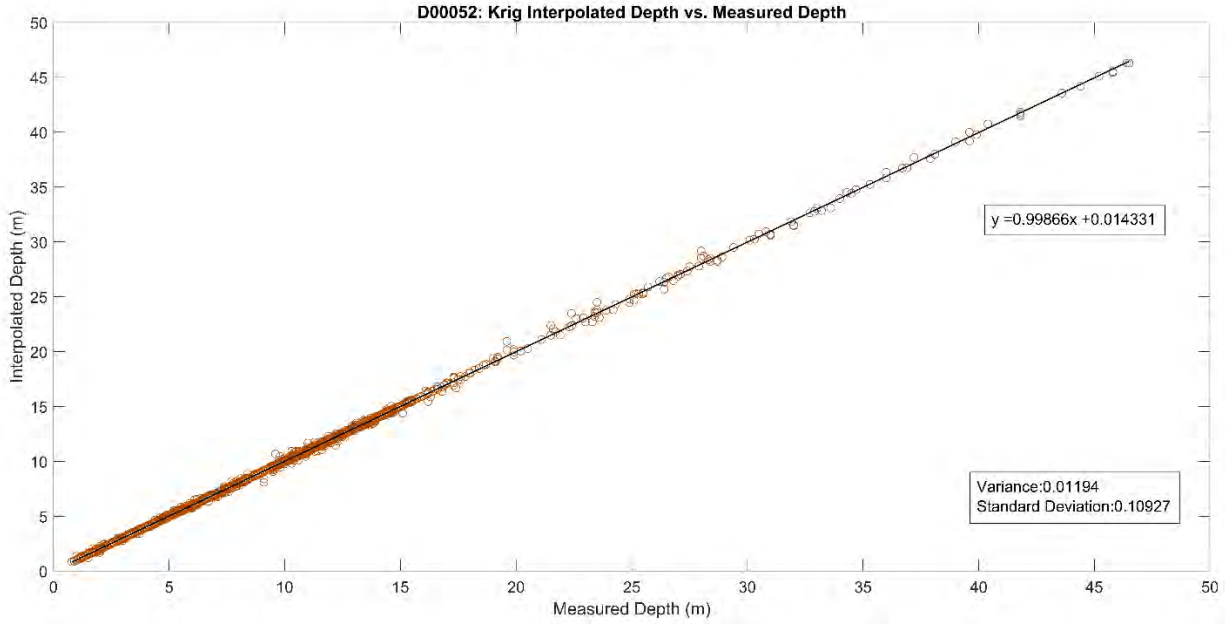

Figure 51: Mid-Layer D00052 kriging interpolated depths versus measured depths.

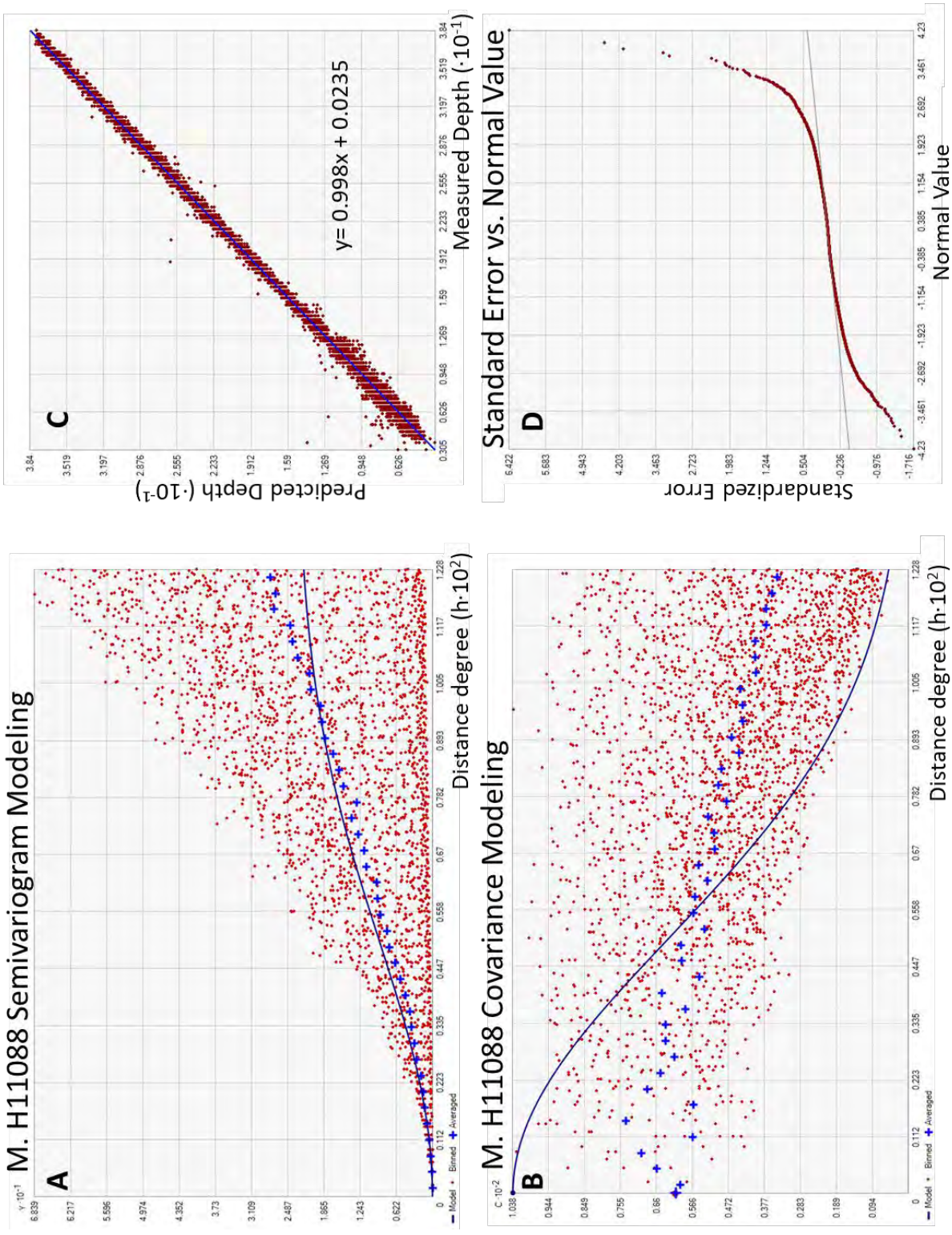

Figure 52: Mid-layer H11088 graphs used to determine kriging parameters. (A) Empirical Semivariogram Gaussian Model comparison. (B) Covariance Gaussian Model comparison. Plots (A) and (B) incorporate binned (red dots) and average values (blue crosses) of the data within the set lag size to help the user determine which statistical model (solid blue line) fits the each data set

the best. (C) Predicted depth vs. measured depth graph with trend line equation that shows how much error could occur at known data points using the parameters chosen. (D) Standardized error vs. normal value graph.

Location	**M. H11088**
Northeast Extent	38.4708 N, 76.2906 W
Southwest Extent	38.3427 N, 76.4294 W
Number of Points	42,718
Prediction Errors	
Mean	0.001691649
Root-Mean-Square	0.2737156
Mean Standardized	0.01103378
RMS Standardized	1.667314
Average Standard Error	0.1650757

Table 18: Mid-layer H11088 extent and kriging bathymetry prediction errors.

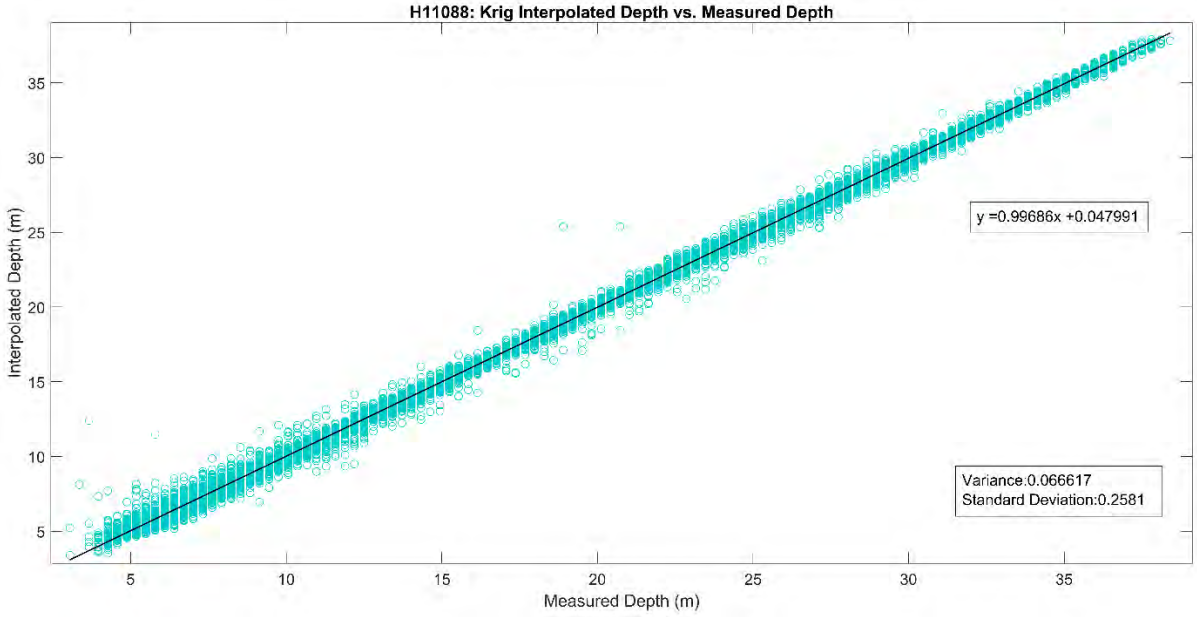

Figure 53: Mid-Layer H11088 kriging interpolated depths versus measured depths.

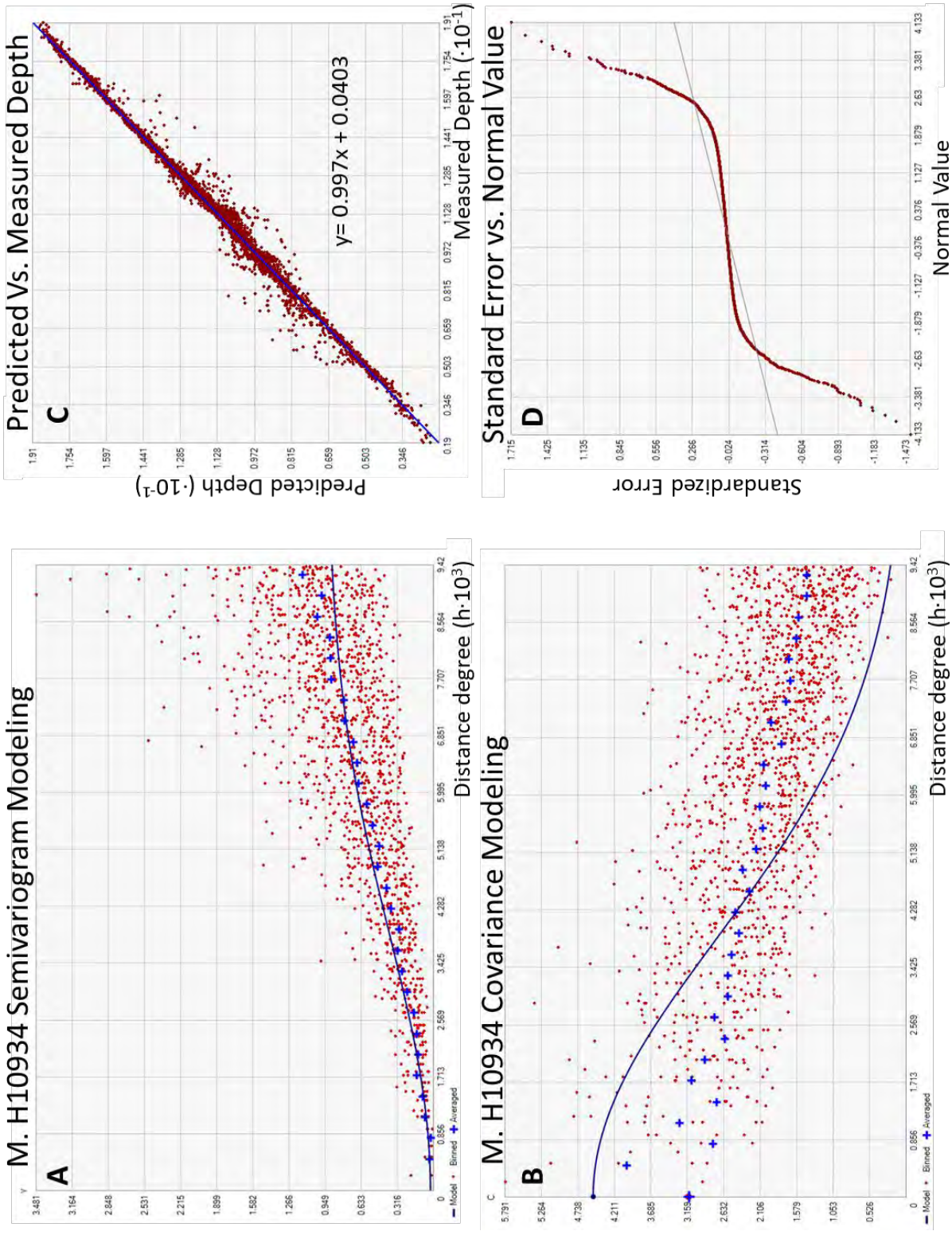

Figure 54: Mid-layer H10934 graphs used to determine kriging parameters. (A) Empirical Semivariogram Gaussian Model comparison. (B) Covariance Gaussian Model comparison. Plots (A) and (B) incorporate binned (red dots) and average values (blue

crosses) of the data within the set lag size to help the user determine which statistical model (solid blue line) fits the each data set the best. (C) Predicted depth vs. measured depth graph with trend line equation that shows how much error could occur at known data points using the parameters chosen. (D) Standardized error vs. normal value graph.

Location	**M. H10934**
Northeast Extent	38.0394 N, 76.2069 W
Southwest Extent	37.9292 N, 76.3658 W
Number of Points	27,899
Prediction Errors	
Mean	-0.0006286584
Root-Mean-Square	0.1372092
Mean Standardized	-0.003697011
RMS Standardized	0.798035
Average Standard Error	0.1723181

Table 19: Mid-layer H10934 extent and kriging bathymetry prediction errors.

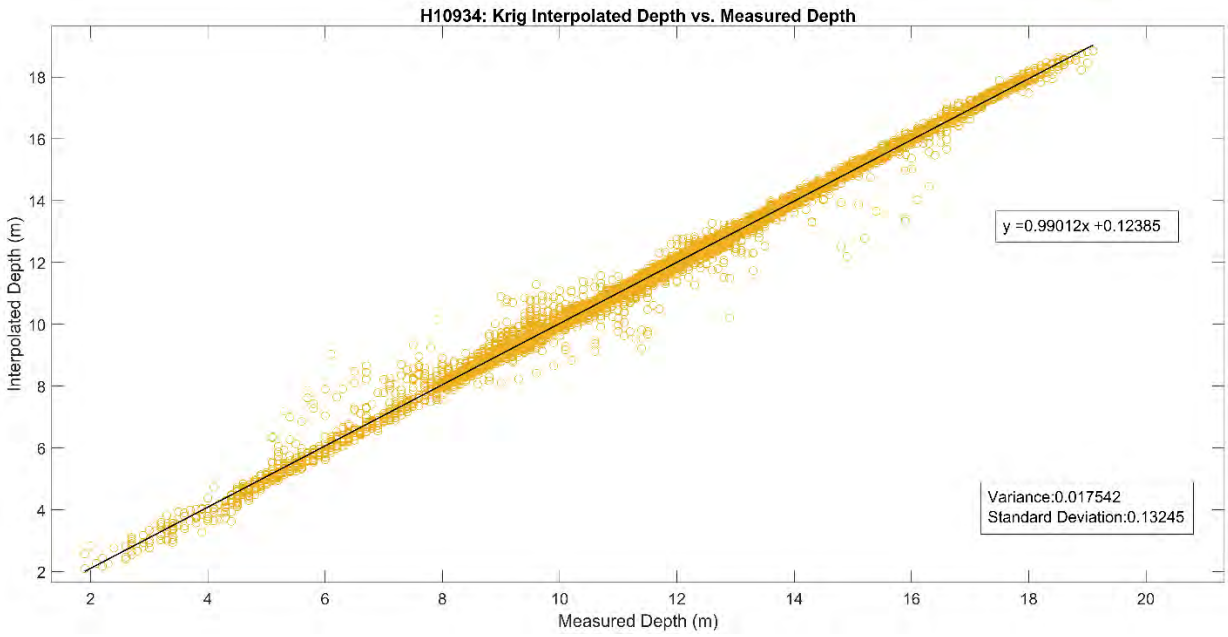

Figure 55: Mid-Layer H10934 kriging interpolated depths versus measured depths.

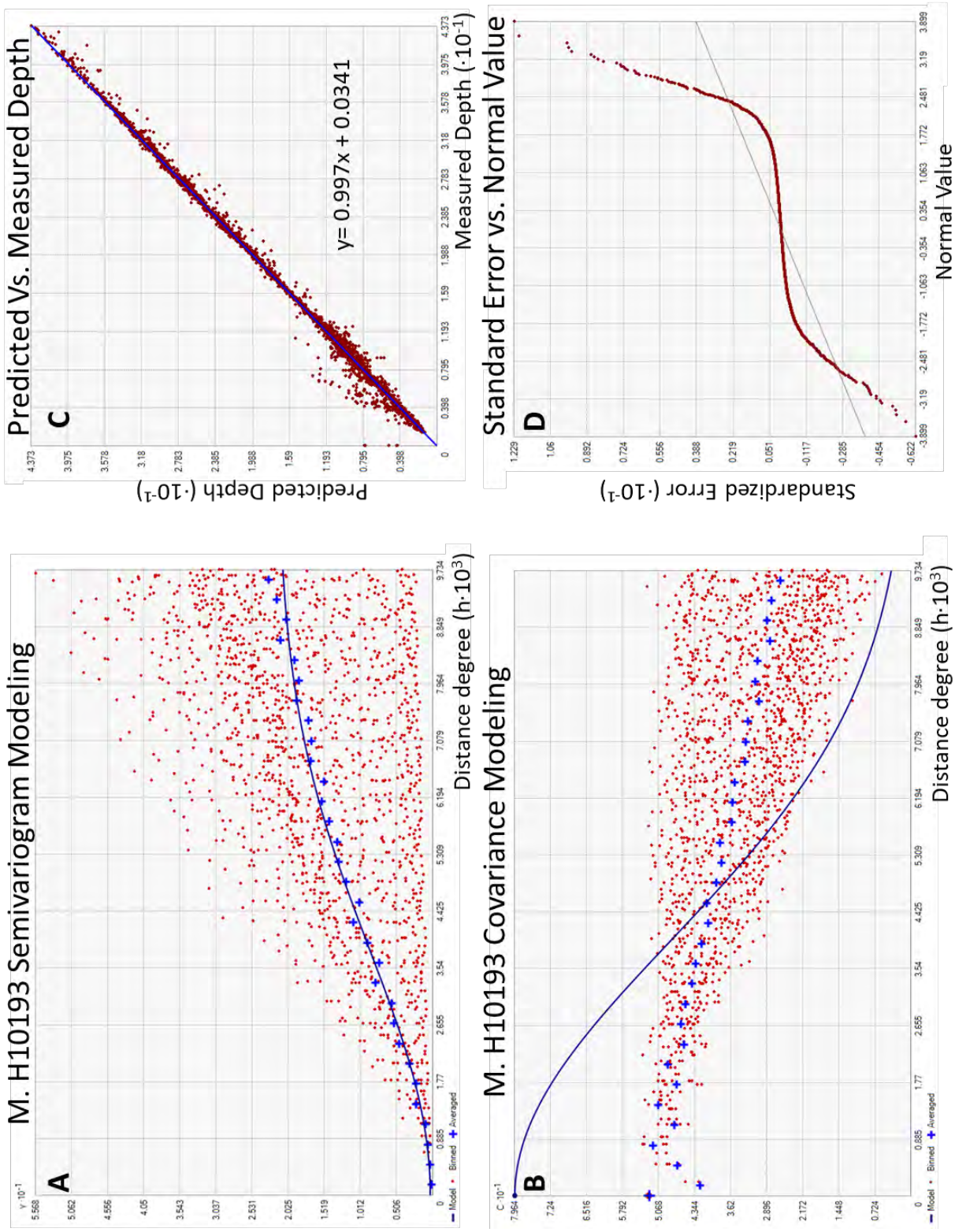

Figure 56: Mid-layer H10193 graphs used to determine kriging parameters. (A) Empirical Semivariogram Gaussian Model comparison. (B) Covariance Gaussian Model comparison. Plots (A) and (B) incorporate binned (red dots) and average values (blue

crosses) of the data within the set lag size to help the user determine which statistical model (solid blue line) fits the each data set the best. (C) Predicted depth vs. measured depth graph with trend line equation that shows how much error could occur at known data points using the parameters chosen. (D) Standardized error vs. normal value graph.

Location	**M. H10193**
Northeast Extent	38.3351 N, 76.2817 W
Southwest Extent	38.2905 N, 76.3853 W
Number of Points	10,341
Prediction Errors	
Mean	0.002754618
Root-Mean-Square	0.413769
Mean Standardized	0.004839575
RMS Standardized	0.6654018
Average Standard Error	0.630334

Table 20: Mid-layer H10193 extent and kriging bathymetric prediction errors.

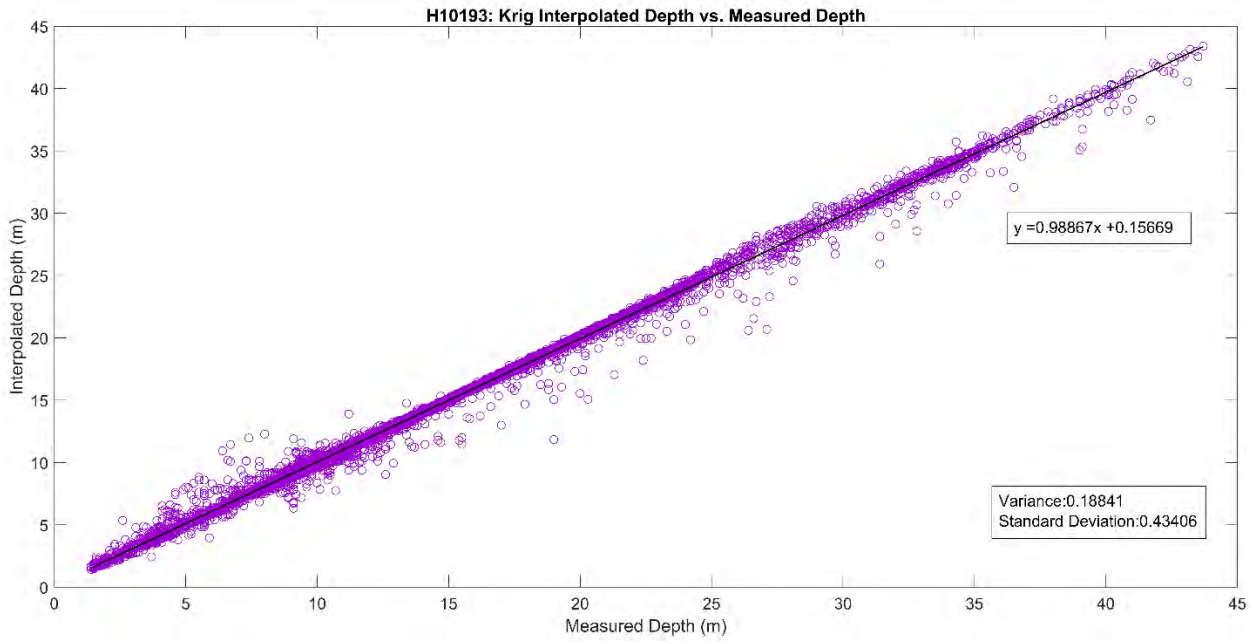

Figure 57: Mid-Layer H10193 kriging interpolated depths versus measured depths.